2013

GUMBOS and NanoGUMBOS: Applications as Photosensitizers in Dye-sensitized Solar Cells

Atiya Nicole Jordan
Louisiana State University and Agricultural and Mechanical College

GUMBOS AND NANOGUMBOS: APPLICATIONS AS PHOTOSENSITIZERS IN DYE-SENSITIZED SOLAR CELLS

A Dissertation

Submitted to the Graduate Faculty of the
Louisiana State University and
Agricultural and Mechanical College
in partial fulfillment of the
requirements for the degree of
Doctor of Philosophy

in

The Department of Chemistry

by
Atiya N. Jordan
B.S., Virginia Commonwealth University, 2008
December 2013

To my best friend and other half, Reginald Brown II, for his steadfast love, encouragement, and faith in me.

To my parents, Jimmy and Vendella Jordan, and my siblings, Toesia Mims and Alysia Jordan for their infinite love and support over the years.

To my grandfather for the constant reminder that "while climbing the ladder of success, remember everything is a test."

To my entire family past, present, and future.

ACKNOWLEDGEMENTS

I am truly grateful to the following people for their generosity and support:

Prof. Isiah M. Warner for his mentorship and constant faith in me. It has been a privilege to work in your research group. I appreciate your encouragement and guidance that has facilitated my growth as a researcher. Thank you for the amazing opportunities to experience science abroad, beyond the laboratory.

Doctoral Committee Members: Profs. Jayne Garno, Daniel Hayes, Ying Wang, Dooyoung Hah, and Jeffrey Blackmon for their time and helpful suggestions regarding this dissertation.

Profs. Robert Chang, Evgueni Nesterov, Matthew Tarr, and Ying Wang for use of their instrumentation for this dissertation work.

Profs. Samuel Gilman and Theda Daniels-Race for their encouragement and support during my graduate school tenure.

Dr. Susmita Das and Dr. Noureen Siraj for sharing their knowledge of fluorescence spectroscopy and electrochemistry with me. Thank you for the helpful discussions and review of my manuscripts.

Dr. Vivian Fernand for her guidance, helpful suggestions, and proofreading of my manuscripts and dissertation.

Dr. Bilal El-Zahab, Dr. Min Li, and Dr. Farhana Hasan for their time, support, and helpful suggestions regarding this dissertation work.

Warner Research Group for their dynamic discussions, support, and friendship over the years.

Funding Agencies: National Science Foundation, Philip W. West Endowment, Louisiana Board of Regents Fellowship, and GAANN Fellowship

TABLE OF CONTENTS

LIST OF TABLES

LIST OF FIGURES

LIST OF ABBREVIATIONS

Abbreviation	Name
η	energy conversion efficiency
λ	wavelength
λ_{int}	intersect wavelength
λ_{onset}	onset wavelength
A	absorbance
AIEE	aggregation-induced emission enhancement
BTU	British thermal units
CCD	charge-couple device
CdTe	cadmium telluride
CIGS	gallium diselenide
CV	cyclic voltammetry
DSSCs	dye-sensitized solar cells
ε	molar extinction coefficient
E	energy transfer efficiency
$E_{0\text{-}0}$	0-0 transition energy state
E^*_{red}	excited state reduction potential
E_{pa}	anodic peak potential
E_{pc}	cathodic peak potential
E_g	band gap
$E_{g\ EC}$	electrochemical band gap
E_{ox}	oxidation potential

eV	electron volt
f(λ)	normalized emission spectrum of the donor
F_d	fluorescence intensities of donor in the absence of acceptor
F_{da}	fluorescence intensities of donor in the presence of acceptor
Fc^+/Fc	ferrocene/ferrocenium
FF	fill factor
FONs	fluorescent organic nanoparticles
FRET	Förster resonance energy transfer
FTO	fluorine-doped tin oxide
GaAs	gallium arsenide
GUMBOS	Group of Uniform Materials Based on Organic Salts
H-	hypsochromic aggregates
HOMO	highest unoccupied molecular orbital
I_{max}	maximum current
I_{sc}	short-circuit current
IC	internal conversion
ILs	ionic liquids
ISC	intersystem crossing
I-V	current-voltage
J-	Jelley aggregates
J(λ)	spectral overlap integral
LiBETI	lithium bis(perfluoroethylsulfonyl)imide

$LiNTf_2$	lithium bis(trifluoromethanesulfonyl)imide
LUMO	lowest unoccupied molecular orbital
NHE	normal hydrogen electrode
P_{in}	power input
P_{max}	maximum power output
PICI	pseudoisocyanine iodide
[PIC][BETI]	pseudoisocyanine bis(perfluoroethylsulfonyl)imide
$[PIC][NTf_2]$	pseudoisocyanine bis(trifluoromethanesulfonyl)imide
POM	polarized optical microscopy
Pt	Platinum
QDs	quantum dots
r	anisotropy
redox	reduction-oxidation
RIR	restriction in intramolecular rotation
RTILs	room temperature ionic liquids
SAED	selected area electron diffraction
SEM	scanning electron microscopy
TAC	time-to-amplitude converter
$TBAPF_6$	tetrabutylammonium hexafluorophosphate
TCO	transparent conductive oxide
TCSPC	time-correlated single-photon counting
TEM	transmission electron microscopy
TICT	twisted intramolecular charge transfer

TiO_2	titanium dioxide
TW	terawatts
UV-Vis	ultraviolet-visible
V_{max}	maximum voltage
V_{oc}	open-current voltage

ABSTRACT

Renewable energy is a major concern due to increased world energy consumption. In particular, solar energy is a type of renewable energy source that uses devices known as solar cells to convert sunlight to electricity. Specifically, devices referred to as dye-sensitized solar cells (DSSCs) employ dyes to absorb solar energy. Dyes derived from ruthenium complexes have been typically used in DSSCs. Unfortunately, several disadvantages are associated with current ruthenium complex photosensitizers, which can be attributed to limited supply and expense of metals, as well as reduced absorption in the near-infrared region of the electromagnetic spectrum. Accordingly, this dissertation is a discussion of novel dyes referred to as **g**roup of **u**niform **m**aterials **b**ased on **o**rganic **s**alts (GUMBOS) for application as photosensitizers in DSSCs. These GUMBOS are solid phase organic salts composed of bulky ions that have melting points from 25°C to 250°C. Importantly, GUMBOS can be tuned for multiple functions based on selected ions resulting in interesting physiochemical properties. In addition, nanomaterials derived from GUMBOS (nanoGUMBOS) can also result in significant properties.

The first part of this dissertation involves the synthesis and characterization of nanoGUMBOS from cyanine dyes. These nanomaterials are prepared via a facile self-assembly approach, and spectral and electrochemical properties are investigated. In one study, controlled properties of cyanine-based nanoGUMBOS are found to be dependent on the counterion associated with the cationic dye. In another study, GUMBOS derived from cyanine dyes with increasing methine chain lengths are synthesized. In addition, binary nanomaterials consisting of two different cyanine

methine chain length GUMBOS are prepared. The effect of Förster resonance energy transfer between these latter nanomaterials enhances fluorescence into the near-infrared region of the electromagnetic spectrum. The individual and binary nanoGUMBOS offer possible use as sensitizers that extend into the near-infrared region of the electromagnetic spectrum.

The second part of this dissertation entails the incorporation of cyanine-based GUMBOS and nanoGUMBOS into DSSCs. In this study, various preparation methods are used for formation of titanium dioxide semiconductor electrodes. Solar cells comprised of these electrodes and cyanine-based GUMBOS are fabricated, and the performances of these DSSCs are investigated.

CHAPTER 1
INTRODUCTION

1.1 Solar Energy

Advances in renewable energy production are a major concern in recent years due to increased world energy consumption. In 2011, the United States energy consumption was 97.5 quadrillion British thermal units (Btu), or 3.26 terawatts (TW).[1] A major source of this energy consumption was provided by use of nonrenewable carbon-based fuels, i.e. petroleum, natural gas, and coal (Figure 1.1).[1] Unfortunately, nonrenewable energy sources are known to be detrimental to the environment, primarily as a result of carbon dioxide emissions.

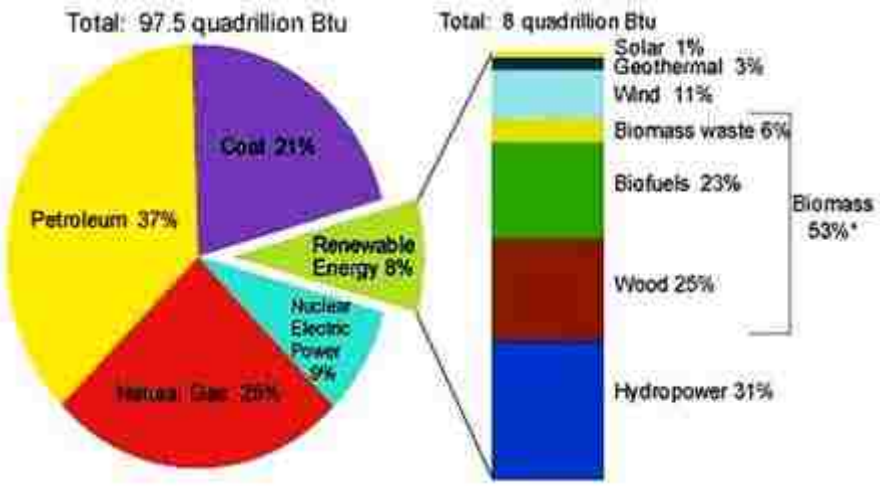

Figure 1.1 United States energy consumption in 2011 reproduced from the U.S. Energy Information Administration (March 2012).[1]

The use of renewable energy sources affords promising methods to reduce fuel dependence by replenishing energy over a short period of time. In particular, solar energy is a continuous and abundant energy source obtained directly from sunlight. More than 120,000 TW of solar energy reaches the surface of the earth,[2] which is five orders of magnitude greater than the energy consumed in the United States in 2011. In

such applications, energy from solar emission is converted to electricity by use of devices known as photovoltaics, or solar cells. However, with only 1% of energy consumption obtained by solar energy, continued research and development is a driving force to efficiently harness and exploit this natural source of energy.

1.2 Development of Solar Cells

Solar cells absorb energy in the form of photons from sunlight, which is used to generate electricity by migration of electrons through an external load. This concept of converting sunlight to electricity was initially established as a result of the discovery of the photovoltaic effect by Becquerel in 1839.[3] In this experiment, the production of current was achieved between two platinum electrodes by illumination while the electrodes were immersed in an electrolyte solution containing silver halide salt. This discovery became a foundation of the development of solar cells. Thereafter, an advancement by Ohl at Bell Laboratories in 1941 used a p-n junction of a doped single silicon crystal to produce two types of semiconductor material known as p-type (positive) and n-type (negative) semiconductors (Figure 1.2).[4] When these semiconductors are in contact, positive (hole) and negative (electron) charge carriers diffuse to opposite charged regions generating an intrinsic electric field. At equilibrium, the p-n junction does not have a net charge resulting in a depletion region that forms at this junction. Upon illumination, photons with energy greater than the band gap (E_g), i.e. the energy difference between the valence band (E_v) and conduction band (E_c), are absorbed by a semiconductor and result in generation of an exciton, or electron-hole pair. The intrinsic electric field separates the charge carriers and forces the electron to

migrate through an external load to ultimately generate current before recombining with a hole.

It was not until 1954 that a commercial solar cell was developed by Chapin, Fuller, and Pearson at Bell Laboratories.[5] This solar cell was based on a p-n junction composed of silicon and yielded an energy conversion efficiency of 6%. More recently, Green has reported the highest energy conversion efficiency of 24.7% for single crystalline silicon solar cells based on use of a p-n junction.[6] Unfortunately, these first generation solar cells require expensive manufacturing of greater than $1/watt for production of high purity single crystals (Figure 1.3).[7] In addition, silicon absorbs only ultraviolet light that results in the need for a thick silicon layer to obtain adequate electromagnetic absorption.

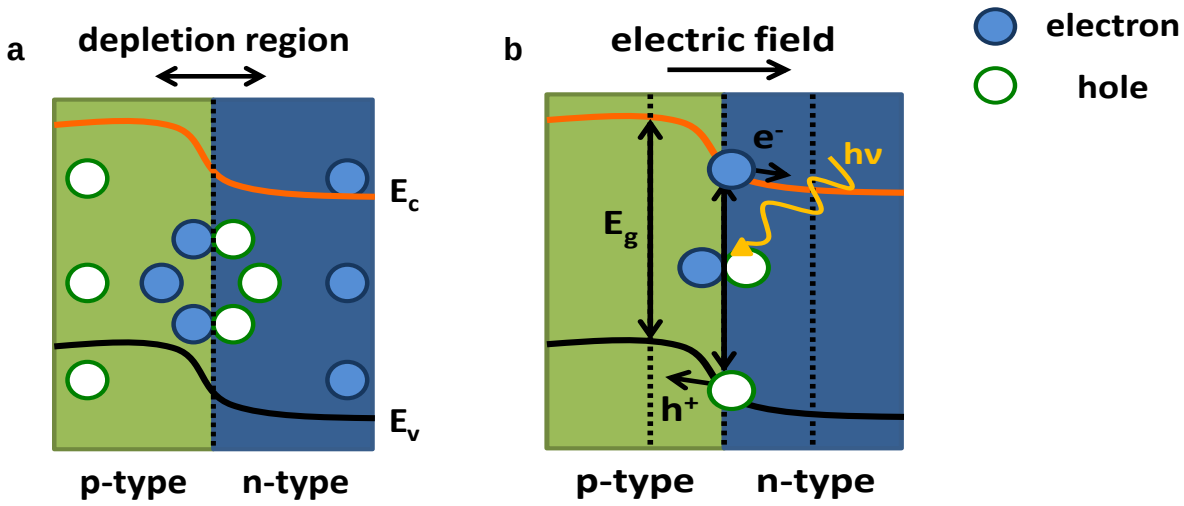

Figure 1.2 Diagram of a p-n junction (a) at equilibrium and (b) under illumination.

Thin film solar cells, classified as second generation devices, have been developed based on binary and multi-junction semiconductors to overcome the absorption disadvantage of crystalline silicon solar cells. These semiconductors provide better absorption which allows for use of less material and reduces manufacturing cost

as low as $0.50/watt.[7] Thin film solar cells include materials such as amorphous silicon, cadmium telluride (CdTe), copper indium gallium diselenide (CIGS), and gallium arsenide (GaAs). In that regard, a conversion efficiency of 10.1% has been achieved for amorphous silicon solar cells, which are typically used in low power devices such as calculators.[8] Thin film solar cells consisting of CdTe and CIGS have been reported to exhibit a conversion efficiency of 17.3% and 19.9%, respectively.[9,10] Although the aforementioned thin film solar cells are relatively less expensive, efficiencies are lower than crystalline silicon solar cells. A more expensive thin film solar cell comprised of GaAs has been found to exhibit a high conversion efficiency of 28.8% and is mainly used for space applications.[9]

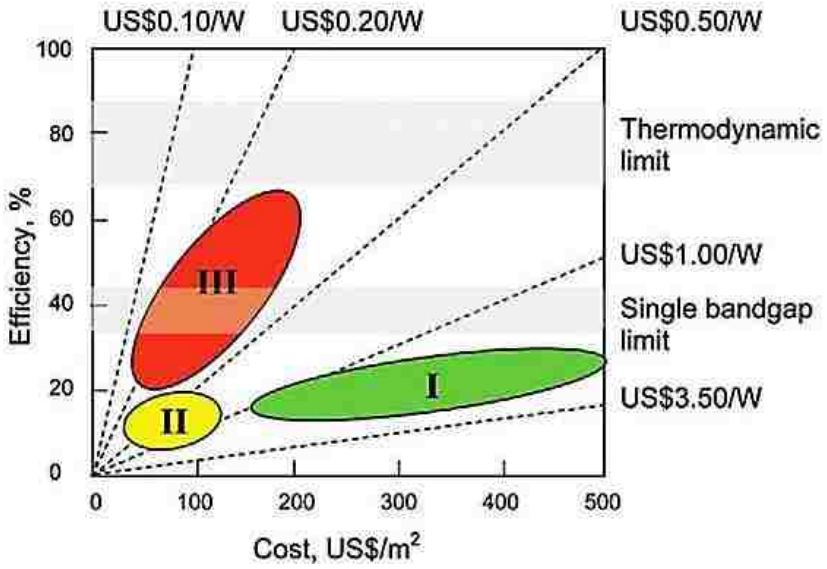

Figure 1.3 Classification of solar cells into three categories i.e. first, second, and third generation, based on materials used, maximum conversion efficiency obtained, and associated cost of power. Obtained from reference.[7]

The desire to develop low cost solar cells with increased efficiency is dependent on maximum energy conversion. However, achieving maximum energy conversion is limited due to energy loss by heat and inadequate photon absorption. This hindrance

results in a maximum thermodynamic efficiency of 30% for p-n junction solar cells, which was calculated by Shockley and Queisser.[11] Research to increase efficiency greater than the Shockley-Queisser limit at low cost has led to the development of a third generation of solar cells. In particular, a third generation device known as dye-sensitized solar cells (DSSCs) employs nanomaterials to broaden the potential to optimize efficiency.

1.3 Nanomaterials in DSSCs

The field of nanotechnology focuses on developments and applications of materials and devices at the molecular level. Materials at the nanoscale, ranging from 1 to 100 nm, are found to exhibit distinct physical, chemical, and electrical properties as compared to bulk materials due to a higher surface area to volume ratio. For instance, nanomaterials have been reported to have tunable absorption and energy level depending on the size of the nanostructures.[12] These properties are commonly found in semiconductor nanomaterials resulting in absorption onset shifts to shorter wavelengths and increase band gap as the size of the nanomaterials decrease. Research on such significant physiochemical properties has led to innovative applications of engineered nanomaterials in areas such as medicine,[13,14] electronics,[15] and energy.[16,17]

The use of nanomaterials in DSSCs was developed by Gratzel and O'Regan in 1991 via nanocrystalline titanium dioxide (TiO_2) particles.[18] This DSSC consisted of a dye derived from a ruthenium complex that was adsorbed on the surface of TiO_2 nanoparticles and generated a conversion efficiency of 7.9%. Since development, research related to DSSCs continues to increase over the years (Figure 1.4). As a result, a conversion efficiency of 11% has been achieved for DSSCs using ruthenium

complexes.[19,20] In comparison to silicon and thin film solar cells, DSSCs are have been found to be more cost efficient (less than $0.50/watt) due to the abundance of TiO_2.[7] The following section involves examination of the principle of DSSCs.

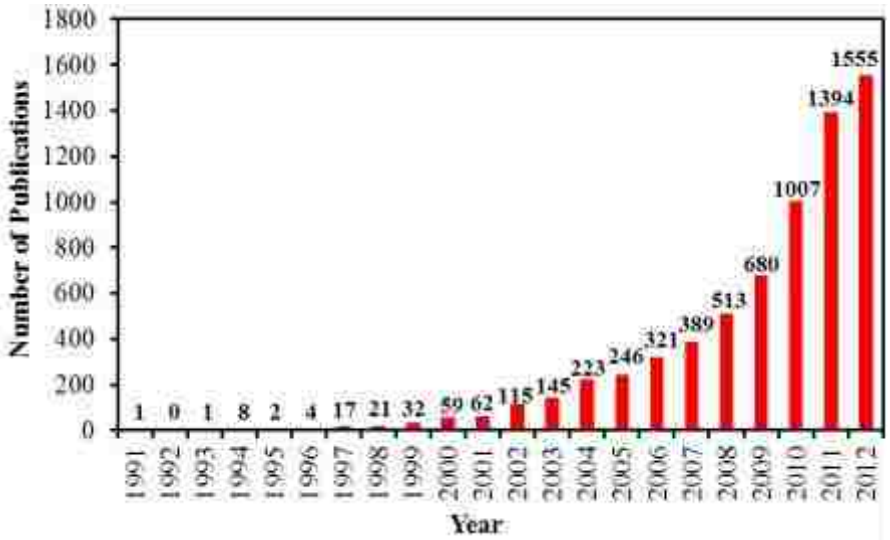

Figure 1.4 Number of publications per year since 1991 based on a literature search using the keywords “solar” and “dye-sensitized.”

1.3.1 Principles of DSSCs

The operating principle of DSSCs consists of the photoexcitation of a dye upon irradiation of light and the transfer of electrons to generate current (Figure 1.5). This device is assembled in a sandwich-like structure by the use of two transparent conductive oxide (TCO) glass substrates. Several components are incorporated in DSSCs including a working and counter electrode, electrolyte, and dye sensitizer. In that regard, the working electrode is composed of an oxide semiconductor such as TiO_2 nanoparticles with dye molecules adsorbed on the semiconductor surface. An electron in the dye is excited to a higher energy state upon absorption of photons. This electron is transferred from the excited state energy level of the dye to the conduction band of TiO_2. The electron migrates through a TiO_2 nanocrystalline network to the TCO electrode and reaches an external load to produce current. Subsequently, the electron

travels through a catalyst TCO counter electrode and reduction-oxidation (redox) couple electrolyte to regenerate the dye to the ground state.

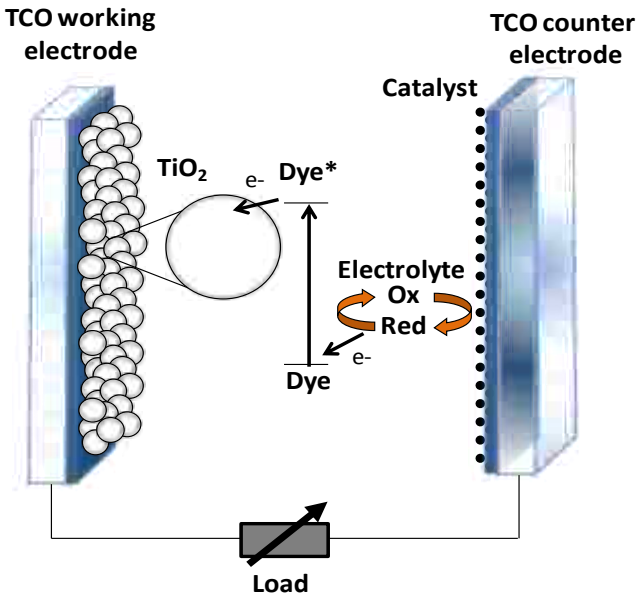

Figure 1.5 Diagram of a DSSC consisting of a dye sensitizer, TiO_2 working electrode, catalyst counter electrode, and electrolyte.

For energy conversion to be successful in DSSCs, three main processes must be achieved: light absorption, electron injection, and electron regeneration. The timescale of these electron transfer processes is also important to optimize parameters (Figure 1.6). The initial process entails absorption of photons from sunlight by a dye, which promotes electrons in dye molecules to an excited electronic state in femtoseconds. Subsequently, an electron transfers over a period of picoseconds to the conduction band of TiO_2 resulting in an oxidized dye. The electron migrates through the nanoparticle network in milliseconds generating current at an external load. Following current generation, the electron passes through the catalyst counter electrode to the electrolyte. A mediator in the electrolyte restores the oxidized dye via electron transfer over a period of nanoseconds to the ground state.

Unfortunately, competitive transitions can also occur that reduce energy conversion. Upon excitation, the electron can undergo radiative and non-radiative processes that cause dye molecules to decay from the excited state to the ground state in nanoseconds. A process known as recombination can also occur that transfers the electron in milliseconds from the conduction band of TiO_2 to the ground state of a dye or to the electrolyte mediator. The key components of DSSCs have been investigated to overcome recombination processes and optimize conversion efficiency. The subsequent sections involve discussion of the ideal requirements for each component and emphasis of conducted studies.

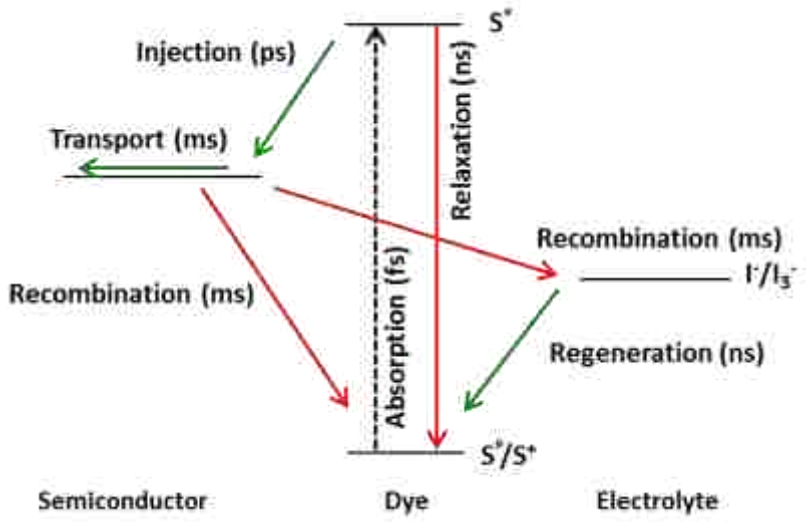

Figure 1.6 Schematic of the primary (green) and recombination (red) electron transfer processes and timescale of DSSCs.

1.3.2 Working Electrode

An important function for DSSCs is the capability to transport electrons to an external load. Electron transport is achieved by a working electrode that consists of a wide band gap oxide semiconductor deposited on a TCO glass substrate. A wide band gap oxide semiconductor only absorbs in the ultraviolet region of the electromagnetic

spectrum, which allows for absorption of photons by dye molecules with limited interference. Specifically, the use of oxide semiconductor nanomaterials, having an increased surface area relative to bulk materials, enables enhanced dye adsorption on the semiconductor surface.

A variety of nanostructures has been studied to optimize conversion efficiency, i.e. nanoparticles, nanotubes, and nanorods (Figure 1.7). Generally, an anatase crystalline form of TiO_2 nanoparticles has been used in DSSCs due to a large band gap of 3.2 eV and stability against photocorrosion. These nanoparticles are typically deposited on a fluorine-doped tin oxide (FTO) glass substrate due to its thermal stability and low resistance that allows for better electron transport. Thus far, fabrication of DSSCs employing a mesoporous network composed of uniform TiO_2 nanoparticles has led to a high conversion efficiency of 11%.[19,20]

As compared to nanoparticles, the use of ordered TiO_2 nanotube arrays provides increased surface area via two-dimensional cylindrical nanostructures with a hollow core. In such nanotube arrays, a conversion efficiency around 3% has been reported using dyes derived from ruthenium complexes.[21,22,23] Additionally, an increase in conversion efficiency to 4.9% and 6.9% has been observed for longer nanotubes.[24,25] Nanorods and nanowires have a cylindrical shape similar to nanotubes but lack a hollow core. The use of TiO_2 nanowires has been found to exhibit an increased conversion efficiency of 9.3% as compared to nanorods, which are similar to nanotube arrays with a conversion efficiency of 3%[26,27] This increase has been attributed to the network of nanowires.

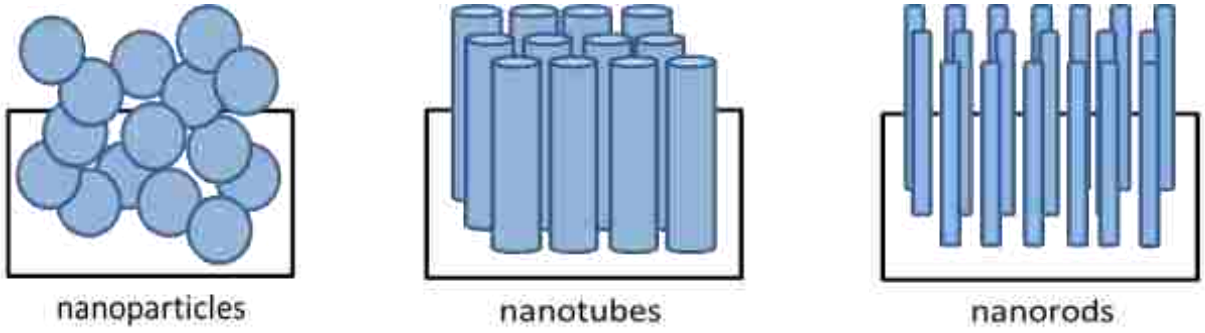

Figure 1.7 Types of nanostructures used in DSSCs, i.e. nanoparticles, nanotubes, and nanorods.

Other oxide semiconductors have also been investigated using a variety of nanostructures. For instance, the use of different zinc oxide (ZnO) nanostructures has led to an increase in conversion efficiency due to higher surface area and better orientation.[28,29] Law *et al.* prepared ZnO nanowires that exhibited one-fifth the surface area of a nanoparticle electrode resulting in increased dye adsorption and a conversion efficiency of 1.5%.[28] This efficiency was greater than both ZnO and TiO_2 nanoparticles under the same conditions. Similar conversion efficiencies of 1.1% for ZnO nanowires and 1.6% for ZnO nanotubes have been reported.[30,31] Conversely, Hosono *et al.* fabricated ZnO nanosheets that generated a conversion efficiency of 3.9% that was attributed to the upright standing orientation of these sheet-like particles.[29]

1.3.3 Counter Electrode

The counter electrode in DSSCs is used to transport electrons from an external load to a redox mediator in the electrolyte. Such electrodes consist of a catalyst deposited on a TCO glass substrate to reduce energy loss. Typically, a thin layer of platinum (Pt) has been used as preferred material due to its high catalytic activity. However, the desire to further reduce cost of solar cells has led to research for cost efficient materials such as carbon materials and polymers.

Carbon materials have been reported as promising low cost alternatives to Pt for counter electrodes due to good catalytic activity, high conductivity, and corrosion stability. Carbon materials such as activated carbon,[32] mesoporous carbon,[33] and carbon nanotubes[34] have been found to generate conversion efficiencies ranging from 3.5% to 7.7%, which are similar to Pt counter electrodes studied under the same conditions. Conversely, a relatively high conversion efficiency of 9.1% has been reported by Murakami *et al.* using carbon black as a catalyst for the counter electrode.[35] This enhanced performance using carbon black was attributed to the use of a thick carbon layer that resulted in a decrease in the charge transfer resistance.

Polymers have also been applied as catalyst for counter electrodes. For instance, a counter electrode consisting of doped poly(3,4-ethylenedioxythiophene) (PEDOT) has resulting in a conversion efficiency of about 3.7%.[36] Furthermore, the use of PEDOT in polymer-carbon and polymer-Pt composites has been found to yield a conversion efficiency of about 4.4%.[37,38] In addition, the use of polymers has led to the development of flexible plastic substrates resulting in conversion efficiencies ranging from 5.4% to 7.4%.[39,40,41,42]

1.3.4 Electrolyte

Another important consideration for DSSCs is the need to restore the oxidized dye to the ground state via electron transfer from a redox couple mediator in the electrolyte. An ideal redox couple mediator consists of suitable kinetics for rapid regeneration of the oxidized dye and slow recombination between electrons in the conduction band of TiO_2. Based on these factors, the most preferred electrolyte is composed of an iodide/triiodide redox couple dissolved in organic solvent. However,

new redox mediators including cobalt-based electrolytes have been investigated as alternatives to the iodide/triiodide redox couple to improve the conversion efficiency. For instance, Yella *et al.* have reported a conversion efficiency of 12% using a porphyrin dye and cobalt$^{(II/III)}$tris(bipyridyl)-based redox electrolyte in acetonitrile.[43] Although the aforementioned redox electrolytes have resulted in high solar cell performance, the use of organic solvents can result in solvent evaporation and solar cell instability attributed to low boiling point and volatility.

Electrolytes composed of ionic liquids (ILs) have been studied to reduce the effects of solvent evaporation and instability in DSSCs. These ILs are molten salts composed of ions with opposing charge. Compared to uniformly packed salts such as sodium chloride that has a melting point of 800 °C, ILs are arranged in asymmetric packing due to a bulky ion resulting in a reduced melting point at or below 100 °C. Specifically, ILs with melting points at or below 25 °C are referred to as room temperature ionic liquids while ILs that extend to 100 °C are known as frozen ionic liquids. Interesting physiochemical properties of ILs such as negligible vapor pressure, tunable viscosity, high ionic conductivity, and high chemical and thermal stability have led to application as solvents in synthesis and catalysis,[44] as well as separations.[45] The fields of electrochemistry[46] and energy conversion[47] have also been influenced by ILs.

The aforementioned properties of ILs are particularly ideal for electrolytes in DSSCs.[48] Generally, IL electrolytes are composed of cations such as imidazolium, pyridinum, or quarternary alkylammonium ions and halide or non-coordinating anions including hexaflorophosphate and bis(trifluoromethanesulfonyl)imide (Figure 1.8).[49] Many DSSCs employ the following composition as a typical solvent-based IL electrolyte:

1-propyl-3-methylimidazolium iodide (PMII), iodine, and an additive such as guanidinium thiocyanate dissolved in N-methoxypriopionitrile, acetonitrile, or a mixture of acetonitrile and valeronitrile.[50] For instance, Wang *et al.* have reported a conversion efficiency of 7.0% using a mixture of PMII and 1-ethyl-3-methylimidazolium thiocyanate with a ruthenium-based sensitizer.[51] More recently, solvent-free IL electrolytes have been investigated that use low viscous ILs such as 1,3-dimethylimidazolium iodide and 1-methyl-3-ethylimidazolium iodide to replace organic solvents.[49]

Similar to ILs, polymers have also been incorporated as quasi-solid or solid electrolytes for solid state DSSCs to reduce undesired effects of evaporation and instability.[52] In that regard, the influence of a polymer additive polyaniline has also been examined in a solvent-free IL electrolyte that resulted in an efficiency of 2.81%.[53] Moreover, an IL polymer gel electrolyte composed of PMII and poly(vinylidenefluoride-co-hexafluoropropylene) (PVDF-HFP) has been reported to produce a conversion efficiency of 5.3%.[54]

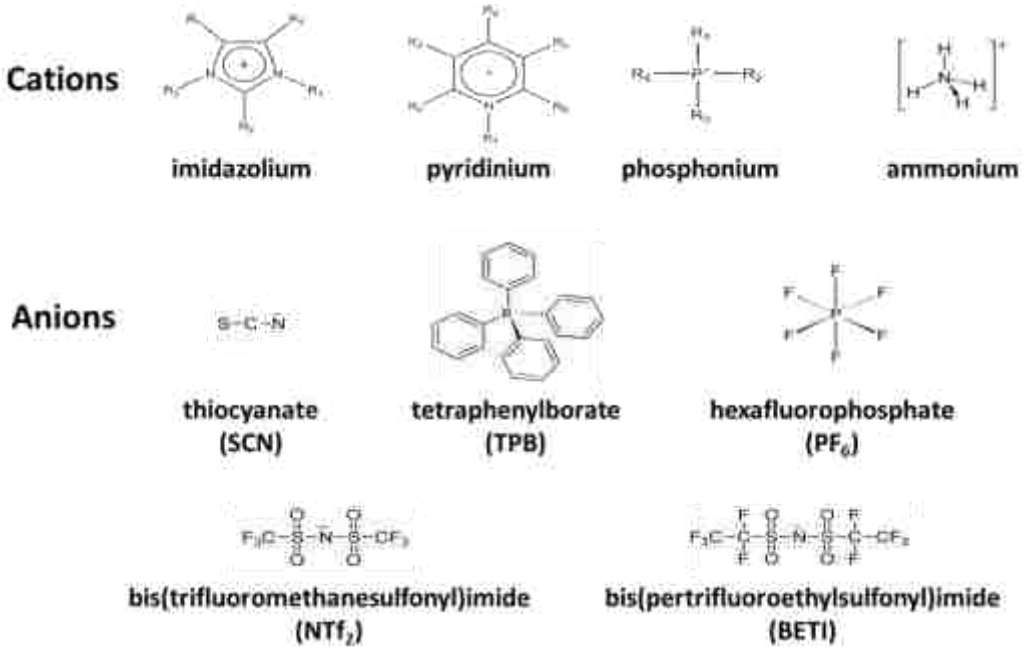

Figure 1.8 Structures of common cations and anions in ionic liquids.

1.3.5 Photosensitizing Dye

Another important component of DSSCs is the photosensitizing dye which is used to absorb photons from sunlight and transfer electrons to generate current. Ideal dye sensitizers absorb photons in the visible and near-infrared regions below 920 nm of the solar irradiance spectrum (Figure 1.9).

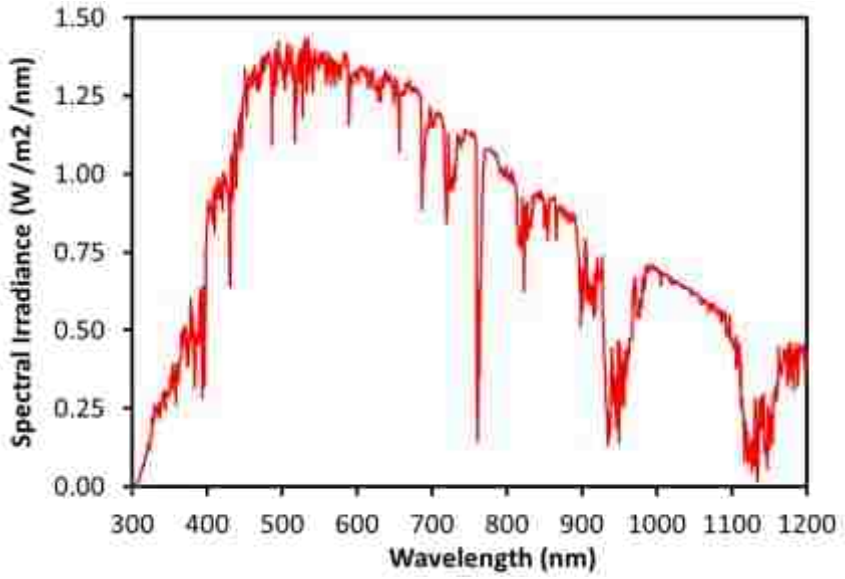

Figure 1.9 Solar irradiance spectrum encompassing the ultra-violet, visible, and infrared regions of the electromagnetic spectrum.[55]

In addition, dye sensitizers possess suitable redox properties for efficient electron transfer to overcome possible recombination and reduce loss of efficiency throughout the solar cell. For this reason, the oxidation potential and excited state oxidation potential of the sensitizer are closely matched with the potentials of the iodide/triiodide electrolyte (0.4 V vs NHE) and conduction band of TiO_2 (-0.5 V vs NHE), respectively. The ideal spectral and redox properties of these dye sensitizers can be optimized by the structure of the dye. For instance, the use of anchoring groups such as carboxyl groups is important to enable for strong interaction with TiO_2 for better charge transfer. The following section involves discussion of the advantages and drawbacks of different

types of photosensitizers: metal complexes, quantum dots, and organic dyes. In particular, organic dyes have been found to overcome limitations of the other photosensitizers.

Dyes derived from ruthenium complexes consisting of have been commonly used in DSSCs since development (Figure 1.10) due to the ability to introduce ligands for optimizing spectral properties and energy levels.[56] These dyes consist of strong donor and anchoring group ligands to increase charge transfer. Currently, an efficiency of 11% has been reported using dye derived from ruthenium complex, namely N3 and Black dye.[19,20] Although the use of ruthenium dyes as sensitizers has produced a high conversion efficiency, these dyes are found to possess disadvantages attributed to the limited supply of these precious metals and reduced absorption in the near-infrared region of the electromagnetic spectrum.[57]

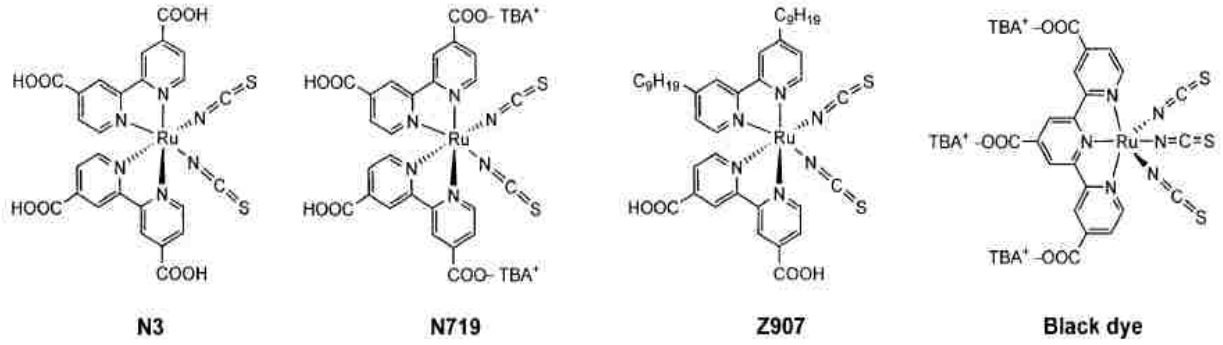

Figure 1.10 Structures of dyes derived from ruthenium complexes.

The use of quantum dots (QDs) can overcome spectral limitations of ruthenium dyes. These nanocrystalline semiconductors are composed of inorganic materials that provide tunable absorption and energy level depending on the size of the nanostructure. As the size of QDs decreases, the absorption onset shifts to shorter wavelengths and the band gap increases. Thus, QDs require varying sizes for simultaneous absorption

in the visible and near-infrared region.[58] Currently, a conversion efficiency of about 4% has been reported for QD-sensitized solar cells using cadmium sulfide and cadmium selenide, independently.[59,60] However, a disadvantage of these sensitizers is the presence of recombination processes that reduce charge transfer, which is necessary for further improvement in the conversion efficiency of QDs.

The development of organic dyes as photosensitizers allows for the design of structures to be tailored for optimal spectral and electrochemical properties. This characteristic provides a broader range of structures to be investigated and has the potential to overcome drawbacks of ruthenium dyes and QDs, i.e. reduced absorption in the near-infrared region of the electromagnetic spectrum and the presence of recombination processes that reduce charge transfer. A variety of organic dyes such as indolines,[61,62] perylenes,[63] and triphenylamines[64,65] have been synthesized at low cost that exhibit desirable properties such as high molar extinction coefficients and broad absorption spectra (Figure 1.11). In particular, various molecular designs of coumarin dyes have been reported that resulted in conversion efficiencies ranging from 4%-7.6%.[66,67,68] A class of cyanine dyes, including merocyanines and squaraines, have also been investigated as sensitizers with conversion efficiencies ranging from 3.1% to 5.4%.[69,70,71] Although organic dyes have been found to provide adequate conversion efficiencies by tailoring the structures, a challenge of these and metal dyes is the presence of aggregation that can reduce conversion efficiency.

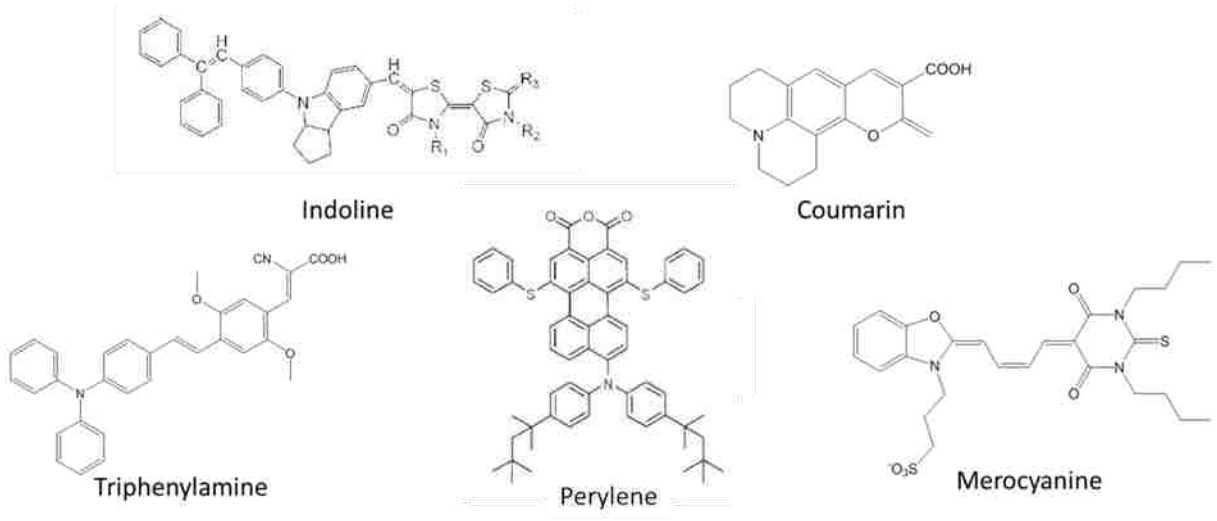

Figure 1.11 Structures of several organic dyes.

1.3.6 Dye Aggregates

Aggregation is the self-association of molecules that results in changes of spectral behavior compared to monomeric species. This phenomenon was first independently discovered by Jelley[72] and Scheibe,[73] who reported the aggregation of pseudoisocyanine iodide (PICI) at high concentrations in aqueous solution and at solid-liquid interfaces.[74] These aggregates are known as Jelley (J) or Scheibe aggregates, appellations honoring these discoverers. As a result, cyanine dyes have been extensively studied for aggregation and used in silver halide emulsions for photography.[74] Moderation of spectral properties in self-assembled molecules is attributed to excitonic splitting, as has been explained by Davydov *et al.*[75] and Kasha *et al.*[76] using molecular exciton coupling theory (Figure 1.12). Such theory allows for variations in aggregation, which lead to interactions between the transition dipole moments of the molecules, resulting in differences in splitting of the excited state. The arrangement of molecules is based on the slip angle (α) which is between the chromophore axes and center-to-center line. The formation of J-aggregates is a result

of head-to-tail molecular stacking and typically exhibits a narrow and bathochromically shifted absorption band with respect to the monomer. In addition, J-aggregation also results in enhanced resonance fluorescence. In contrast, H- (hypsochromic) aggregates are formed as a result of molecular stacking in a card pack manner. This aggregate type is typically found to exhibit a hypsochromically shifted absorption band with respect to the monomer and results in little to no fluorescence. More recently, randomly-oriented aggregates have been classified as those without any specific order of stacking, with conservation of the spectral properties of the monomer. In addition, the extent of aggregation depends on various factors including concentration, solvent polarity, temperature, pH, and ionic strength.[77]

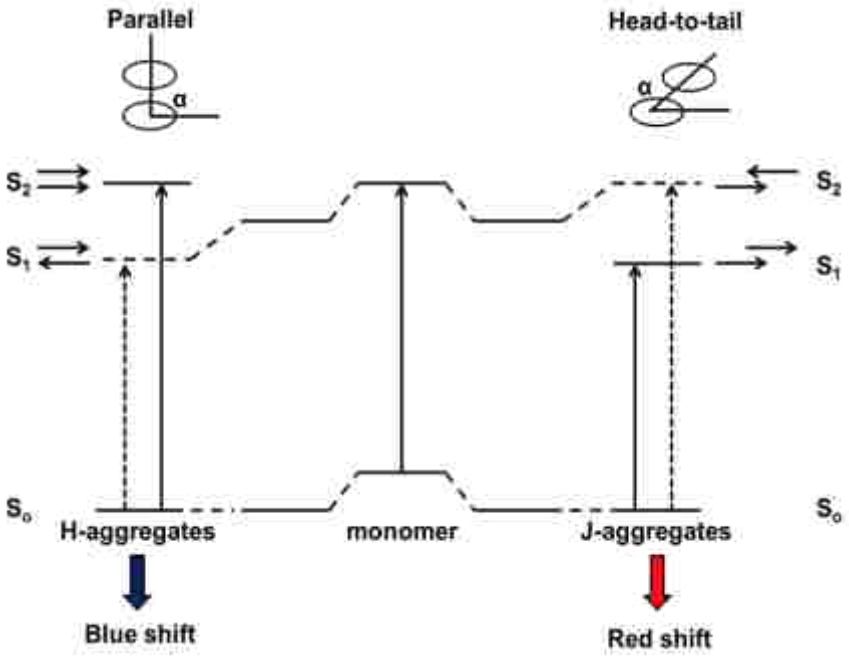

Figure 1.12 Molecular exciton coupling theory containing molecular arrangement of aggregates.

Aggregation of dyes used as sensitizers in DSSCs can result in reduced conversion efficiency due to intermolecular quenching or excess molecules that act as

filters.[78] The ability to reduce or control aggregation is important to improve conversion efficiency. In this regard, molecular design modifications including the use of increased alkyl chains, as well as the addition of π–π stacking and bulky substituents has been applied to various dyes to suppress aggregation.[62,79,80] For instance, Barea *et al.* have reported an increase in conversion efficiency from 3.3% to 6.4% using porphyrin dyes.[81] In addition, the incorporation of coadsorbates such as chenodeoxycholic acid (CDCA) and 4-tert-butylpyridine (TBP) in DSSCs have also been found to limit aggregation and improve conversion efficiency in organic dyes such as indoline and coumarin.[62,67] Similarly, the addition of TBP in DSSCs with ruthenium complexes has also resulted in an increase in conversion efficiency from 5.8% to 7.5%.[82] Overall, these methods reduce aggregation by blocking the effects of charge recombination.[83]

In contrast, beneficial characteristics have been reported in recent studies by controlling dye aggregates. Properties of both J- and H-aggregation have been found to improve conversion efficiency of DSSCs. Mann *et al.* have found that H-aggregates of rhodamine-based dyes result in broad absorption and increased light harvesting efficiency.[84] In particular, the presence of aggregation in cyanine dyes has also been investigated for potential aid in optimizing conversion efficiency of DSSCs.[85] In this regard, the use of controlled J-aggregates of a merocyanine dye has been reported to achieve a conversion efficiency of 4.5% by Sayama *et al.*[86]

1.4 Nanomaterials Derived from a Group of Uniform Materials Based on Organic Salts (nanoGUMBOS)

The Warner research group has developed a class of materials referred to as a **g**roup of **u**niform **m**aterials **b**ased on **o**rganic **s**alts (GUMBOS).[87] These GUMBOS are solid phase organic salts composed of bulky, poorly coordinated ions resembling frozen

ILs, with the exception of melting points that frequently extend well past the conventional upper bound for ILs (100 °C). The melting point could, in practice, fall anywhere in the 25–250 °C window (Figure 1.13). Importantly, GUMBOS retain many of the attractive properties inherent to those of ILs and can be tuned to exhibit multifunctional properties based on the selected cation and anion. In addition, nanomaterials derived from GUMBOS (nanoGUMBOS) combines the interesting properties of both ILs and nanomaterials. Initially reported by Tesfai *et al.*, nanoGUMBOS composed of both tetrafluoroborate (BF_4^-) and tetrachloroferrate ($FeCl_4^-$) anions demonstrated tunability in which nanoparticles containing $FeCl_4^-$ anion were observed to retain magnetic properties.[87] Thus far, nanoGUMBOS of varying ion pairs offer potential as candidates for biomedical,[87] antibacterial,[91] optoelectronic,[92,93] and light harvesting[94,95,96] applications.

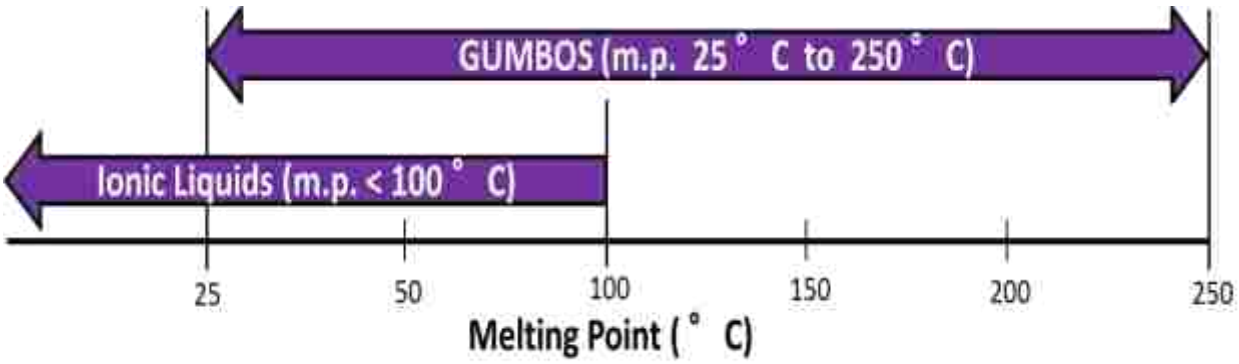

Figure 1.13 Temperature difference between ionic liquids and GUMBOS.

1.4.1 Cyanine-based NanoGUMBOS

In particular, our group has explored the formation of nanoGUMBOS using a heptamethine cyanine dye 1,1',3,3,3',3'-hexamethylindotricarbocyanine (HMT) iodide. Bwambok *et al.* initially observed that nanoGUMBOS containing this cationic near-infrared (NIR) dye resulted in a broad absorption spectrum and slight shift in the

fluorescence emission spectrum as compared to the GUMBOS in solution.[88] These changes in the spectral properties were attributed to aggregation of the cationic dye. In this study, nanomaterials of the NIR fluorescent compound were employed as contrasting agents for biomedical imaging applications. In a subsequent study by Das *et al.* variation of the anions paired with HMT were observed to retain controlled aggregation and spectral properties.[94] These results further suggest the presence of aggregation, specifically of both J- and H- aggregates in different proportions.

1.5 Analytical Techniques Used

1.5.1 Ultraviolet-Visible Spectroscopy

Ultraviolet-visible (UV-Vis) spectroscopy is used to study molecules that absorb light in the ultraviolet and visible regions of the electromagnetic spectrum. When a sample is exposed to light, molecules absorb photons resulting in promotion of an electron in the molecule from the ground state to an excited state. This change in energy is monitored by use of a spectrophotometer. A typical spectrophotometer consists of a light source, monochromator, sample, and detector (Figure 1.14). Light passes through a monochromator that allows for a selected wavelength to transmit through to the sample. This transmitted light is detected by a photodiode array. Absorbance (A) of the sample is determined by $A = \log(I_o/I)$ where I_o is the incident intensity and I is the transmitted intensity. Furthermore, the Beer-Lambert law is used to describe absorbance in relation to concentration denoted as $A = \varepsilon bc$ where ε is the molar extinction coefficient ($M^{-1}cm^{-1}$), b is the pathlength or distance light travels through the sample (cm), and c is the concentration of the sample (M). An absorption spectrum is obtained by plotting absorbance versus wavelength.

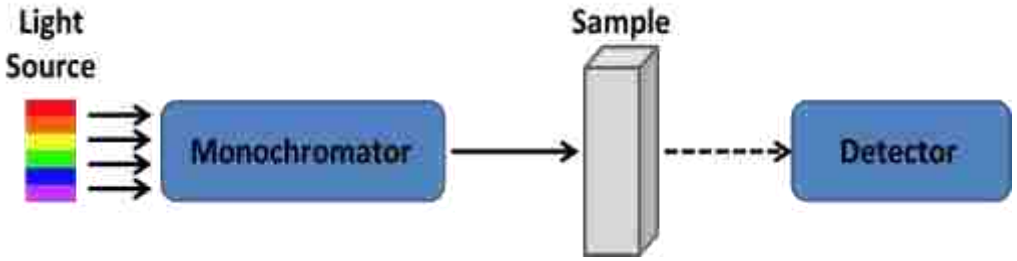

Figure 1.14 Schematic of a UV-Vis spectrophotometer.

1.5.2 Fluorescence Spectroscopy

The processes of fluorescence and other electronic transitions are illustrated using a Jablonski diagram (Figure 1.15). As shown in this energy level diagram, absorption (A) is a process that promotes a molecule to an excited electronic state in femtoseconds. The excited molecule may undergo a non-radiative transition between a higher and lower energy state known as internal conversion (IC) that occurs in picoseconds. A radiative process called fluorescence (F) can occur when the molecule returns from a lower vibrational level of the excited singlet state (S_1) to a ground state (S_o) over a period of nanoseconds.

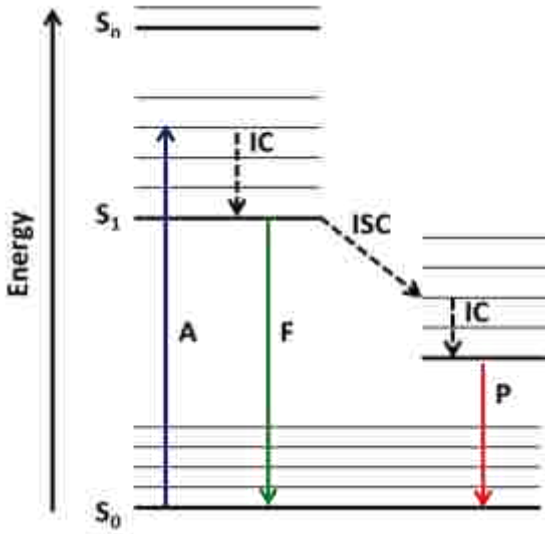

Figure 1.15 Schematic of the Jablonski diagram.

In addition to fluorescence, a non-radiative process called intersystem crossing (ISC) involves a transition from a singlet state to a triplet state (T_1). After undergoing internal conversion to a lower vibrational level of the excited triplet state, a relatively slow radiative process known as phosphorescence (P) can take place over a span of milliseconds. The probability of a molecule to fluoresce or phosphoresce is described by the quantum yield, which is a ratio of the number of photons emitted relative to the number of photons absorbed.

Fluorescence spectroscopy is a technique that measures fluorescence of molecules by use of a spectrofluorometer. A spectrofluorometer consists of a light source, two monochromators, a sample, and a detector (Figure 1.16).

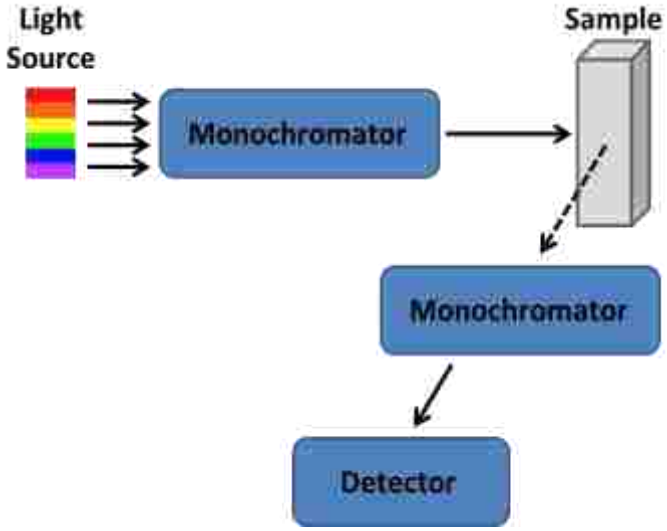

Figure 1.16 Schematic of a spectrofluorometer.

Generally, excitation light ranging from 200 nm to 900 nm passes through an excitation monochromator that allows for a selected excitation wavelength to transmit through the sample. Subsequently, emitted light travels through an emission monochromator to isolate fluorescence emission which is collected by a photomultiplier tube. This emission monochromator is positioned orthogonally from the excitation light to attenuate

light scattering. Data from steady-state fluorescence measurements are presented as an emission spectrum plotting fluorescence intensity versus wavelength. Using this technique, several fluorescence parameters can be investigated including lifetime, anisotropy, and Förster resonance energy transfer.

Fluorescence lifetime is the average time a molecule spends in the excited state before returning to the ground state. This process occurs in nanoseconds and can be examined via a time-domain method. Time-domain fluorescence employs a pulsed excitation source to measure fluorescence intensity as a function of time. This time-dependent intensity is used to obtain lifetime or decay time from the slope of a plot of log I(t) versus time (t). Time-correlated single-photon counting (TCSPC) is commonly used to measure these decays. The TCSPC counts at least one photon per excitation pulse, which is time-correlated by the time-to-amplitude converter (TAC). This TAC measures voltage over time and consists of a start and stop time, which are related to the detection excitation pulse and first emitted photon, respectively. The time between pulses in the TCSPC is measured up to four times the longest decay time.

Fluorescence anisotropy measurements determine varying fluorescence intensities along different planes. Due to random orientation of fluorophores in solution molecules are particularly excited when exposed to polarized light. Figure 1.17 illustrates the use of polarizers in the measurement of fluorescence anisotropy. The value of fluorescence anisotropy (r) is the average angular displacement of molecules in the excited state[97] after excitation with vertically polarized light and is given by

$$r = \frac{I_{vv} - GI_{vh}}{I_{vv} + 2GI_{vh}} \quad (1)$$

where G is the grating factor to correct for instrumental responses, such as the emission wavelength and detector. Parameters I_{vv} and I_{vh} correspond to the fluorescence emission intensities measured parallel and perpendicular to the vertically polarized excitation, respectively.[97]

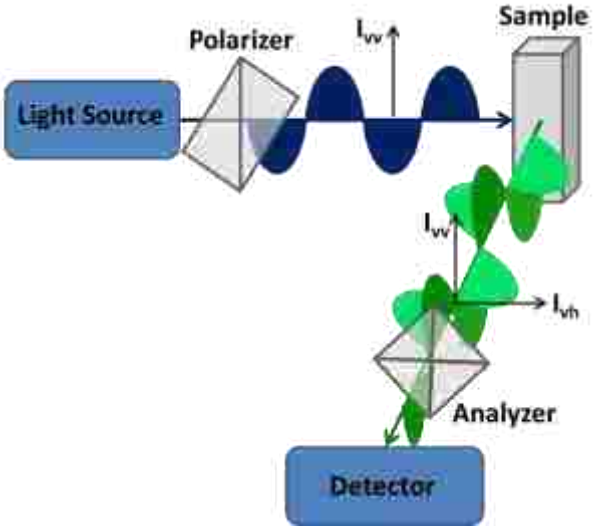

Figure 1.17 Schematic configuration of fluorescence anisotropy.

Förster resonance energy transfer (FRET) is a non-radiative process that occurs between donor molecules in an excited state and acceptor molecules in a ground state. This energy transfer can occur when the distance between the donor and acceptor molecules is 1-10 nm and an overlap of the donor emission spectrum and acceptor absorption spectrum is present (Figure 1.18).[97] The area of overlap known as the spectral overlap integral ($J(\lambda)$) can be determined using the following formula

$$J(\lambda) = \frac{\int_0^\infty \varepsilon(\lambda) f(\lambda) \lambda^4 d\lambda}{\int_0^\infty f(\lambda) d\lambda} \quad (2)$$

where ε is the molar extinction coefficient of the acceptor, $f(\lambda)$ is the normalized emission spectrum of the donor, and λ is the wavelength. The energy transfer efficiency (E) can be obtained using the given equation

$$E = 1 - \frac{F_{da}}{F_d} \quad (3)$$

where F_{da} and F_d are the fluorescence intensities of the donor in the presence and absence of the acceptor, respectively.

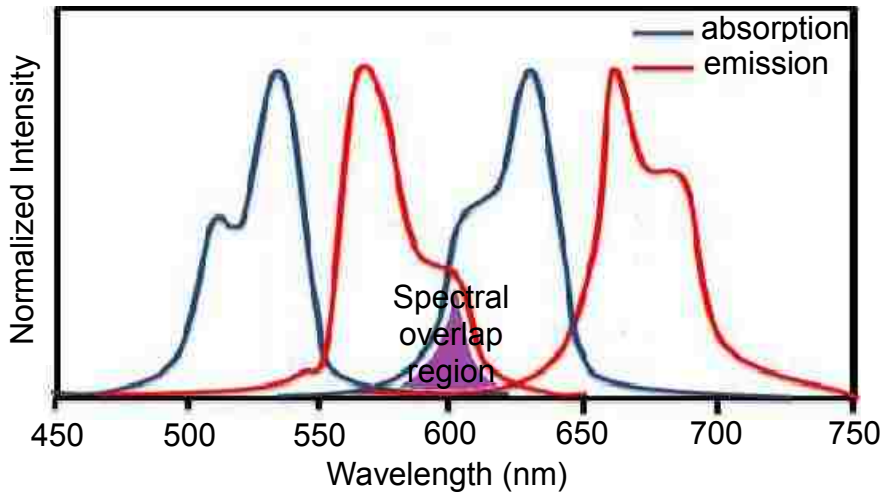

Figure 1.18 Spectral representation of Förster resonance energy transfer between a donor and acceptor.

1.5.3 Transmission Electron Microscopy

Transmission electron microscopy (TEM) is a technique used to visualize and characterize materials (Figure 1.19a). The use of electrons under vacuum allows for higher magnification and resolution of materials as compared to light microscopy. As a result, TEM has become a useful tool for research at the nanoscale. An electron gun is employed to generate an electron beam that is focused by the use of condenser lenses under a magnetic field. Once the electrons penetrate through the sample, transmitted electrons are magnified by objective lenses and projected on a phosphor screen to generate an image. This image can be captured via a photographic or charge-coupled device (CCD) camera. The resulting contrast image is dependent on the density of the sample. In this regard, darker regions of the image identify dense areas of the material

that limits transmission of electrons, while lighter regions characterize less dense areas that allow electrons to pass through the sample.

1.5.4 Scanning Electron Microscopy

Similar to TEM, scanning electron microscopy (SEM) uses lenses to focus an electron beam on a sample to produce an image (Figure 1.19b). For this technique, the electron beam scans across the sample, which is coated with a thin conductive metal layer, using a scanning coil. This scanning process generates secondary electrons that are emitted when incident electrons interact with atoms near the surface of a sample resulting in the release of valance electrons. These signals are detected via a photomultiplier tube and commonly used to obtain an image. This image is based on the surface topography of the sample, in which more secondary electrons escape at the surface as compared to those that travel through the sample.

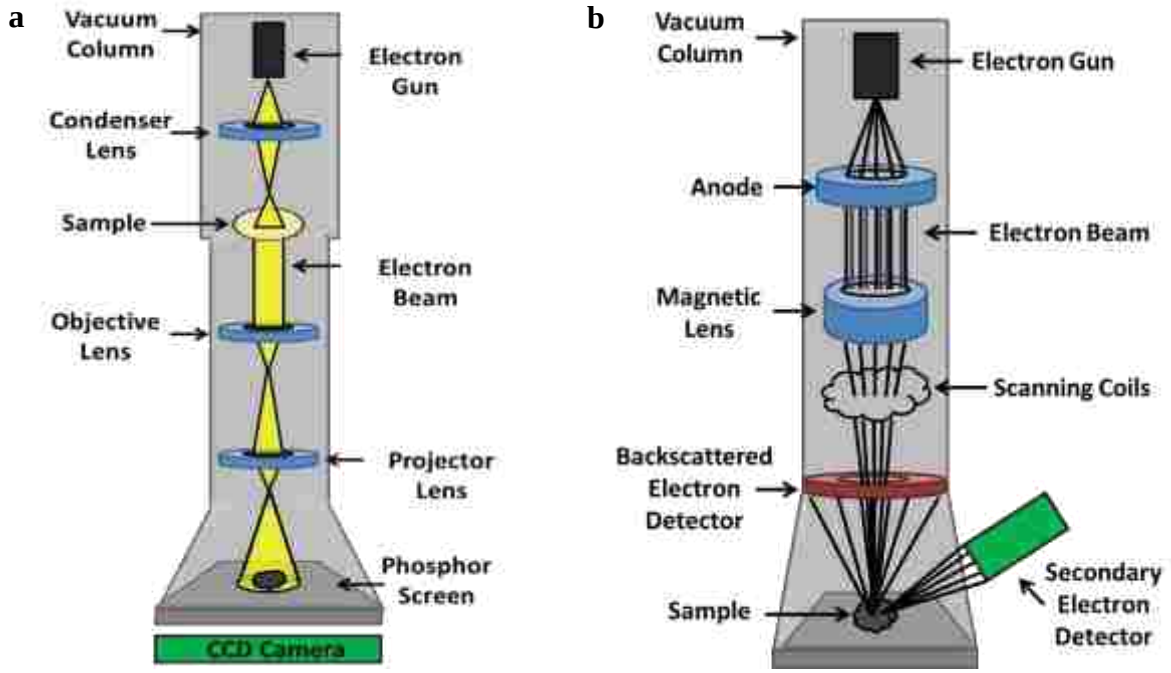

Figure 1.19 Schematic of a (a) transmission electron microscope and (b) scanning electron microscope.

1.5.5 Polarized Optical Microscopy

Polarized optical microscopy (POM) is a technique used to study the crystal structure and organization of a material. Such microscopes are equipped with a light source, polarizer, analyzer, and camera (Figure 1.20). Light, which vibrates in all planes, travels through a polarizer to filter and allow only one vibrational plane to pass (0°). Once the polarized light passes through a sample, the transmitted light proceeds to an analyzer or second polarizer that is in a cross polarized position (90°) and an image is captured using a camera. This resulting image can provide characterization of crystallinity and organization based on the isotropy of a material. Generally, crystalline materials are anisotropic, i.e. having a refractive index that is dependent on directionality. In this regard, an anisotropic sample can cause birefringence, i.e. the splitting of a polarized beam of incident light into two rays as a result of passing through a sample, which produces a bright image. In contrast, an isotropic sample has a refractive index that is equal in all directions which allows polarized light to pass through the material unaltered resulting in the appearance of a dark image.

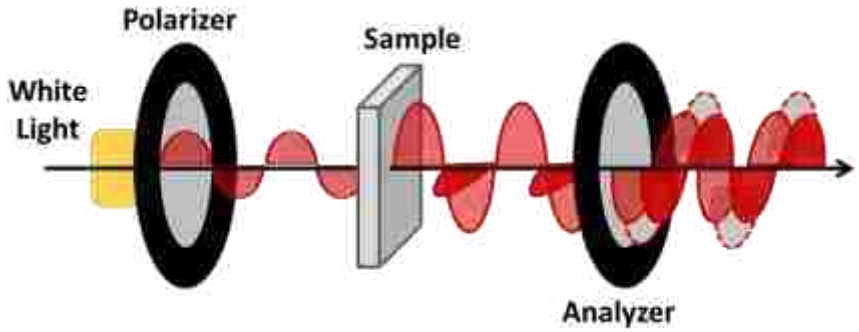

Figure 1.20 Schematic of a polarized optical microscope.

1.5.6 Cyclic Voltammetry

Cyclic voltammetry (CV) is a technique used to study electrochemical processes of a species that can undergo oxidation and reduction reactions by the transfer of

electrons. In such reactions, potential or voltage is applied as a driving force, while current is the electron flow resulting from the reaction. This process is measured using a potentiostat and an electrochemical cell containing three electrodes: working, reference, and counter (Figure 1.21).

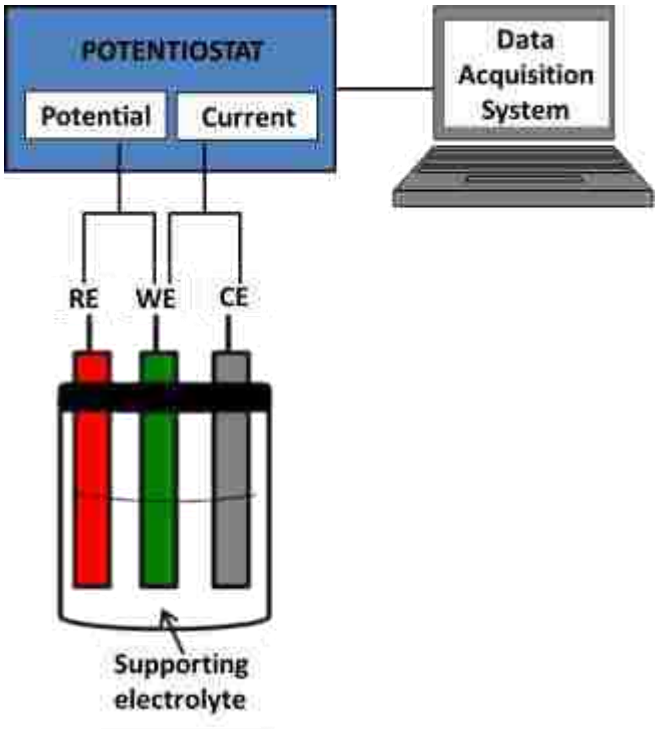

Figure 1.21 Diagram of a CV system containing a potentiostat, data acquisition system, electrochemical cell, and three electrodes i.e. reference (RE), working (WE) and counter (CE) immersed in supporting electrolyte solution.

In that regard, the potentiostat is an electrical instrument that monitors and controls the difference in potential between the working and reference electrodes, as well as measures the current flow between the working and counter electrodes. Overall, the working electrode measures potential and current of a sample on the surface of the electrode where the electrochemical reaction takes place. The potential at this working electrode is varied over time with respect to a reference electrode of constant potential. In addition, the working electrode measures current response relative to a counter electrode that introduces current into the system. These electrodes are immersed in a

solution containing a supporting electrolyte composed of a nonreactive ionic species that provides excess electrons. When potential is applied to the electrodes, a fixed range is scanned in a forward and reverse manner at a constant rate (Figure 1.22a). In CV, a cyclic voltammogram is obtained by plotting the measured current against potential at a given range (Figure 1.22b).

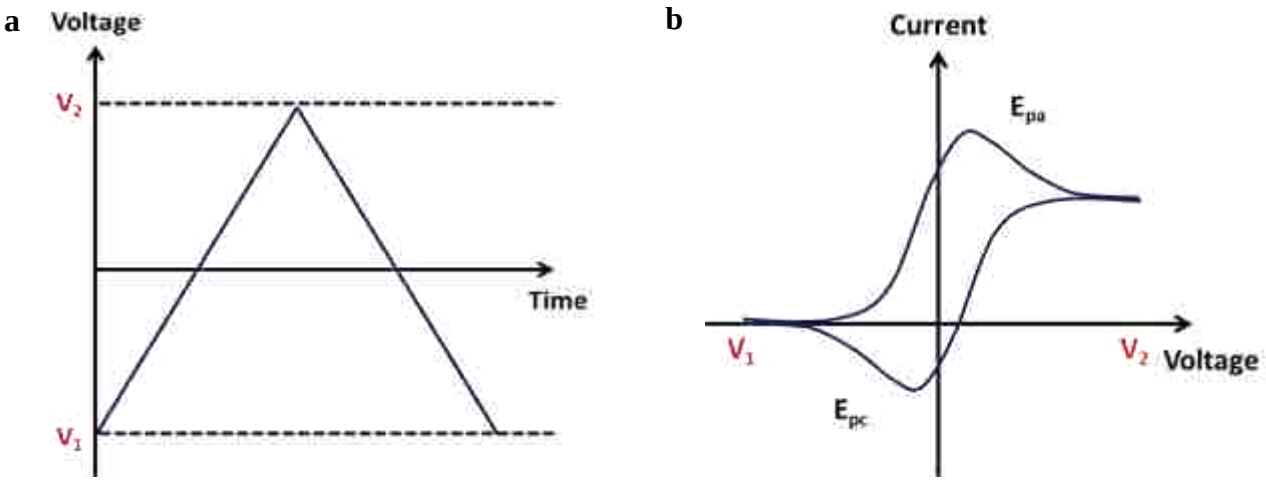

Figure 1.22 Representation of a (a) potential versus time plot and (b) current versus potential plot.

The use of CV provides information on electron transfer properties such as redox potential and band gap. In this regard, the redox potential of a species is calculated by an average of the anodic (E_{pa}) and cathodic (E_{pc}) peak potentials. The band gap (E_g) of a species can also be determined using the following equations.

$$E_{g\,EC}(eV) = E_{LUMO} - E_{HOMO} \tag{4}$$

$$\mathrm{E_{HOMO}\left(eV\right) = -1e^{-}\left[E_{pa}\left(V\ vs\ Fc^{+}/Fc\right) + 4.8\left(V\ Fc^{+}/Fc\ vs\ Zero\right)\right]} \tag{5}$$

The electrochemical band gap ($E_{g\ EC}$) is calculated by use of the difference in the energy level of the lowest unoccupied molecular orbital (LUMO) and highest occupied

molecular orbital (HOMO). These values are ascertained versus a vacuum with ferrocene (Fc^+/Fc) as an internal reference.

1.5.7 Solar Cell Conversion Efficiency

Solar cell characterization involves the measurement of current as a function of voltage under illumination to determine conversion efficiency. Generally, a solar simulator containing a xenon arc lamp is used as a light source which is calibrated by use of an air mass filter (AM 1.5G) to generate a spectrum comparable to the solar irradiance spectrum (Figure 1.9). Under illumination, a difference in potential between the working and counter electrodes of a solar cell causes electrons to migrate through the cell and generate current. This resulting current is measured by use of a sourcemeter to obtain a current-voltage (I-V) curve (Figure 1.23).

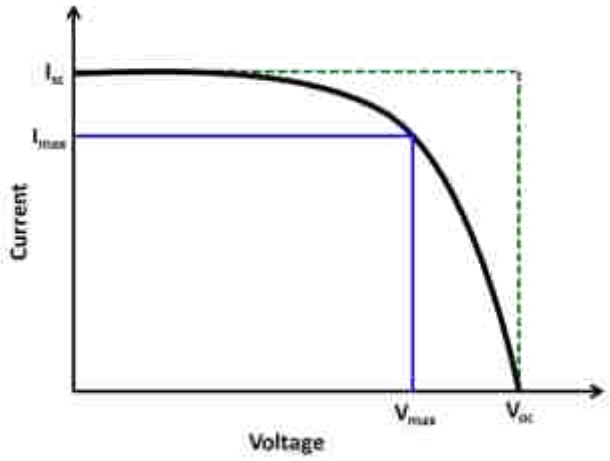

Figure 1.23 Representation of an I-V curve used to characterize a solar cell.

Using the I-V curve, several critical parameters can be obtained to determine the performance of the solar cell. In particular, the fill factor (FF) measures the I-V characteristic of an actual solar cell relative to an ideal cell using the formula

$$FF = \frac{V_{max} \times I_{max}}{V_{oc} \times J_{sc}} \quad (6)$$

where V_{max} and I_{max} are the respective maximum voltage and current at the maximum power output. The open-current voltage (V_{oc}) is the voltage when current is zero and provides detail about the structure and energy of the solar cell. Whereas, the photocurrent density at short-circuit current (J_{sc}) is the measured current when voltage is zero for a given area of the cell. A ratio of the maximum power output (P_{max}) to the power input (P_{in}) is defined as the conversion efficiency (η) using the following formula

$$\eta = \frac{P_{max}}{P_{in}} = \frac{V_{oc} \times J_{sc} \times FF}{P_{in}} \times 100\% \quad (7)$$

where the power input is generally maintained at a standard condition of 100 $mWcm^{-2}$ by the solar simulator.

1.6 Scope of the Dissertation

This dissertation is a summary of the morphological, spectral, and electrochemical properties of GUMBOS and nanoGUMBOS derived from cyanine dyes. Furthermore, these cyanine-based dyes were utilized as photosensitizers in DSSCs. The second chapter is a description of the synthesis of GUMBOS with various anions and the preparation of their corresponding nanostructures. The use of the anions NTf_2^- and $BETI^-$ resulted in different morphologies and broad absorption spectra. In addition, the electrochemical properties of cyanine-based GUMBOS were examined using cyclic voltammetry. This study was found to exhibit suitable potential values which suggest that these materials may be beneficial for application as photosensitizers in DSSCs. In the third chapter, the cation of the cyanine-based nanoGUMBOS was altered by increasing the methine chain lengths. A mixture of these GUMBOS was used to form binary nanomaterials, which were characterized by UV-Vis absorption spectroscopy, fluorescence spectroscopy, and cyclic voltammetry. It was found that the binary

nanomaterials exhibited broad absorption spectra, as well as tunable emission due to the occurrence of FRET. This tunable emission of the binary nanomaterials suggests potential for application as sensitizers in the visible to near-infrared region of the electromagnetic spectrum. Furthermore, adequate electrochemical properties also indicate the use of these materials in DSSCs. Application of cyanine-based GUMBOS as photosensitizers in DSSCs was investigated in the fourth chapter. Solar cells were fabricated using various methods for syntheses of TiO_2, as well as incorporating the GUMBOS. Characterization of the solar cells resulted in a conversion efficiency of 0.73% by use of electrospun nanofibers doped with TiO_2 nanoparticles and cyanine-based GUMBOS.

1.7 References

1. U.S. Energy Information Administration. *Monthly Energy Review* **2012**.
2. Gratzel, M., Photoelectrochemical cells. *Nature* **2001,** *414* (6861), 338-344.
3. Becquerel, A. E., *C. R. Acad. Sci.* **1839,** *9*, 561-567.
4. Ohl, R. S. Light-sensitive electric device. U.S. Patent 2,402,662, filed May 27 1941.
5. Chapin, D. M.; Fuller, C. S.; Pearson, G. L., A New Silicon p-n Junction Photocell for Converting Solar Radiation into Electrical Power. *J. Appl. Phys.* **1954,** *25* (5), 676-677.
6. Zhao, J. H.; Wang, A. H.; Green, M. A.; Ferrazza, F., 19.8% efficient "honeycomb" textured multicrystalline and 24.4% monocrystalline silicon solar cells. *Appl. Phys. Lett.* **1998,** *73* (14), 1991-1993.
7. Green, M. A., *Third generation photovoltaics: advanced solar energy conversion*. Berlin ; New York: 2006.
8. Borrello, D.; Vallat-Sauvain, E.; Meier, J.; Kroll, U., High-efficiency Amorphous Silicon Devices on LPCVD-ZNO TCO Prepared in Industrial KAI-M R&D Reactor. *24 EUR PHOT SOL EN C* **2009**.

9. Green, M. A.; Emery, K.; Hishikawa, Y.; Warta, W.; Dunlop, E. D., Solar cell efficiency tables (version 40). *Prog. Photovoltaics* **2012,** *20* (5), 606-614.

10. Repins, I.; Contreras, M. A.; Egaas, B.; DeHart, C.; Scharf, J.; Perkins, C. L.; To, B.; Noufi, R., 19.9%-efficient ZnO/CdS/CuInGaSe2 solar cell with 81.2% fill factor. *Prog. Photovoltaics* **2008,** *16* (3), 235-239.

11. Shockley, W.; Queisser, H. J., Detailed Balance Limit of Efficiency of p-n Junction Solar Cells. *J. Appl. Phys.* **1961,** *32* (3), 510-519.

12. Kamat, P. V., Quantum Dot Solar Cells. Semiconductor Nanocrystals as Light Harvesters. *J. Phys. Chem. C* **2008,** *112* (48), 18737-18753.

13. West, J. L.; Halas, N. J., Engineered nanomaterials for biophotonics applications: Improving sensing, imaging, and therapeutics. *Annu. Rev. Biomed. Eng.* **2003,** *5*, 285-292.

14. Goldberg, M.; Langer, R.; Jia, X. Q., Nanostructured materials for applications in drug delivery and tissue engineering. *J. Biomater. Sci.-Polym. Ed.* **2007,** *18* (3), 241-268.

15. Xia, Y. N.; Yang, P. D.; Sun, Y. G.; Wu, Y. Y.; Mayers, B.; Gates, B.; Yin, Y. D.; Kim, F.; Yan, Y. Q., One-dimensional nanostructures: Synthesis, characterization, and applications. *Adv. Mater.* **2003,** *15* (5), 353-389.

16. Arico, A. S.; Bruce, P.; Scrosati, B.; Tarascon, J. M.; Van Schalkwijk, W., Nanostructured materials for advanced energy conversion and storage devices. *Nat. Mater.* **2005,** *4* (5), 366-377.

17. Kamat, P. V., Meeting the clean energy demand: Nanostructure architectures for solar energy conversion. *J. Phys. Chem. C* **2007,** *111* (7), 2834-2860.

18. Oregan, B.; Gratzel, M., A Low-Cost, High-Efficiency Solar Cell Based on Dye-Sensitized Colloidal TiO2 Films. *Nature* **1991,** *353* (6346), 737-740.

19. Nazeeruddin, M. K.; De Angelis, F.; Fantacci, S.; Selloni, A.; Viscardi, G.; Liska, P.; Ito, S.; Bessho, T.; Gratzel, M., Combined experimental and DFT-TDDFT computational study of photoelectrochemical cell ruthenium sensitizers. *J. Am. Chem. Soc.* **2005,** *127* (48), 16835-16847.

20. Chiba, Y.; Islam, A.; Watanabe, Y.; Komiya, R.; Koide, N.; Han, L., Dye-Sensitized Solar Cells with Conversion Efficiency of 11.1%. *Jpn. J. Appl. Phys.* **2006,** *45* (25), L638-L640.

21. Mor, G. K.; Shankar, K.; Paulose, M.; Varghese, O. K.; Grimes, C. A., Use of Highly-Ordered TiO2 Nanotube Arrays in Dye-Sensitized Solar Cells. *Nano Lett.* **2006,** *6* (2), 215-218.

22. Zhu, K.; Neale, N. R.; Miedaner, A.; Frank, A. J., Enhanced Charge-Collection Efficiencies and Light Scattering in Dye-Sensitized Solar Cells Using Oriented TiO2 Nanotubes Arrays. *Nano Lett.* **2007,** *7* (1), 69-74.

23. Jennings, J. R.; Ghicov, A.; Peter, L. M.; Schmuki, P.; Walker, A. B., Dye-Sensitized Solar Cells Based on Oriented TiO2 Nanotube Arrays: Transport, Trapping, and Transfer of Electrons. *J. Am. Chem. Soc.* **2008,** *130* (40), 13364-13372.

24. Adachi, M.; Murata, Y.; Okada, I.; Yoshikawa, S., Formation of titania nanotubes and applications for dye-sensitized solar cells. *J. Electrochem. Soc.* **2003,** *150* (8), G488-G493.

25. Varghese, O. K.; Paulose, M.; Grimes, C. A., Long vertically aligned titania nanotubes on transparent conducting oxide for highly efficient solar cells. *Nat. Nanotechnol.* **2009,** *4* (9), 592-597.

26. Adachi, M.; Murata, Y.; Takao, J.; Jiu, J.; Sakamoto, M.; Wang, F., Highly Efficient Dye-Sensitized Solar Cells with a Titania Thin-Film Electrode Composed of a Network Structure of Single-Crystal-like TiO2 Nanowires Made by the "Oriented Attachment" Mechanism. *J. Am. Chem. Soc.* **2004,** *126* (45), 14943-14949.

27. Liu, B.; Aydil, E. S., Growth of Oriented Single-Crystalline Rutile TiO2 Nanorods on Transparent Conducting Substrates for Dye-Sensitized Solar Cells. *J. Am. Chem. Soc.* **2009,** *131* (11), 3985-3990.

28. Law, M.; Greene, L. E.; Johnson, J. C.; Saykally, R.; Yang, P. D., Nanowire dye-sensitized solar cells. *Nat. Mater.* **2005,** *4* (6), 455-459.

29. Hosono, E.; Fujihara, S.; Honma, I.; Zhou, H., The fabrication of an upright-standing zinc oxide nanosheet for use in dye-sensitized solar cells. *Adv. Mater.* **2005,** *17* (17), 2091-2094.

30. Baxter, J. B.; Walker, A. M.; van, O. K.; Aydil, E. S., Synthesis and characterization of ZnO nanowires and their integration into dye-sensitized solar cells. *Nanotechnology* **2006,** *17* (11), S304-S312.

31. Martinson, A. B. F.; Elam, J. W.; Hupp, J. T.; Pellin, M. J., ZnO Nanotube Based Dye-Sensitized Solar Cells. *Nano Lett.* **2007,** *7* (8), 2183-2187.

32. Suzuki, K.; Yamaguchi, M.; Kumagai, M.; Yanagida, S., Application of carbon nanotubes to counter electrodes of dye-sensitized solar cells. *Chem. Lett.* **2003,** *32* (1), 28-29.

33. Wang, G.; Xing, W.; Zhuo, S., Application of mesoporous carbon to counter electrode for dye-sensitized solar cells. *J. Power Sources* **2009,** *194* (1), 568-573.

34. Lee, W. J.; Ramasamy, E.; Lee, D. Y.; Song, J. S., Efficient Dye-Sensitized Cells with Catalytic Multiwall Carbon Nanotube Counter Electrodes. *ACS Appl. Mater. Interfaces* **2009,** *1* (6), 1145-1149.

35. Murakami, T. N.; Ito, S.; Wang, Q.; Nazeeruddin, M. K.; Bessho, T.; Cesar, I.; Liska, P.; Humphry-Baker, R.; Comte, P.; Pechy, P.; Graetzel, M., Highly efficient dye-sensitized solar cells based on carbon black counter electrodes. *J. Electrochem. Soc.* **2006,** *153* (12), A2255-A2261.

36. Saito, Y.; Kubo, W.; Kitamura, T.; Wada, Y.; Yanagida, S., I-/I-3(-) redox reaction behavior on poly(3,4-ethylenedioxythiophene) counter electrode in dye-sensitized solar cells. *J. Photochem. Photobiol. A-Chem.* **2004,** *164* (1-3), 153-157.

37. Muto, T.; Ikegami, M.; Miyasaka, T., Polythiophene-Based Mesoporous Counter Electrodes for Plastic Dye-Sensitized Solar Cells. *J. Electrochem. Soc.* **2010,** *157* (8), B1195-B1200.

38. Hong, W.; Xu, Y.; Lu, G.; Li, C.; Shi, G., Transparent graphene/PEDOT-PSS composite films as counter electrodes of dye-sensitized solar cells. *Electrochem. Commun.* **2008,** *10* (10), 1555-1558.

39. Ma, T. L.; Fang, X. M.; Akiyama, M.; Inoue, K.; Noma, H.; Abe, E., Properties of several types of novel counter electrodes for dye-sensitized solar cells. *J. Electroanal. Chem.* **2004,** *574* (1), 77-83.

40. Chen, L.; Tan, W.; Zhang, J.; Zhou, X.; Zhang, X.; Lin, Y., Fabrication of high performance Pt counter electrodes on conductive plastic substrate for flexible dye-sensitized solar cells. *Electrochim. Acta* **2010,** *55* (11), 3721-3726.

41. Ito, S.; Ha, N.-L. C.; Rothenberger, G.; Liska, P.; Comte, P.; Zakeeruddin, S. M.; Pechy, P.; Nazeeruddin, M. K.; Graetzel, M., High-efficiency (7.2%) flexible dye-sensitized solar cells with Ti-metal substrate for nanocrystalline-TiO2 photoanode. *Chem. Commun.* **2006,** (38), 4004-4006.

42. Sun, H.; Luo, Y.; Zhang, Y.; Li, D.; Yu, Z.; Li, K.; Meng, Q., In Situ Preparation of a Flexible Polyaniline/Carbon Composite Counter Electrode and Its Application in Dye-Sensitized Solar Cells. *J. Phys. Chem. C* **2010,** *114* (26), 11673-11679

43. Yella, A.; Lee, H. W.; Tsao, H. N.; Yi, C. Y.; Chandiran, A. K.; Nazeeruddin, M. K.; Diau, E. W. G.; Yeh, C. Y.; Zakeeruddin, S. M.; Gratzel, M., Porphyrin-Sensitized Solar Cells with Cobalt (II/III)-Based Redox Electrolyte Exceed 12 Percent Efficiency. *Science* **2011,** *334* (6056), 629-634.

44. Welton, T., Room-temperature ionic liquids. Solvents for synthesis and catalysis. *Chem. Rev.* **1999,** *99* (8), 2071-2083.

45. Han, X.; Armstrong, D. W., Ionic liquids in separations. *Accounts Chem. Res.* **2007,** *40* (11), 1079-1086.

46. Buzzeo, M. C.; Evans, R. G.; Compton, R. G., Non-haloaluminate room-temperature ionic liquids in electrochemistry - A review. *Chemphyschem* **2004,** *5* (8), 1106-1120.

47. Gratzel, M., Dye-sensitized solar cells. *J. Photochem. Photobiol. C-Photochem. Rev.* **2003,** *4* (2), 145-153.

48. Baker G. A., B. S. N., Pandey S., Bright F. V., An Analytical View of Ionic Liquids. *Analyst* **2005,** *130*, 800-808.

49. Zakeeruddin, S. M.; Gratzel, M., Solvent-Free Ionic Liquid Electrolytes for Mesoscopic Dye-Sensitized Solar Cells. *Adv. Funct. Mater.* **2009,** *19* (14), 2187-2202.

50. Kalyanasundaram, K., *Dye-Sensitized Solar Cells*. EPFL Press: Lausanne, Switzerland, 2012.

51. Wang, P.; Zakeeruddin, S. M.; Humphry-Baker, R.; Graetzel, M., A Binary Ionic Liquid Electrolyte to Achieve ≥7% Power Conversion Efficiencies in Dye-Sensitized Solar Cells. *Chem. Mater.* **2004,** *16* (14), 2694-2696.

52. Gorlov, M.; Kloo, L., Ionic liquid electrolytes for dye-sensitized solar cells. *Dalton Trans.* **2008,** (20), 2655-2666.

53. Lee, J. K.; Nath, N. C. D.; Cha, E. H.; Sarker, S.; Park, H. S.; Jeong, W. S.; Hong, S. H.; Lee, J. J., Effects of Polyaniline Additive in Solvent-Free Ionic Liquid Electrolyte for Dye-Sensitized Solar Cell. *Bull. Korean Chem. Soc.* **2010,** *31* (11), 3411-3414.

54. Wang, P.; Zakeeruddin, S. M.; Exnar, I.; Graetzel, M., High efficiency dye-sensitized nanocrystalline solar cells based on ionic liquid polymer gel electrolyte. *Chem. Commun.* **2002,** (24), 2972-2973.

55. Reference Solar Spectral Irradiance: Air Mass 1.5. American Society for Testing and Materials. http://rredc.nrel.gov/solar/spectra/am1.5/.

56. Polo, A. S.; Itokazu, M. K.; Iha, N. Y. M., Metal complex sensitizers in dye-sensitized solar cells. *Coord. Chem. Rev.* **2004,** *248* (13-14), 1343-1361.

57. Hagfeldt, A.; Boschloo, G.; Sun, L.; Kloo, L.; Pettersson, H., Dye-Sensitized Solar Cells. *Chem. Rev.* **2010,** *110* (11), 6595-6663.

58. Kamat, P. V., Quantum Dot Solar Cells. Semiconductor Nanocrystals as Light Harvesters. *J. Phys. Chem. C* **2008,** *112* (48), 18737-18753.

59. Sun, W.-T.; Yu, Y.; Pan, H.-Y.; Gao, X.-F.; Chen, Q.; Peng, L.-M., CdS Quantum Dots Sensitized TiO2 Nanotube-Array Photoelectrodes. *J. Am. Chem. Soc.* **2008,** *130* (4), 1124-1125.

60. Gonzalez-Pedro, V.; Xu, X.; Mora-Sero, I.; Bisquert, J., Modeling High-Efficiency Quantum Dot Sensitized Solar Cells. *ACS Nano* **2010,** *4* (10), 5783-5790.

61. Horiuchi, T.; Miura, H.; Uchida, S., Highly efficient metal-free organic dyes for dye-sensitized solar cells. *J. Photochem. Photobiol. A-Chem.* **2004,** *164* (1-3), 29-32.

62. Ito, S.; Miura, H.; Uchida, S.; Takata, M.; Sumioka, K.; Liska, P.; Comte, P.; Pechy, P.; Graetzel, M., High-conversion-efficiency organic dye-sensitized solar cells with a novel indoline dye. *Chem. Commun.* **2008,** (41), 5194-5196.

63. Li, C.; Yum, J. H.; Moon, S. J.; Herrmann, A.; Eickemeyer, F.; Pschirer, N. G.; Erk, P.; Schoeboom, J.; Mullen, K.; Gratzel, M.; Nazeeruddin, M. K., An Improved Perylene Sensitizer for Solar Cell Applications. *ChemSusChem* **2008,** *1* (7), 615-618.

64. Liang, M.; Xu, W.; Cai, F. S.; Chen, P. Q.; Peng, B.; Chen, J.; Li, Z. M., New triphenylamine-based organic dyes for efficient dye-sensitized solar cells. *J. Phys. Chem. C* **2007,** *111* (11), 4465-4472.

65. Liang, Y.; Cheng, F.; Liang, J.; Chen, J., Triphenylamine-Based Ionic Dyes with Simple Structures: Broad Photoresponse and Limitations on Open-Circuit Voltage in Dye-Sensitized Solar Cells. *J. Phys. Chem. C* **2010,** *114* (37), 15842-15848.

66. Hara, K.; Sayama, K.; Arakawa, H.; Ohga, Y.; Shinpo, A.; Suga, S., A coumarin-derivative dye sensitized nanocrystalline TiO2 solar cell having a high solar-energy conversion efficiency up to 5.6%. *Chem. Commun.* **2001,** (6), 569-570.

67. Hara, K.; Dan-oh, Y.; Kasada, C.; Ohga, Y.; Shinpo, A.; Suga, S.; Sayama, K.; Arakawa, H., Effect of Additives on the Photovoltaic Performance of Coumarin-Dye-Sensitized Nanocrystalline TiO2 Solar Cells. *Langmuir* **2004,** *20* (10), 4205-4210.

68. Wang, Z. S.; Cui, Y.; Dan-Oh, Y.; Kasada, C.; Shinpo, A.; Hara, K., Molecular Design of Coumarin Dyes for Stable and Efficient Organic Dye-Sensitized Solar Cells. *J. Phys. Chem. C* **2008,** *112* (43), 17011-17017.

69. Sayama, K.; Tsukagoshi, S.; Mori, T.; Hara, K.; Ohga, Y.; Shinpou, A.; Abe, Y.; Suga, S.; Arakawa, H., Efficient sensitization of nanocrystalline TiO2 films with cyanine and merocyanine organic dyes. *Sol. Energy Mater. Sol. Cells* **2003,** *80* (1), 47-71.

70. Chen, Y. S.; Li, C.; Zeng, Z. H.; Wang, W. B.; Wang, X. S.; Zhang, B. W., Efficient electron injection due to a special adsorbing group's combination of carboxyl and hydroxyl: dye-sensitized solar cells based on new hemicyanine dyes. *J. Mater. Chem.* **2005,** *15* (16), 1654-1661.

71. Geiger, T.; Kuster, S.; Yum, J. H.; Moon, S. J.; Nazeeruddin, M. K.; Gratzel, M.; Nuesch, F., Molecular Design of Unsymmetrical Squaraine Dyes for High Efficiency Conversion of Low Energy Photons into Electrons Using TiO2 Nanocrystalline Films. *Adv. Funct. Mater.* **2009,** *19* (17), 2720-2727.

72. Jelley, E. E., Spectral absorption and fluorescence of dyes in the molecular state. *Nature* **1936,** *138*, 1009-1010.

73. Scheibe, G., *Angew. Chem.* **1936,** *49*.

74. Mobius, D., Scheibe Aggregates. *Adv. Mater.* **1995,** *7* (5), 437-444.

75. Davydov, A. S., *Theory of Molecular Excitons*. McGraw-Hill: New York, 1962.

76. Kasha, M., *Pure Appl Chem* **1965,** *11*.

77. Mishra, A.; Behera, R. K.; Behera, P. K.; Mishra, B. K.; Behera, G. B., Cyanines during the 1990s: A review. *Chem. Rev.* **2000,** *100* (6), 1973-2011.

78. Khazraji, A. C.; Hotchandani, S.; Das, S.; Kamat, P. V., Controlling dye (Merocyanine-540) aggregation on nanostructured TiO2 films. An organized assembly approach for enhancing the efficiency of photosensitization. *J. Phys. Chem. B* **1999,** *103* (22), 4693-4700.

79. Koumura, N.; Wang, Z.-S.; Mori, S.; Miyashita, M.; Suzuki, E.; Hara, K., Alkyl-Functionalized Organic Dyes for Efficient Molecular Photovoltaics. *J. Am. Chem. Soc.* **2006,** *128* (44), 14256-14257.

80. Imahori, H.; Umeyama, T.; Ito, S., Large pi-Aromatic Molecules as Potential Sensitizers for Highly Efficient Dye-Sensitized Solar Cells. *Accounts Chem. Res.* **2009,** *42* (11), 1809-1818.

81. Barea, E. M.; Gonzalez-Pedro, V.; Ripolles-Sanchis, T.; Wu, H. P.; Li, L. L.; Yeh, C. Y.; Diau, E. W. G.; Bisquert, J., Porphyrin Dyes with High Injection and Low Recombination for Highly Efficient Mesoscopic Dye-Sensitized Solar Cells. *J. Phys. Chem. C* **2011,** *115* (21), 10898-10902.

82. Huang, S. Y.; Schlichthoerl, G.; Nozik, A. J.; Graetzel, M.; Frank, A. J., Charge Recombination in Dye-Sensitized Nanocrystalline TiO2 Solar Cells. *J. Phys. Chem. B* **1997,** *101* (14), 2576-2582.

83. Kay, A.; Gratzel, M., Artificial Photosynthesis. 1. Photosensitization of TiO2 Solar Cells with Chlorophyll Derivatives and Related Natural Porphyrins. *J. Phys. Chem.* **1993,** *97* (23), 6272-6277.

84. Mann, J. R.; Gannon, M. K.; Fitzgibbons, T. C.; Detty, M. R.; Watson, D. F., Optimizing the photocurrent efficiency of dye-sensitized solar cells through the controlled aggregation of chalcogenoxanthylium dyes on nanocrystalline titania films. *J. Phys. Chem. C* **2008,** *112* (34), 13057-13061.

85. Ehret, A.; Stuhl, L.; Spitler, M. T., Spectral sensitization of TiO2 nanocrystalline electrodes with aggregated cyanine dyes. *J. Phys. Chem. B* **2001,** *105* (41), 9960-9965.

86. Sayama, K.; Tsukagoshi, S.; Hara, K.; Ohga, Y.; Shinpou, A.; Abe, Y.; Suga, S.; Arakawa, H., Photoelectrochemical properties of J aggregates of benzothiazole merocyanine dyes on a nanostructured TiO2 film. *J. Phys. Chem. B* **2002,** *106* (6), 1363-1371.

87. Tesfai, A.; El-Zahab, B.; Kelley, A. T.; Li, M.; Garno, J. C.; Baker, G. A.; Warner, I. M., Magnetic and Nonmagnetic Nanoparticles from a Group of Uniform Materials Based on Organic Salts. *ACS Nano* **2009,** *3* (10), 3244-3250.

88. Bwambok, D. K.; El-Zahab, B.; Challa, S. K.; Li, M.; Chandler, L.; Baker, G. A.; Warner, I. M., Near-Infrared Fluorescent NanoGUMBOS for Biomedical Imaging. *ACS Nano* **2009,** *3* (12), 3854-3860.

89. Das, S.; de Rooy, S. L.; Jordan, A. N.; Chandler, L.; Negulescu, I. I.; El-Zahab, B.; Warner, I. M., Tunable Size and Spectral Properties of Fluorescent NanoGUMBOS in Modified Sodium Deoxycholate Hydrogels. *Langmuir* **2012,** *28* (1), 757-765.

90. Lu, C.; Das, S.; Magut, P. K. S.; Li, M.; El-Zahab, B.; Warner, I. M., Irradiation Induced Fluorescence Enhancement in PEGylated Cyanine-Based NIR Nano- and Mesoscale GUMBOS. *Langmuir* **2012,** *28* (40), 14415-14423.

91. Cole, M. R.; Li, M.; El-Zahab, B.; Janes, M. E.; Hayes, D.; Warner, I. M., Design, Synthesis, and Biological Evaluation of beta-Lactam Antibiotic-Based

Imidazolium- and Pyridinium-Type Ionic Liquids. *Chem. Bio. Drug Des.* **2011,** *78* (1), 33-41.

92. Dumke, J. C.; El-Zahab, B.; Challa, S.; Das, S.; Chandler, L.; Tolocka, M.; Hayes, D. J.; Warner, I. M., Lanthanide-Based Luminescent NanoGUMBOS. *Langmuir* **2010,** *26* (19), 15599-15603.

93. de Rooy, S. L.; El-Zahab, B.; Li, M.; Das, S.; Broering, E.; Chandler, L.; Warner, I. M., Fluorescent one-dimensional nanostructures from a group of uniform materials based on organic salts. *Chem. Commun.* **2011,** *47* (31), 8916-8918.

94. Das, S.; Bwambok, D.; Ei-Zahab, B.; Monk, J.; de Rooy, S. L.; Challa, S.; Li, M.; Hung, F. R.; Baker, G. A.; Warner, I. M., Nontemplated Approach to Tuning the Spectral Properties of Cyanine-Based Fluorescent NanoGUMBOS. *Langmuir* **2010,** *26* (15), 12867-12876.

95. de Rooy, S. L.; Das, S.; Li, M.; El-Zahab, B.; Jordan, A.; Lodes, R.; Weber, A.; Chandler, L.; Baker, G. A.; Warner, I. M., Ionically Self-Assembled, Multi-Luminophore One-Dimensional Micro- and Nanoscale Aggregates of Thiacarbocyanine GUMBOS. *J. Phys. Chem. C* **2012,** *116* (14), 8251-8260.

96. Jordan, A. N.; Das, S.; Siraj, N.; de Rooy, S. L.; Li, M.; El-Zahab, B.; Chandler, L.; Baker, G. A.; Warner, I. M., Anion-controlled morphologies and spectral features of cyanine-based nanoGUMBOS - an improved photosensitizer. *Nanoscale* **2012,** *4* (16), 5031-5038.

97. Lakowicz, J. R., *Principles of Fluorescence Spectroscopy*. 3 ed.; Springer: New York, 2006.

CHAPTER 2
ANION-CONTROLLED MORPHOLOGIES AND SPECTRAL FEATURES OF CYANINE-BASED NANOGUMBOS – AN IMPROVED PHOTOSENSITIZER*

2.1 Introduction

Nanomaterials based on functional organic molecules are of considerable interest due to their strikingly different optoelectronic properties[1] and high photoluminescence[2] as compared to their inorganic counterparts. Low-dimensional organic nanostructures are of further significance for their applications as optical waveguides,[3,4,5] lasers,[1,6] field effect transistors,[7] sensors,[8] and optoelectronic devices.[9] Several strategies have been employed for fabrication of organic nanostructures with variable morphologies and properties. Strategies reported thus far include both non-templated and template-induced molecular self-assemblies.[10,11,12] The non-templated approach primarily involves the driving forces of assembly of the molecules themselves through properties such as hydrogen bonding, van der Waals forces, π-π stacking, cation- π and donor-acceptor interactions, and so forth. The perfect design of an organic molecule that will yield desirable properties in self-assembled nanostructures has been the focus of various studies performed over the last decade.[13,14]

Nakanishi and coworkers have developed perylene microcrystals using a simple reprecipitation method.[15,16] The development of this reprecipitation process has overcome the difficulties of nano- and microcrystal fabrication. The formation of microcrystalline perylene was induced as a result of aggregation. Notably, aggregation

* This chapter previously appeared as Jordan, A. N.; Das, S.; Siraj, N.; de Rooy, S. L.; Li, M.; El-Zahab, B.; Chandler, L.; Baker, G. A.; Warner, I. M., Anion-controlled morphologies and spectral features of cyanine-based nanoGUMBOS - an improved photosensitizer. *Nanoscale* **2012,** *4* (16), 5031-5038. It is reproduced by permission of The Royal Society of Chemistry.

via ordered self-association of molecules can result in changes of spectral behavior as compared to the monomeric species. The formation of J-aggregates, for example, is a result of head-to-tail molecular stacking and typically exhibits a narrow and bathochromically shifted absorption band with respect to the monomer. In addition, J-aggregation also results in enhanced resonance fluorescence. In contrast, H-(hypsochromic) aggregates are formed as a result of molecular stacking in a card pack (stacking) manner. This aggregate type typically exhibits a hypsochromically shifted absorption band with respect to the monomer and typically displays little to no fluorescence. More recently, randomly-oriented aggregates have been classified as those without any specific order of stacking, with conservation of the spectral properties of the monomer. Moderation of these spectral properties in self-assembled nanostructures is attributed to excitonic splitting, as has been explained by Davydov et al.[17] and Kasha et al.[18] using molecular exciton coupling theory. Such theory allows for variations in aggregation, which lead to interactions between the transition dipole moments of the molecules, resulting in differences in splitting of the excited state. Knowledge of aggregation characteristics has been applied to further understanding the behavior of fluorescent organic nanoparticles (FONs). A common challenge of FONs is fluorescence quenching, which is either considered to be an effect of the solid state or an effect of H-aggregation of the chromophores. Conversely, a phenomenon called aggregation-induced emission enhancement (AIEE) exhibits an opposite effect. Instead of fluorescence quenching, FONs can display an enhanced emission due to formation of J-aggregates. Examples of this process have been reported by Tang and coworkers

who have developed numerous biological[19,20] and chemical[21,22] sensors based on AIEE tetraphenylethene derivatives.

FONs studied thus far have exhibited various sizes, shapes, and spectral properties. These properties are attributed to chemical composition and intermolecular interactions that can result in highly ordered molecular self-assemblies. Recently, our group has reported the non-templated control of spectral properties in nanoGUMBOS derived from a near-infrared dye.[23] However, to the best of our knowledge, control of the morphology of these nanoparticles using a template-free approach remains an outstanding challenge. Thus, the ability to simultaneously influence the morphology and spectral features of organic low-dimensional nanomaterials without alteration in the primary dye's skeleton is an exciting development.

Cyanine dyes, in particular, are well-known to form aggregates by self-assembly. This was first independently discovered by Jelley[24] and Scheibe,[25] who reported the aggregation of pseudoisocyanine at high concentrations in aqueous solution and at solid-liquid interfaces.[26] These aggregates were initially called Jelley (J) or Scheibe aggregates, appellations honoring these discoverers. As a result, cyanine dyes have been extensively studied for aggregation and used in silver halide emulsions for photography. Further studies have led to application of these dyes in biosensors[27] and semiconductor materials,[28] as well as possible uses in gold and silver nanoparticle coatings.[29] Recently, Pandey and coworkers have reported the formation of controlled aggregation states of anionic cyanine dyes in aqueous solution using water-miscible ionic liquids (ILs).[30] Cyanine dye aggregates have also displayed different morphologies depending on their molecular structures.[31,32] The formation of spherical

pseudoisocyanine nanoparticles has been previously studied by use of an ion association approach with borate anions at varying ratios in which no aggregates were observed.[33] Pseudoisocyanine nanocrystals have also been examined with polyelectrolyte capsules that formed aggregates at a concentration of 3 μM.[34] However, to the best of our knowledge, thus far there exists no report on the demonstration of counterion controlled morphologies and aggregation properties in nanomaterials derived from salts of pseudoisocyanine. Hence, this study is the first report of the kind, especially from the point of view of a non-templated approach to controlled morphology and enhanced fluorescence of nanomaterials at low concentrations.

In this study, pseudoisocyanine iodide (PICI) was modified by use of an anion exchange reaction with lithium bis(trifluoromethanesulfonyl)imide ($LiNTf_2$) and lithium bis(perfluoroethylsulfonyl)imide (LiBETI) to produce the water-insoluble salts pseudoisocyanine bis(trifluoromethanesulfonyl)imide and pseudoisocyanine bis(perfluoroethylsulfonyl)imide, [PIC][NTf_2] and [PIC][BETI], respectively. These dyes are representative of a class of materials which we have come to refer to as GUMBOS (i.e., groups of uniform materials based on organic salts).[35,36] As described in the previous chapter, GUMBOS are essentially ionic organic salts that retain many of the attractive properties inherent to those of ILs. NanoGUMBOS were synthesized from [PIC][NTf_2] and [PIC][BETI] GUMBOS by employing a simple reprecipitation method in an aqueous dispersion. The properties of the nanoGUMBOS were examined by use of various techniques such as transmission and scanning electron microscopy (TEM and SEM), as well as absorption and fluorescence spectroscopies. Investigation of the electrochemical properties of the GUMBOS was also evaluated via cyclic voltammetry.

As a result of the studies reported here, we have established a rapid and facile approach to control the overall shape and associated optical features of low-dimensional nanoGUMBOS fabricated at low concentrations from an identical cationic building block. These nanomaterials have potential applications as nanosensors and dye sensitizers in photovoltaics.

2.2 Materials and Methods

2.2.1 Materials

1,1'-diethyl-2,2'-cyanine iodide or pseudoisocyanine iodide (97%) and lithium bis(trifluoromethanesulfonyl)imide (99.95%) were purchased from Sigma Aldrich and used as received. Lithium bis(perfluoroethylsulfonyl)imide was obtained from 3M. Ethanol was purchased from Pharmaco-AAPER and used as received. Ultrapure water (18.2 MΩ cm) was used from ELGA model PURELAB ultra water filtration system. A BRANSON 3510RDTH model bath ulstrasonicator (335W, 40kHz frequency) was used at room temperature for syntheses of the nanoGUMBOS. Carbon-coated copper grids (CF400-Cu, Electron Microscopy Sciences, Hatfield, PA) were used for TEM imaging.

2.2.2 Synthesis and Characterization of PIC-based GUMBOS

Pseudoisocyanine iodide (PICI) was modified by use of an anion exchange reaction (Figure 2.1) using a method previously reported.[23,35] Two novel dyes were synthesized using $LiNTf_2$ and LiBETI. In a typical synthesis, a mixture of PICI and $LiNTf_2$ (1.1 eq) was dissolved in a biphasic solution of methylene chloride and water (2:1, v/v) and stirred for one day at room temperature. The ion-exchanged dye product was insoluble in water and transferred to the lower organic layer. The methylene chloride layer was collected and washed several times with fresh deionized water to

completely remove residual LiI byproduct. Subsequently, the methylene chloride was removed under vacuum at 40 °C by use of a rotary evaporator followed by freeze-drying overnight to afford solid [PIC][NTf_2]. A similar procedure was implemented to synthesize [PIC][BETI]. The melting points of [PIC][NTf_2] and [PIC][BETI] GUMBOS were determined by use of a MEL-TEMP capillary melting point apparatus. The PIC-based GUMBOS were characterized using ^{13}C NMR (Bruker Avance 400MHz, [D_6] DMSO), ^{19}F NMR (Bruker DPX 250MHz, [D_6] DMSO), and elemental microanalysis (Atlantic Microlab, Norcross, GA).

2.2.3 Preparation of PIC-based NanoGUMBOS

[PIC][NTf_2] and [PIC][BETI] nanoGUMBOS were prepared by use of an additive-free reprecipitation method.[23,35] The procedure consists of the addition of 150 µL of a 1 mM ethanolic solution of GUMBOS to 5 mL (~30 µM) of DI water under sonication for 5 min.

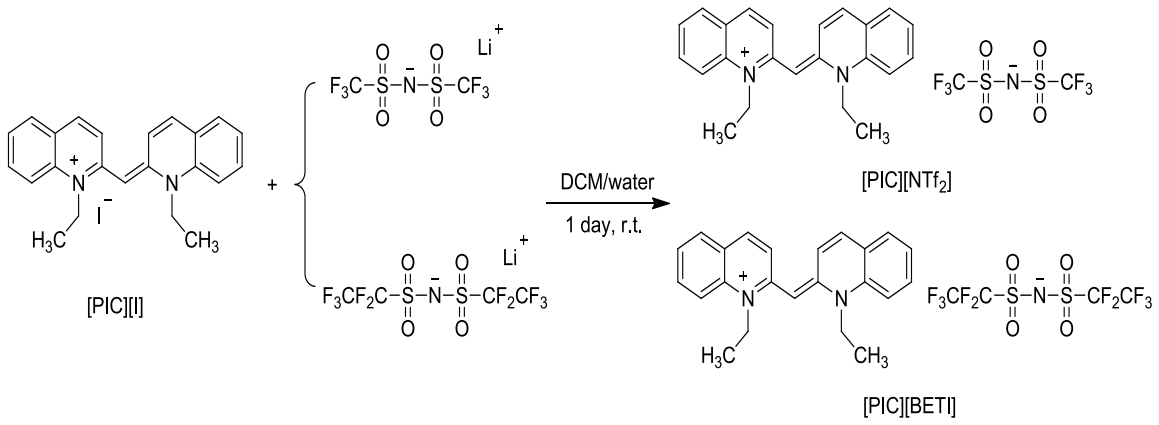

Figure 2.1 Synthesis of [PIC][NTf_2] and [PIC][BETI] using an anion exchange reaction.

2.2.4 Microscopy Characterization of NanoGUMBOS

Electron micrographs were obtained for characterization of the size and morphology using a JEOL100CX transmission electron microscope and JSM-

6610, JSM-6610LV high and low vacuum scanning electron microscope (JEOL USA, Inc., Peabody, MA). Height characterization was confirmed by AFM using Nano-R AFM system, which was operated in contact mode with an n-type silicon probe (Pacific Nanotechnology, Inc./Agilent Technologies, Santa Clara, CA). Selected area electron diffraction (SAED) was performed to determine crystallinity by the use of a JEOL JEM-2010 high-resolution transmission electron microscope at an accelerating voltage of 200 kV. An aliquot (5 µL) of PIC-based nanoGUMBOS was drop-casted onto a carbon-coated copper grid or gold-coated mica substrate and air dried at room temperature. Polarized optical microscopy was performed using an Olympus BH polarizing optical microscope with an MD 1900 camera. For these measurements, a few microliters of the sample were dropped onto a pre-cleaned glass slide and air dried. The images were then captured using a variety of angles between the polarizer and the analyzer.

2.2.5 Absorption and Fluorescence Studies of GUMBOS and NanoGUMBOS

Absorbance measurements were obtained using a Shimadzu UV-3101PC UV-Vis-NIR scanning spectrometer (Shimadzu, Columbia, MD) at 20 °C with a slit width of 2 nm. Fluorescence emission, fluorescence quantum yield, and fluorescence anisotropy were performed on a Spex Fluorolog-3 spectrofluorimeter (model FL3-22TAU3; Jobin Yvon, Edison, NJ) at room temperature with slitwidths of 5 nm. A 0.4 cm quartz cuvet (Starna Cells) was used to collect the absorbance and fluorescence measurements. A second 0.4 cm quartz cuvet was filled with water for use as a control blank. Fluorescence studies were all performed through adoption of a synchronous scan protocol with right angle geometry. Fluorescence spectra were corrected for inner filter effects using a standard formula.[37] Quantum yield (Φ) measurements were performed

using Rhodamine 6G (R6G) (Φ = 0.92 in water) as a standard. The nanoGUMBOS were prepared using a reprecipitation method and diluted to obtain absorbance below 0.1, at and above the excitation wavelength (524 nm). The same protocol was followed for the standard as well. Fluorescence lifetime measurements were performed at Horiba Jobin Yvon, NJ using time domain mode. A picoseconds pulsed excitation source of 495 nm was used and emission was collected at 550 nm with a TBX detector. The time correlated single photon counting (TSCPC) mode was used for data acquisition with a resolution of 7 ps/ channel.

2.2.6 Electrochemical Studies of GUMBOS

Electrochemical measurements were performed under anaerobic conditions using an Autolab PGSTAT 302 potentiostat from Eco. Chemie. A three-electrode system consisting of an Ag/Ag^+ reference electrode, Pt working electrode, and Pt counter electrode was employed. Measurements were conducted in acetonitrile with 0.1 M tetrabutylammonium hexafluorophosphate ($TBAPF_6$) as a supporting electrolyte and ferrocene (Fc^+/Fc) as an internal reference having a formal potential of 0.63 V vs NHE.

2.3 Results and Discussion

2.3.1 Synthesis and Characterization of [PIC][NTf_2] and [PIC][BETI] GUMBOS

Pseudoisocyanine iodide was reacted with 1.1 molar equivalent of lithium bis(trifluoromethanesulfonyl)imide to yield [PIC][NTf_2] with a melting point of 245 °C. A similar procedure was employed to produce [PIC][BETI] with a melting point of 170 °C. Elemental analysis characterization for the GUMBOS is shown in Table 2.1.

[PIC][NTf_2]: ^{13}C NMR (400MHz, [D_6] DMSO), δ (ppm): 153.52 (s), 139.18 (s), 138.39 (s), 133.30 (s), 129.76 (s), 125.55 (s), 122.15 (s), 116.86 (s), 89.51 (s), 44.79 (s), 12.26 (s). ^{19}F NMR (250MHz, [D_6] DMSO), -79.17 (s).

[PIC][BETI]: ^{13}C NMR (400MHz, [D_6] DMSO), δ (ppm): 153.53 (s), 139.04 (s), 138.39 (s), 133.29 (s), 129.76 (s), 125.54 (s), 125.07 (s), 122.15 (s), 116.86 (s), 89.51 (s), 44.78 (s), 12.26 (s). ^{19}F NMR (250MHz, [D_6] DMSO), δ (ppm): -78.99 (s), -117.85 (s).

Table 2.1 Elemental analysis of PIC-based GUMBOS

PIC-based	C		H		N		F	
GUMBOS	Theory	Found	Theory	Found	Theory	Found	Theory	Found
[PIC][NTf_2]	49.37%	49.61%	3.79%	3.81%	6.91%	6.91%	18.76%	18.57%
[PIC][BETI]	45.86%	46.19%	3.25%	3.24%	5.94%	5.97%	26.89%	25.75%

2.3.2 Characterization of Size and Morphology of NanoGUMBOS

Examination of TEM and SEM micrographs of [PIC][NTf_2] and [PIC][BETI] nanoGUMBOS revealed interesting and dramatic changes in morphology upon variation in the counteranion associated with the PIC cation (Figure 2.2). The [PIC][NTf_2] nanoGUMBOS were found to form distinct diamond-like structures with an average respective length, width, and height of 656 ± 139 nm, 334 ± 74 nm, and 66 ± 30 nm. In contrast, [PIC][BETI] nanoGUMBOS exhibited rod-like structures with an average respective length and width of 1.5 ± 0.83 μm and 88 ± 26 nm. The distinct change in morphology of these nanomaterials was attributed to ordered repetition of the molecular stacking. The head-to-tail type of molecular orientation within the [PIC][NTf_2] nanoGUMBOS led to the diamond-like structures. Likewise, the repetition of the parallel stacked units led to the formation of [PIC][BETI] nanorods. Similar self-assembly structures and properties have been reported using the reprecipitation method to prepare rubrene[38] and quinacridone derivatives.[39] These compounds consist of

relatively similar aromatic structures that could contribute to the rod and diamond-like nanostructures.

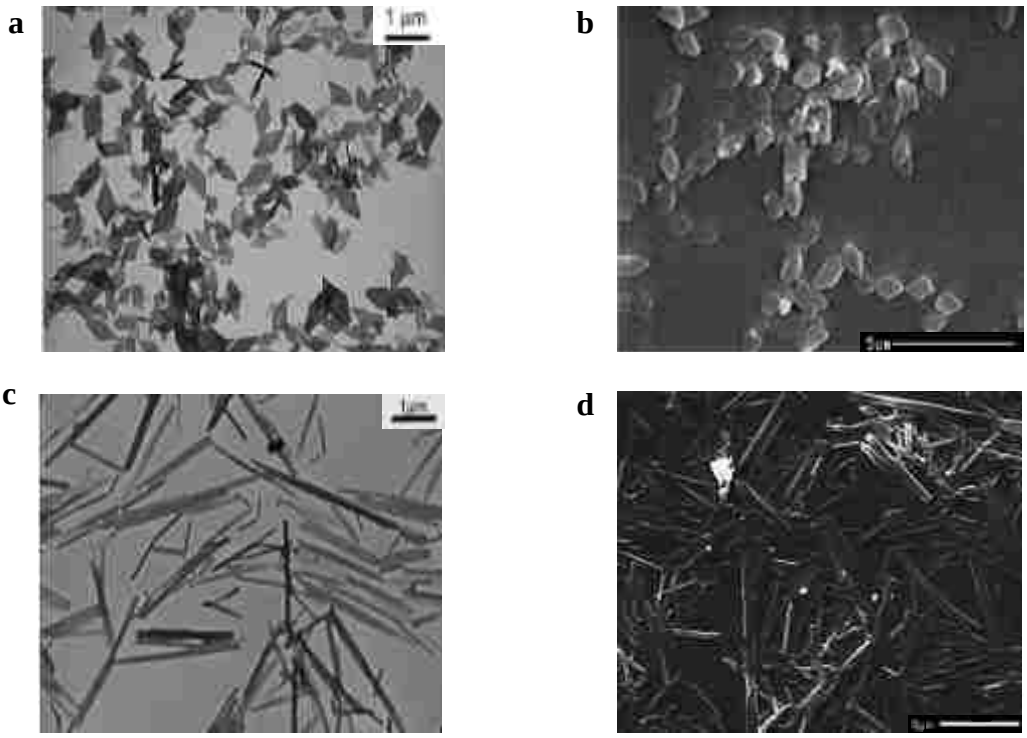

Figure 2.2 TEM (left) micrographs of (a) [PIC][NTf_2] and (c) [PIC][BETI] nanoGUMBOS. Scale bars are 1 µm. SEM (right) micrographs of (b) [PIC][NTf_2] and (d) [PIC][BETI] nanoGUMBOS. Scale bars are 5 µm.

The use of polarized optical microscopy (POM) revealed appreciable birefringence for [PIC][NTf_2] nanoGUMBOS, while [PIC][BETI] nanoGUMBOS exhibited very little to no birefringence (Figure 2.3). SAED suggested that both the nanoGUMBOS were amorphous. Thus, birefringence of the nanomaterials was attributed to the anisotropic ordered molecular arrangement in the J- and H-aggregates. Previous studies have observed the birefringent property of cyanine dyes in aqueous solution at concentrations of 10^{-3} molar.[40,41] Although the distinct [PIC][NTf_2] and [PIC][BETI] nanostructures were not observed under POM, likely due to the low resolution of the instrument, birefringence of the nanoGUMBOS was clearly visible from

these micrographs. This property enhances the potential application of these nanomaterials as building blocks for optoelectronic devices.[5]

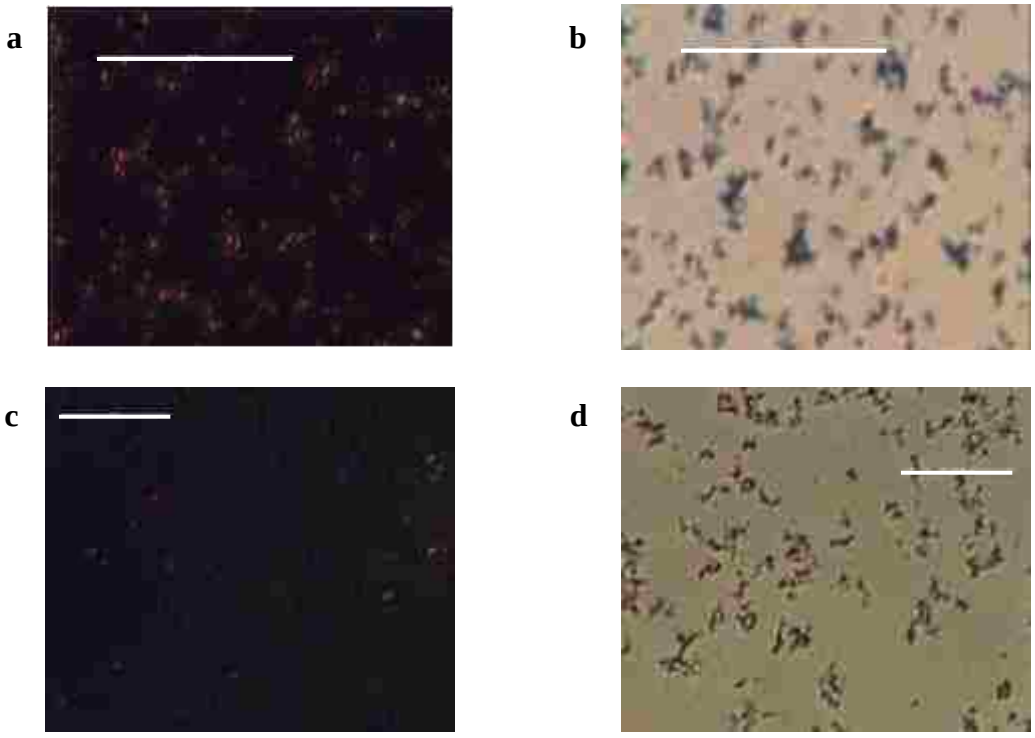

Figure 2.3 POM of [PIC][NTf_2] (top) and [PIC][BETI] (bottom) nanoGUMBOS at various angles 0° (a,b) and 45° (c,d). The scale bars are 50 µm.

2.3.3 Absorption Studies of GUMBOS and NanoGUMBOS

Examination of absorption spectra of PICI, [PIC][BETI], and [PIC][NTf_2] GUMBOS in ethanolic solution showed similar spectra (Figure 2.4). Two monomeric peaks at 490 and 524 nm were observed, due to two different vibrational transitions.[42] However, dramatic changes in spectral properties were noticed upon formation of the nanoGUMBOS in aqueous dispersion (Figure 2.5). An increase in absorbance was observed as the concentration increased (Figure 2.6). However, concentrations above 60 µM resulted in precipitation in the aqueous dispersion. More specifically, [PIC][BETI] nanoGUMBOS exhibited a reduced monomer absorbance at ~524 nm. In addition, a new blue shifted peak appeared at 450 nm with tail broadening in the longer wavelength

region. The hypsochromic shift in the absorption spectrum of [PIC][BETI] nanorods was attributed to the formation of H-aggregates or sandwich-like arrangements of the dye molecules within this nanomaterial. The [PIC][NTf_2] nanoGUMBOS exhibited a similar decrease in the monomer absorbance, with the appearance of a new strong red shifted band at 590 nm. This new red shifted peak suggests formation of J-aggregates within the diamond-like nanostructures. The molar extinction coefficients of the nanoGUMBOS were in ranges from 1.2–1.5 × 10^4 $M^{-1}cm^{-1}$ (Table 2.2).

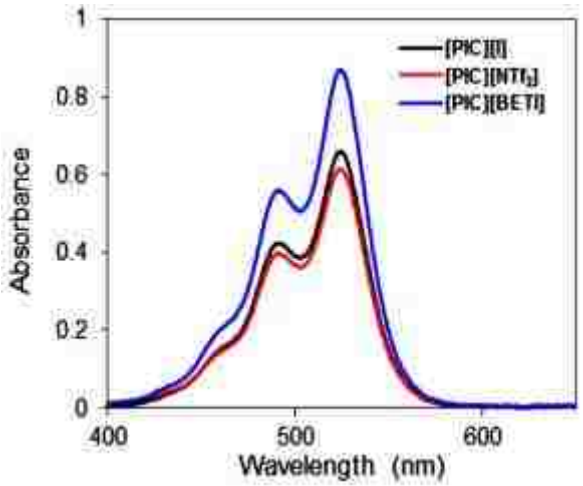

Figure 2.4 Absorption spectra of PICI, [PIC][NTf_2], and [PIC][BETI] in ethanolic solution.

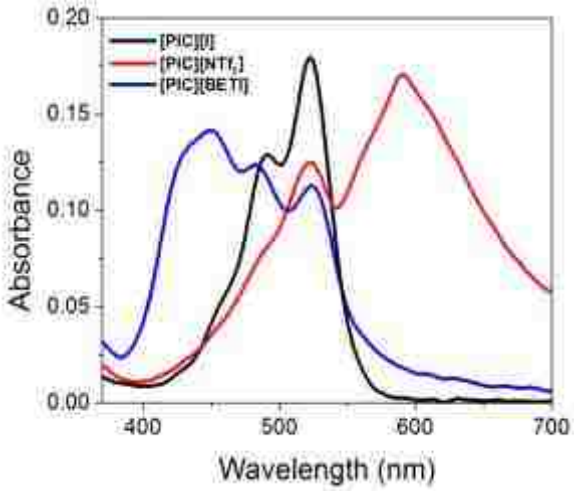

Figure 2.5 Absorption spectra of PICI in aqueous solution and [PIC][NTf_2] and [PIC][BETI] nanoGUMBOS suspended in water at a concentration of 30 µM.

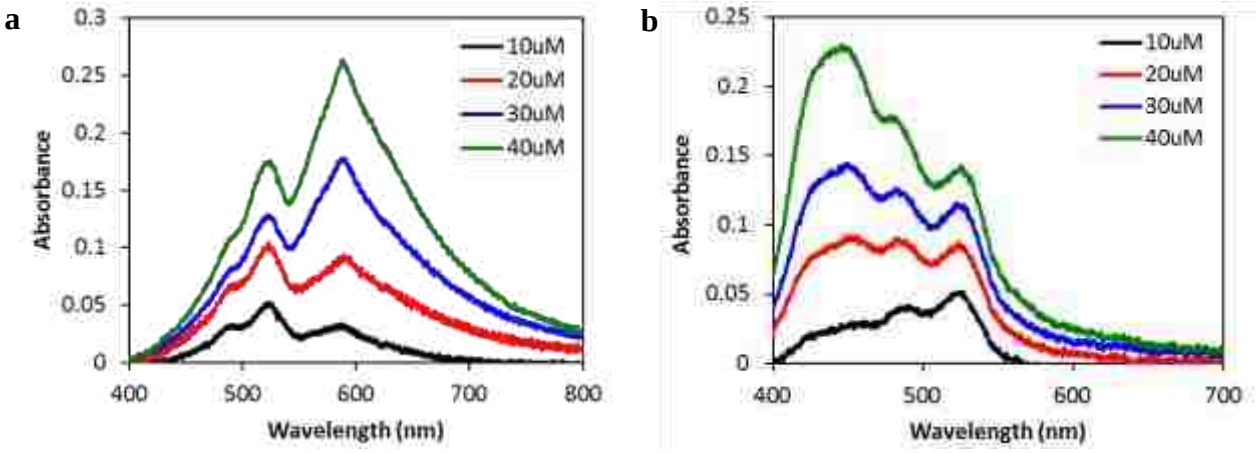

Figure 2.6 Absorption spectra of (a) [PIC][NTf_2] and (b) [PIC][BETI] nanoGUMBOS at various concentrations.

In studies reported to date, J-aggregates usually display a narrow, bathochromically shifted absorption spectrum.[24,25] However, this signature is mostly encountered for J-aggregates in solution. A relatively broader J-aggregate peak has been observed for nanoparticles as a result of less optimal J-aggregation and a lack of motional narrowing in the nanoparticles.[8,43] Lattice disorder is considered to be another possible explanation for this spectral broadening.[44] To the best of our knowledge, this is the first observation that reports a non-templated control of J- and H-aggregates in FONs derived from PIC dyes at an extremely low concentration (30 µM). Moreover, the broadness of the absorption spectra achieved in these nanomaterials encompassing the entire visible region and extending to the near infrared region can be considered extremely important for their application as photosensitizers in energy harvesting devices such as solar cells.

2.3.4 Fluorescence Studies of GUMBOS and NanoGUMBOS

The fluorescence data complements our conclusions from absorption data (Figure 2.7). Formation of J-aggregates in the [PIC][NTf_2] nanoGUMBOS resulted in a new red shifted fluorescence peak at 590 nm, with 590 times enhancement in

fluorescence intensity as compared to an aqueous PICI solution (575 nm) of the same concentration. Fluorescence was also observed near the same wavelength as the J-aggregate absorption peak. This resonance fluorescence of [PIC][NTf_2] nanoGUMBOS reconfirms the presence of J-aggregates in these diamond-like nanostructures. The observed striking enhancement in fluorescence emission intensity in the [PIC][NTf_2] nanoGUMBOS is considered to be a combined effect of J-aggregation and restriction in intramolecular rotation (RIR) in the solid state.[45] In contrast, [PIC][BETI] nanoGUMBOS displayed a weaker fluorescence peak at ~577 nm that was a result of H-aggregation. In spite of H-aggregation, the fluorescence emission intensity of [PIC][BETI] nanoGUMBOS was 40 times higher than the emission of PICI in water. This observation was attributed to RIR within the nanoGUMBOS.

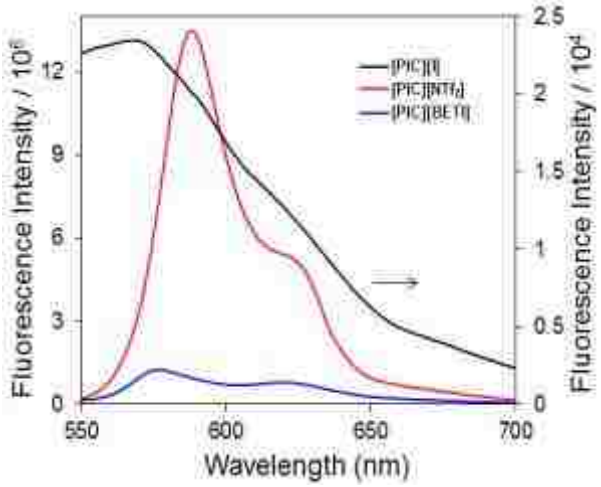

Figure 2.7 Fluorescence spectra of PICI in aqueous solution and [PIC][NTf_2] and [PIC][BETI] nanoGUMBOS suspended in water at a concentration of 30 µM.

Fluorescence quantum yields (Table 2.2) for PICI in water and [PIC][NTf_2] and [PIC][BETI] nanoGUMBOS coincided with the fluorescence spectra. The PICI compound exhibited an extremely low quantum yield, 3.89×10^{-4}, in water which was attributed to twisted intramolecular charge transfer (TICT) states. In contrast,

[PIC][NTf_2] nanoGUMBOS exhibited two orders of magnitude enhancement in fluorescence quantum yield as compared to the parent compound in aqueous solution. This was attributed to the presence of highly fluorescent J-aggregates and restricted TICT in the nanomaterials due to enhanced rigidity. The quantum yield of [PIC][BETI] nanoGUMBOS also revealed an order of magnitude enhancement in fluorescence quantum yield as compared to the parent compound. This increase in the quantum yield is due to the RIR within the nanoGUMBOS as previously noted. The quantum yield values obtained in our studies for PICI without J-aggregation at the experimental concentration of 30 μM and in [PIC][NTf_2] nanomaterials with J-aggregation are close to the values reported in the literature.[46,47] However, in the studies performed so far, J-aggregation or the 100 times enhancement in quantum yield was observed at very high concentrations (~1 mM) and/or in the presence of certain templates.[46,47] Our study demonstrates similar improvements at nearly 100 times lower concentration in the nanomaterials using a template free approach.

Table 2.2 Fluorescence quantum yields and lifetimes[a] of PICI in aqueous system and [PIC][NTf_2] and [PIC][BETI] nanoGUMBOS

Dyes	λ_{max}[b] /H_2O (nm)	ε_{max}[b] /10^4 ($M^{-1}cm^{-1}$)	Quantum Yield (Φ)	Lifetime (τ)
PICI	524	1.5	3.89×10^{-4}	11–16 ps[c]
[PIC][NTf_2]	590	1.4	1.09×10^{-2}	98 ps (98%), 1.22 ns (2%)
[PIC][BETI]	450	1.2	2.16×10^{-3}	234 ps (30%), 4.52 ns (70%)

[a]These values include the percent of contribution for each component. [b]The maximum absorption wavelength and molar extinction coefficient. [c]Obtained from reference 48.

2.3.5 Fluorescence Lifetime Measurements

Lifetime decay (Table 2.2) of [PIC][NTf_2] nanoGUMBOS was best fitted to a biexponential decay with 98% contribution from a 98 ps component and 2% contribution from a 1.22 ns component. The short-lived component was assigned to the

J-aggregates. The presence of J-aggregates as indicated by the red-shifted absorption band and resonance steady state fluorescence is complementary to the lifetime data. The significantly low contribution from a longer component may be attributed to the presence of very small amounts of randomly oriented aggregates in which the lifetime is enhanced due to restricted rotation in the solid state.[47] The lifetime decay of [PIC][BETI] nanorods was also best described by a double exponential decay model and the data revealed the likely presence of two major components. The value with 30% contribution possessed a lifetime of 234 ps and 70% contribution was from a longer component of 4.52 ns. Since H-aggregates are non-fluorescent, they will not contribute to fluorescence decays. As observed from the absorption spectrum, the major fluorescing species in this case was the randomly oriented component which has characteristics similar to that of the monomer.[23] Hence, the longer lifetime component was assigned to randomly oriented species in the nanorods. The fairly long-lived lifetime of the major lifetime component and enhanced fluorescence of the nanorods compared to PICI aqueous solutions suggests highly restricted TICT within the nanorods suspended in aqueous dispersion. PICI solutions in water usually exhibit an extremely short lifetime lying between 11-16 ps which explains its extremely low quantum yield.[48] The shorter component (234 ps) of the nanorods may be assigned to some differently oriented random aggregates. The possibility of J-aggregation in the nanorods can be reasonably excluded based on the steady-state measurements. Dual fluorescence lifetime components and increased quantum yield of PICI has been reported in the literature due to adsorption of the dye on polymeric layers wherein a J-aggregate peak was not observed in the absorption spectrum.[48]

2.3.6 Fluorescence Anisotropy

The formation of J- and H-aggregates in the respective PIC-based nanoGUMBOS was further confirmed by use of fluorescence anisotropy measurements (Figure 2.8). Fluorescence anisotropy (r) is a measure of the average angular displacement of molecules in the excited state[37] after excitation with vertically polarized light and is given by

$$r = \frac{I_{vv} - GI_{vh}}{I_{vv} + 2GI_{vh}} \quad (1)$$

where G is the grating factor to correct for instrumental responses, such as the emission wavelength and detector. Parameters I_{vv} and I_{vh} correspond to the fluorescence emission intensities measured parallel and perpendicular to the vertically polarized excitation, respectively.[37] Upon excitation at 524 nm, anisotropy spectra of [PIC][NTf_2] and [PIC][BETI] nanoGUMBOS exhibited peak minima at 590 and 578 nm, respectively. These peak minima were similar to the emission maxima of [PIC][NTf_2] and [PIC][BETI] nanoGUMBOS.

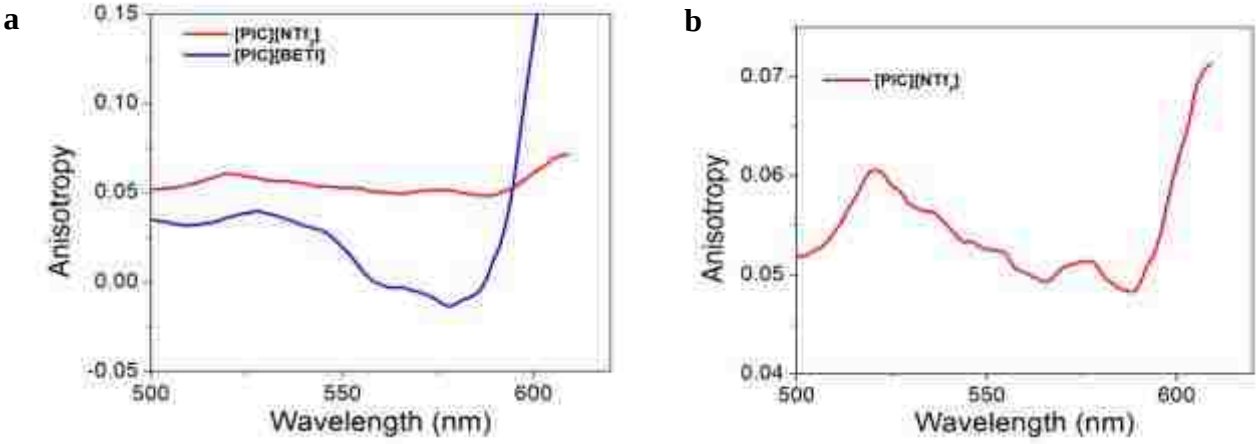

Figure 2.8 (a) Fluorescence anisotropy of [PIC][NTf_2] and [PIC][BETI] nanoGUMBOS. (b) Magnified plot of [PIC][NTf_2] shown in panel (a).

Anisotropy studies of PIC aggregates have reported values close to the theoretical anisotropy values that range from -0.2 to +0.4, with the anisotropy being low (< 0) in the H-aggregate region and increasing sharply to 0.35 in the J-aggregate region.[49] In this study, it was observed that [PIC][NTf_2] nanoGUMBOS, comprised of J-aggregates, had higher positive anisotropy values than [PIC][BETI] nanoGUMBOS that are mainly composed of H-aggregates. This contrast was attributed to slower rotational diffusion within the [PIC][NTf_2] nanoGUMBOS as a result of higher ordered stacking in these nanostructures, suggested by the diamond-like structures of [PIC][NTf_2]. The negative fluorescence anisotropy of [PIC][BETI] nanorods may be attributed to the faster rotational diffusion of the individual molecules within the nanorods. It was observed from the absorption study, as well as both the steady-state and time domain fluorescence studies that the nanorods are comprised mainly of H-aggregates and randomly oriented aggregates, of which the H-aggregates are non-fluorescent. Thus, only the randomly oriented aggregates contribute to the fluorescence anisotropy.

It is well documented in the literature that the fluorescence of cyanine dyes is quenched by *cis-trans* isomerization. This process can very easily occur in randomly oriented aggregates due to the absence of any definite π-π stacking.[50] In contrast, the ordered stacking within the highly fluorescent J-aggregates of [PIC][NTf_2] can substantially reduce the *cis-trans* isomerization, thereby explaining its positive fluorescence anisotropy values. Although the anisotropy values were attenuated, they still agreed with previous findings regarding PIC J- and H-aggregates in solution. This difference is hypothesized to result from aggregates formed in the nanoGUMBOS

suspension in the present study as compared to those commonly observed in PIC solutions.

2.3.7 Electrochemical Energy Levels and Band Gap Calculations

Cyclic voltammetry was performed in acetonitrile using the PIC-based GUMBOS, as well as the parent compound for comparison. Cyclic voltammograms of the PIC-based GUMBOS revealed a reversible oxidation profile at a potential range from 1.2 V to 0.5 V, which were identified as the reactions of $PIC^{\cdot 2+}/PIC^{+}$ (Figure 2.9). The increase in current and multiple electron transfer processes exhibited by the parent compound, PICI, was attributed to the presence of iodide, which can also undergo oxidation and reduction reactions.

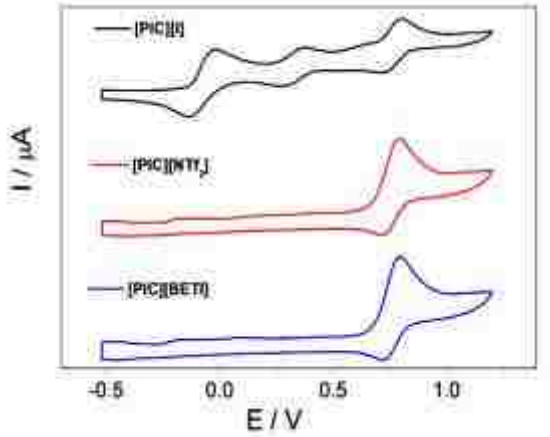

Figure 2.9 Cyclic voltammograms of PIC-based GUMBOS (1 mM) in acetonitrile with 0.1 M $TBAPF_6$ on Ag/Ag^{+} electrode at 0.1 V/s.

The oxidation potential (E_{ox}) was calculated by the average of the anodic and cathodic peak potentials. This oxidation potential along with the absorption and emission spectra of the PIC-based GUMBOS were used to determine the excited state reduction potential (E^{*}_{red}) where $E_{0\text{-}0}$ represents the 0-0 transition energy state and λ_{int} is the intersect wavelength of the normalized absorbance and emission spectra.[51] Normalized absorption and emission spectra of the PICI, [PIC][BETI], and $[PIC][NTf_2]$

GUMBOS in acetonitrile displayed similar spectra that were used to determine a λ_{int} of 534 nm (Figure 2.10).

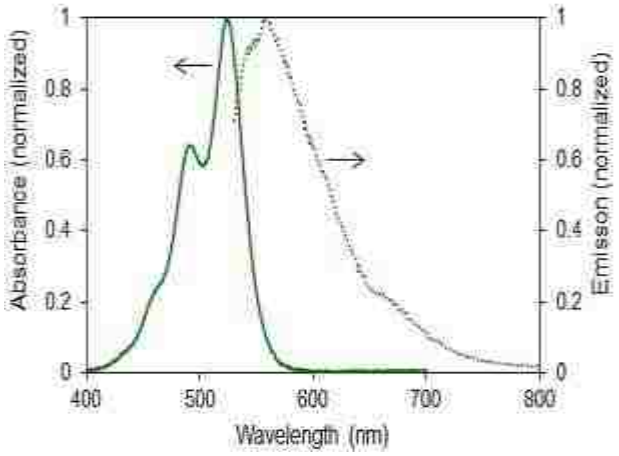

Figure 2.10 Normalized absorption and emission spectra of PIC-based GUMBOS in acetonitrile (30 μM) used to determine the intersect wavelength (λ_{int}).

The band gap (E_g) of the PIC-based GUMBOS was determined by the onset wavelength (λ_{onset}) at which the negative tangent line of the lowest energy absorbance peak intersects with the linear tangent line of the absorption tail (Figure 2.11).[52] The λ_{onset} of the PIC-based GUMBOS in acetonitrile was ascertained at 556 nm. The highest occupied molecular orbital (HOMO) energy level was calculated vs vacuum with Fc^+/Fc as a reference by the following equation

$$E_{HOMO}(eV) = -1e^{-}\left[E_{pa}\left(V \text{ vs } Fc^{+}/Fc\right) + 4.8\left(V\ Fc^{+}/Fc \text{ vs Zero}\right)\right] \quad (2)$$

where E_{pa} is the anodic potential. The sum of the HOMO values and band gaps afforded the values of the energy level of the lowest unoccupied molecular orbital (LUMO). The aforementioned potentials and band gaps were reported in Table 2.3.

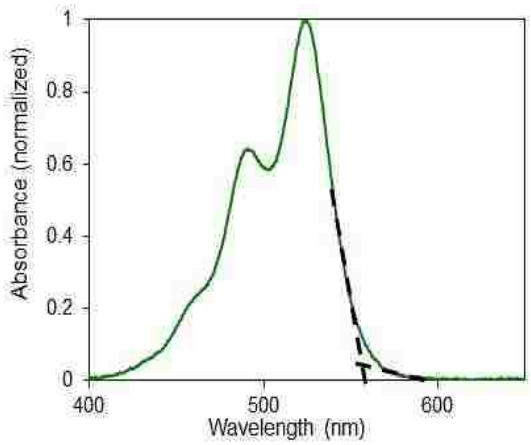

Figure 2.11 Absorption spectra of PIC-based GUMBOS in acetonitrile (30 μM) used to determine the onset wavelength (λ_{onset}).

Table 2.3 Redox potentials and band gap of PIC-based GUMBOS obtained from UV-Vis absorption

Dyes	E_{ox}[a] (V)	$E_{0\text{-}0}$[a] (V)	E^*_{red}[b] (V)	HOMO[c] (eV)	LUMO[c] (eV)	E_g (eV)
PICl	1.30	2.33	-1.03	-5.53	-3.23	2.24
[PIC][NTf_2]	1.29	2.32	-1.02	-5.50	-3.25	2.23
[PIC][BETI]	1.31	2.32	-1.02	-5.56	-3.24	2.22

[a]The potentials were reported as V vs NHE. [b]The excited state reduction potential was obtained by equation $E^*_{red} = E_{ox} - E_{0-0}$ [c]The LUMO value was calculated by equation $E_{LUMO}(eV) = E_{HOMO} + E_g$.

The electrochemical properties of the PIC-based GUMBOS suggested the potential application of these solutions, and possibly the nanoGUMBOS, in dye-sensitized solar cells (DSSCs). Ideal dye sensitizers should absorb photons over a wide range, particularly in the wavelength maximum of solar irradiance. It should also possess a closely matched excited state and TiO_2 conduction band energy as well as a positive redox potential to overcome possible recombination and reduce loss of efficiency throughout the cell.[53] Using an energy level scheme of a DSSC (Figure 2.12), the GUMBOS presented favorable electron injection from the excited state of the dye to the conduction band of a titanium dioxide semiconductor with a potential of -0.5 V vs NHE. These features also indicated the ability for regeneration of the oxidized dye from an iodide/triiodie redox couple electrolyte with a potential of 0.4 V vs NHE.

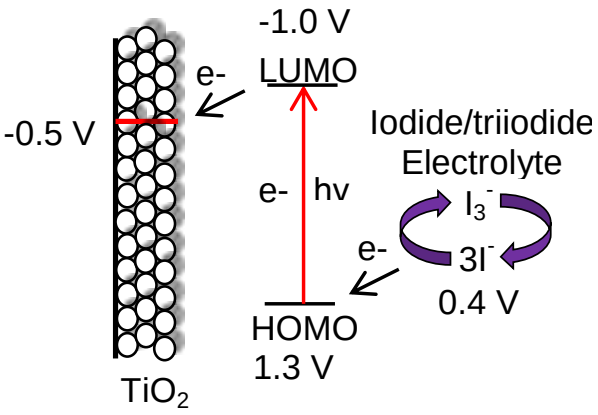

Figure 2.12 Energy level schematic of PIC-based GUMBOS in a DSSC reported as V vs NHE.

2.4 Conclusions

We have successfully demonstrated, for the first time, a novel template-free approach to controlling the morphology and aggregation in nanomaterials by simple variation of the counteranion. The J-aggregation of [PIC][NTf_2] with diamond-like nanostructures induced 590 times enhancement in fluorescence intensity and two orders of magnitude enhancement in fluorescence quantum yield as compared to the parent compound. This work is considered a significant contribution towards controlling the morphology of fluorescent organic nanomaterials. [PIC][NTf_2] nanoGUMBOS also exhibited high birefringence that can enhance the potential application of these nanomaterials. Examination of [PIC][BETI] nanoGUMBOS reflects the presence of H-aggregation with strong and broad blue shifted absorption. The [PIC][BETI] nanorods also revealed low birefringence and one order of magnitude enhancement in fluorescence quantum yield as compared to the parent compound. It is evident from the present study that the counterion associated with the dye cation can govern the morphology, as well as the spectral and optical properties of the nanomaterials. The broadness of the absorption spectra encompassing the visible and near infrared regions

emphasizes the possible use of these nanomaterials as photosensitizers in solar cells. Investigation of the electrochemical properties of the PIC-based GUMBOS displayed potentials that may be beneficial for further applications as photosensitizers in solar cells. We believe that the template-free controlled morphology of PIC-based nanoGUMBOS opens a new direction in the field of low-dimensional nanomaterials. These classes of nanomaterials may be potential candidates for applications as dye sensitizers in photovoltaics, nanosensors, optical waveguides, and optoelectronic devices, some of which are currently under investigation.

2.5 References

1. Menard, E.; Meitl, M. A.; Sun, Y. G.; Park, J. U.; Shir, D. J. L.; Nam, Y. S.; Jeon, S.; Rogers, J. A., Micro- and nanopatterning techniques for organic electronic and optoelectronic systems. *Chem. Rev.* **2007,** *107* (4), 1117-1160.

2. An, B. K.; Gihm, S. H.; Chung, J. W.; Park, C. R.; Kwon, S. K.; Park, S. Y., Color-Tuned Highly Fluorescent Organic Nanowires/Nanofabrics: Easy Massive Fabrication and Molecular Structural Origin. *J. Am. Chem. Soc.* **2009,** *131* (11), 3950-3957.

3. Zhao, Y. S.; Zhan, P.; Kim, J.; Sun, C.; Huang, J. X., Patterned Growth of Vertically Aligned Organic Nanowire Waveguide Arrays. *ACS Nano* **2010,** *4* (3), 1630-1636.

4. Zhao, Y. S.; Xu, J. J.; Peng, A. D.; Fu, H. B.; Ma, Y.; Jiang, L.; Yao, J. N., Optical waveguide based on crystalline organic microtubes and microrods. *Angew. Chem.-Int. Edit.* **2008,** *47* (38), 7301-7305.

5. Bao, Q. L.; Goh, B. M.; Yan, B.; Yu, T.; Shen, Z. A.; Loh, K. P., Polarized Emission and Optical Waveguide in Crystalline Perylene Diimide Microwires. *Adv. Mater.* **2010,** *22* (33), 3661-3666.

6. Samuel, I. D. W.; Turnbull, G. A., Organic semiconductor lasers. *Chem. Rev.* **2007,** *107* (4), 1272-1295.

7. Katz, H. E., Recent advances in semiconductor performance and printing processes for organic transistor-based electronics. *Chem. Mat.* **2004,** *16* (23), 4748-4756.

8. An, B. K.; Kwon, S. K.; Jung, S. D.; Park, S. Y., Enhanced emission and its switching in fluorescent organic nanoparticles. *J. Am. Chem. Soc.* **2002,** *124* (48), 14410-14415.

9. Zhao, Y. S.; Fu, H. B.; Peng, A. D.; Ma, Y.; Liao, Q.; Yao, J. N., Construction and Optoelectronic Properties of Organic One-Dimensional Nanostructures. *Accounts Chem. Res.* **2010,** *43* (3), 409-418.

10. Ujiiye-Ishii, K.; Kwon, E.; Kasai, H.; Nakanishi, H.; Oikawa, H., Methodological features of the emulsion and reprecipitation methods for organic nanocrystal fabrication. *Cryst. Growth Des.* **2008,** *8* (2), 369-371.

11. Wang, M. M.; Silva, G. L.; Armitage, B. A., DNA-templated formation of a helical cyanine dye J-aggregate. *J. Am. Chem. Soc.* **2000,** *122* (41), 9977-9986.

12. Dahne, L., Self-organization of polymethine dyes in thin solid layers. *J. Am. Chem. Soc.* **1995,** *117* (51), 12855-12860.

13. Spillmann, C. M.; Naciri, J.; Anderson, G. P.; Chen, M. S.; Ratna, B. R., Spectral Tuning of Organic Nanocolloids by Controlled Molecular Interactions. *ACS Nano* **2009,** *3* (10), 3214-3220.

14. Gesquiere, A. J.; Uwada, T.; Asahi, T.; Masuhara, H.; Barbara, P. F., Single molecule spectroscopy of organic dye nanoparticles. *Nano Lett.* **2005,** *5* (7), 1321-1325.

15. Kasai, H.; Kamatani, H.; Okada, S.; Oikawa, H.; Matsuda, H.; Nakanishi, H., Size-dependent colors and luminescences of organic microcrystals. *Jpn. J. Appl. Phys. 2* **1996,** *35* (2B), L221-L223.

16. Kasai, H.; Oikawa, H.; Okada, S.; Nakanishi, H., Crystal growth of perylene microcrystals in the reprecipitation method. *Bull. Chem. Soc. Jpn* **1998,** *71* (11), 2597-2601.

17. Davydov, A. S., *Theory of Molecular Excitons*. McGraw-Hill: New York, 1962.

18. Kasha, M.; Rawls, H. R.; Ashraf El-Bayoumi, M., The Exciton Model in Molecular Spectroscopy. *Pure Appl Chem* **1965,** *11*, 371-392.

19. Tong, H.; Hong, Y. N.; Dong, Y. Q.; Haussler, M.; Lam, J. W. Y.; Li, Z.; Guo, Z. F.; Guo, Z. H.; Tang, B. Z., Fluorescent "light-up" bioprobes based on tetraphenylethylene derivatives with aggregation-induced emission characteristics. *Chem. Commun.* **2006,** (35), 3705-3707.

20. Tong, H.; Hong, Y. N.; Dong, Y. Q.; Haeussler, M.; Li, Z.; Lam, J. W. Y.; Dong, Y. P.; Sung, H. H. Y.; Williams, I. D.; Tang, B. Z., Protein detection and quantitation

by tetraphenylethene-based fluorescent probes with aggregation-induced emission characteristics. *J. Phys. Chem. B* **2007,** *111* (40), 11817-11823.

21. Dong, Y. Q.; Lam, J. W. Y.; Qin, A. J.; Liu, J. Z.; Li, Z.; Tang, B. Z., Aggregation-induced emissions of tetraphenylethene derivatives and their utilities as chemical vapor sensors and in organic light-emitting diodes. *Appl. Phys. Lett.* **2007,** *91* (1), 1-3.

22. Wang, M.; Zhang, G. X.; Zhang, D. Q.; Zhu, D. B.; Tang, B., Fluorescent bio/chemosensors based on silole and tetraphenylethene luminogens with aggregation-induced emission feature. *J. Mater. Chem.* **2010,** *20* (10), 1858-1867.

23. Das, S.; Bwambok, D.; Ei-Zahab, B.; Monk, J.; de Rooy, S. L.; Challa, S.; Li, M.; Hung, F. R.; Baker, G. A.; Warner, I. M., Nontemplated Approach to Tuning the Spectral Properties of Cyanine-Based Fluorescent NanoGUMBOS. *Langmuir* **2010,** *26* (15), 12867-12876.

24. Jelley, E. E., Spectral absorption and fluorescence of dyes in the molecular state. *Nature* **1936,** *138*, 1009-1010.

25. Scheibe, G.; Rivas, A., A new method in quantitive emission spectral analysis adaptable also as a micro method. *Angew. Chem.* **1936,** *49*, 0443-0446.

26. Mobius, D., Scheibe Aggregates. *Adv. Mater.* **1995,** *7* (5), 437-444.

27. Slavnova, T. D.; Gorner, H.; Chibisov, A. K., J-aggregation of anionic ethyl meso-Thiacarbocyanine dyes induced by binding to proteins. *J. Phys. Chem. B* **2007,** *111* (33), 10023-10031.

28. Mishra, A.; Behera, R. K.; Behera, P. K.; Mishra, B. K.; Behera, G. B., Cyanines during the 1990s: A review. *Chem. Rev.* **2000,** *100* (6), 1973-2011.

29. Lim, I. I. S.; Goroleski, F.; Mott, D.; Kariuki, N.; Ip, W.; Luo, J.; Zhong, C. J., Adsorption of cyanine dyes on gold nanoparticles and formation of J-aggregates in the nanoparticle assembly. *J. Phys. Chem. B* **2006,** *110* (13), 6673-6682.

30. Kumar, V.; Baker, G. A.; Pandey, S., Ionic liquid-controlled J- versus H-aggregation of cyanine dyes. *Chem. Commun.* **2011,** *47* (16), 4730-4732.

31. Kirstein, S.; Daehne, S., J-aggregates of amphiphilic cyanine dyes: Self-organization of artificial light harvesting complexes. *Int. J. Photoenergy* **2006**, 1-21.

32. Lebedenko, A. N.; Guralchuk, G. Y.; Sorokin, A. V.; Yefimova, S. L.; Malyukin, Y. V., Pseudoisocyanine J-aggregate to optical waveguiding crystallite transition:

Microscopic and microspectroscopic exploration. *J. Phys. Chem. B* **2006,** *110* (36), 17772-17775.

33. Ou, Z. M.; Yao, H.; Kimura, K., Organic nanoparticles of cyanine dye in aqueous solution. *Bull. Chem. Soc. Jpn.* **2007,** *80* (2), 295-302.

34. Peyratout, C. S.; Mohwald, H.; Dahne, L., Preparation of photosensitive dye aggregates and fluorescent nanocrystals in microreaction containers. *Adv. Mater.* **2003,** *15* (20), 1722-1726.

35. Bwambok, D. K.; El-Zahab, B.; Challa, S. K.; Li, M.; Chandler, L.; Baker, G. A.; Warner, I. M., Near-Infrared Fluorescent NanoGUMBOS for Biomedical Imaging. *ACS Nano* **2009,** *3* (12), 3854-3860.

36. Tesfai, A.; El-Zahab, B.; Kelley, A. T.; Li, M.; Garno, J. C.; Baker, G. A.; Warner, I. M., Magnetic and Nonmagnetic Nanoparticles from a Group of Uniform Materials Based on Organic Salts. *ACS Nano* **2009,** *3* (10), 3244-3250.

37. Lakowicz, J. R., *Principles of Fluorescence Spectroscopy*. 3 ed.; Springer: New York, 2006.

38. Huang, L. W.; Liao, Q.; Shi, Q.; Fu, H. B.; Ma, J. S.; Yao, J. N., Rubrene micro-crystals from solution routes: their crystallography, morphology and optical properties. *J. Mater. Chem.* **2010,** *20* (1), 159-166.

39. Wang, J.; Zhao, Y. F.; Zhang, J. H.; Zhang, J. Y.; Yang, B.; Wang, Y.; Zhang, D. K.; You, H.; Ma, D. G., Assembly of one-dimensional organic luminescent nanowires based on quinacridone derivatives. *J. Phys. Chem. C* **2007,** *111* (26), 9177-9183.

40. Stegemeyer, H.; Stockel, F., Anisotropic structures in aqueous solutions of aggregated pseudoisocyanine dyes. *Ber. Bunsen-Ges. Phys. Chem.* **1996,** *100* (1), 9-14.

41. Yao, H.; Domoto, K.; Isohashi, T.; Kimura, K., In situ detection of birefringent mesoscopic H and J aggregates of thiacarbocyanine dye in solution. *Langmuir* **2005,** *21* (3), 1067-1073.

42. von Berlepsch, H.; Bottcher, C.; Dahne, L., Structure of J-aggregates of pseudoisocyanine dye in aqueous solution. *J. Phys. Chem. B* **2000,** *104* (37), 8792-8799.

43. Eisfeld, A.; Briggs, J. S., The J-band of organic dyes: lineshape and coherence length. *Chem. Phys.* **2002,** *281* (1), 61-70.

44. Knapp, E. W., Lineshapes of Molecular Aggregates- Exchange Narrowing and Intersite Correlation. *Chem. Phys.* **1984,** *85* (1), 73-82.

45. Chen, J. W.; Law, C. C. W.; Lam, J. W. Y.; Dong, Y. P.; Lo, S. M. F.; Williams, I. D.; Zhu, D. B.; Tang, B. Z., Synthesis, light emission, nanoaggregation, and restricted intramolecular rotation of 1,1-substituted 2,3,4,5-tetraphenylsiloles. *Chem. Mat.* **2003,** *15* (7), 1535-1546.

46. Guralchuk, G. Y.; Katrunov, I. K.; Grynyov, R. S.; Sorokin, A. V.; Yefimova, S. L.; Borovoy, I. A.; Malyukin, Y. V., Anomalous surfactant-induced enhancement of luminescence quantum yield of cyanine dye J-aggregates. *J. Phys. Chem. C* **2008,** *112* (38), 14762-14768.

47. Sanchez-Galvez, A.; Hunt, P.; Robb, M. A.; Olivucci, M.; Vreven, T.; Schlegel, H. B., Ultrafast radiationless deactivation of organic dyes: Evidence for a two-state two-mode pathway in polymethine cyanines. *Journal of the American Chemical Society* **2000,** *122* (12), 2911-2924.

48. Jones, G.; Oh, C., Photophysical and Electron-Transfer Properties of Pseudoisocyanine in the Hydrophobic Microdomain of an Aqueous Polyelectrolyte. *J. Phys. Chem.* **1994,** *98* (9), 2367-2376.

49. Belfield, K. D.; Bondar, M. V.; Hernandez, F. E.; Przhonska, O. V.; Yao, S., Two-photon absorption of a supramolecular pseudoisocyanine J-aggregate assembly. *Chem. Phys.* **2006,** *320* (2-3), 118-124.

50. Shi, X.; Basran, J.; Seward, H. E.; Childs, W.; Bagshaw, C. R.; Boxer, S. G., Anomalous Negative Fluorescence Anisotropy in Yellow Fluorescent Protein (YFP 10C): Quantitative Analysis of FRET in YFP Dimers. *Biochemistry* **2007,** *46* (50), 14403-14417.

51. Liang, M.; Wang, Z.-Y.; Zhang, L.; Han, H.-Y.; Sun, Z.; Xue, S., New organic photosensitizers incorporating carbazole and dimethylarylamine moieties for dye-sensitized solar cells. *Renew. Energ.* **2011,** *36* (10), 2711-2716.

52. Tacca, A.; Po, R.; Caldararo, M.; Chiaberge, S.; Gila, L.; Longo, L.; Mussini, P. R.; Pellegrino, A.; Perin, N.; Salvalaggio, M.; Savoini, A.; Spera, S., Ternary thiophene-X-thiophene semiconductor building blocks (X = fluorene, carbazole, phenothiazine): Modulating electronic properties and electropolymerization ability by tuning the X core. *Electrochim. Acta* **2011,** *56* (19), 6638-6653.

53. Gratzel, M., Conversion of sunlight to electric power by nanocrystalline dye-sensitized solar cells. *J. Photochem. Photobiol. A-Chem.* **2004,** *164* (1-3), 3-14.

CHAPTER 3
NEAR-INFRARED EMITTING BINARY NANOMATERIALS

3.1 Introduction

Nanomaterials, ranging from 1 to 100 nm, have gained considerable attention as compared to bulk materials due to higher surface area to volume ratios that result in distinct physiochemical properties. Research on such significant properties has led to innovative applications of engineered nanomaterials in areas such as medicine,[1,2] electronics,[3] and energy.[4,5] In particular, the use of organic nanomaterials to tune emission is of interest due to use in applications for sensing, optoelectronics, and light harvesting systems.

A common approach to tuning the emission spectra is based on Förster resonance energy transfer (FRET). This non-radiative process involves the transfer of energy from donor molecules in the excited state to acceptor molecules in the ground state.[6] The extent of FRET is dependent on the overlap of the donor emission spectrum and acceptor absorption spectrum, as well as the distance between the donor and acceptor. In this regard, Yao and coworkers have examined the use of organic nanomaterials to tune emission via FRET.[7,8,9] It was found that the energy transfer efficiencies of the nanomaterials were dependent on the molar ratios of the donor and acceptor molecules. These binary organic nanomaterials have demonstrated potential as candidates for applications in electroluminescent, optoelectronic, and sensing devices.

As previously mentioned, our group has reported the formation of nanomaterials derived from a class of materials referred to as **g**roup of **u**niform **m**aterials **b**ased on **o**rganic **s**alts (GUMBOS).[10] These GUMBOS can be tailored for multiple functions

based on the selected cations and anions. In addition, nanomaterials derived from GUMBOS (nanoGUMBOS) can also afford interesting physiochemical properties. Thus far, these nanoGUMBOS have offered potential as candidates for biomedical,[10] antibacterial,[14] sensing,[15] optoelectronic,[16,17] and light harvesting[18,19,20] applications.

Several studies have been reported which involve the formation of nanoGUMBOS using cyanine dyes that form aggregates by self-assembly. Bwambok *et al.* initially observed that nanoGUMBOS containing heptamethine cyanine dye 1,1',3,3,3',3'-hexamethylindotricarbocyanine (HMT) iodide resulted in a broad absorption spectrum and slight shift in the fluorescence emission spectrum as compared to GUMBOS in solution.[11] These changes in the spectral properties were attributed to aggregation of the cationic near-infrared (NIR) dye. In addition, nanomaterials of the NIR fluorescent compound were employed as contrasting agents for biomedical imaging applications. In a subsequent study by Das *et al.*, variation of the anions paired with HMT was found to produce controlled aggregation and spectral properties.[18] The results further suggest the presence of aggregation, specifically of both J- and H- aggregates in different proportions. More recently, de Rooy *et al.* have reported the formation of nanostructures derived from thiacarbocyanine-based GUMBOS of increasing methine chain lengths.[19] Aggregation of these binary and ternary nanomaterials produced tunable fluorescence emission attributed to FRET.

Aggregation is the self-assembly of molecules as a result of forces such as van der Waals, hydrogen bonding, π-π stacking, and cation-π interactions. This self-assembly of molecules with such intermolecular interactions has been found to yield different types of aggregates leading to viable spectral properties. Such aggregation

behavior has been well-studied by Davydov *et al.*[21] and Kasha *et al.*[22] Specifically, head-to-tail stacking of molecules results in the formation of J-aggregates that are generally characterized by a narrow, bathochromatically (red) shifted absorption band and enhanced fluorescence as compared to monomeric species. In contrast, molecules stacked in a card-pack manner are referred to as H-aggregates. Such H-aggregates are typically characterized by a broad, hypsochromatically (blue) shifted absorption band with weak to no fluorescence. Molecules have also been found to form randomly-oriented aggregates without any specific order of stacking that exhibit spectral properties similar to the monomer.

In our previous work, pseudoisocyanine (PIC)-based nanoGUMBOS have been studied that exhibit controlled morphology and spectral properties at low concentration (30 μM) by simple variation of the counteranion.[20] This behavior was attributed to the presence of J- and H-aggregates. In the present work, PIC-based GUMBOS, the shortest methine chain length, and increased methine chain length cyanine-based GUMBOS were synthesized and investigated as binary nanomaterials. In these binary nanomaterials, previously studied PIC-based GUMBOS were selected as donor molecules due to enhanced emission within nanoGUMOBS, while increased methine chain cyanine-based GUMBOS were used as acceptor molecules. Interestingly, the higher methine chain cyanine-based nanoGUMBOS were essentially non-fluorescent in an aqueous environment. However, these materials were found to exhibit significant fluorescence as binary nanoGUMBOS which were attributed to the occurrence of FRET. The binary nanomaterials were found to have broad absorption and fluorescence emission extended to the near-infrared region by tuning the molar ratio. In addition,

stability and electrochemical properties of these GUMBOS were also examined for potential use of these new materials for light harvesting and optoelectronic applications.

3.2 Materials and Methods

3.2.1 Materials

1,1'-diethyl-2,2'-cyanine iodide or pseudoisocyanine (PIC), 1,1'-diethyl-2,2'-carbocyanine iodide or pinacyanol (PC), 1,1'-diethyl-2,2'-dicarbocyanine (DD) iodide, and lithium bis(trifluoromethanesulfonyl)imide (99.95%) were purchased from Sigma Aldrich and used as received. Lithium bis(perfluoroethylsulfonyl)imide was obtained from 3M. Ethanol was purchased from Pharmaco-AAPER and used as received. Ultrapure water (18.2 MΩ cm) was used from Aries High Purity Water System. A BRANSON 3510RDTH model bath ulstrasonicator (335W, 40kHz frequency) was used at room temperature for syntheses of nanoGUMBOS. Carbon-coated copper grids (CF400-Cu, Electron Microscopy Sciences, Hatfield, PA) were used for TEM imaging.

3.2.2 Syntheses of Cyanine-based GUMBOS and NanoGUMBOS

Cyanine-based GUMBOS were synthesized by an anion exchange reaction of pseudoisocyanine (PIC) iodide, pinacyanol (PC) iodide, and 1,1'-diethyl-2,2'-dicarbocyanine (DD) iodide with lithium bis(trifluoromethanesulfonyl)imide ($LiNTf_2$) and lithium bis(perfluoroethylsulfonyl)imide (LiBETI) using a method previously reported (Figure 3.1).[20] Binary nanomaterials were prepared for each anion by use of PIC GUMBOS as donors and increased methine chain GUMBOS (PC and DD) as acceptors. Different molar ratios of binary GUMBOS were prepared by keeping PIC donor GUMBOS constant while varying PC or DD GUMBOS. NanoGUMBOS were formed by use of a reprecipitation method in which 150 µL of the mixture of GUMBOS

was added to 5 mL of DI water under sonication for 5 min. This procedure was also used for synthesis of individual cyanine-based nanoGUMBOS.

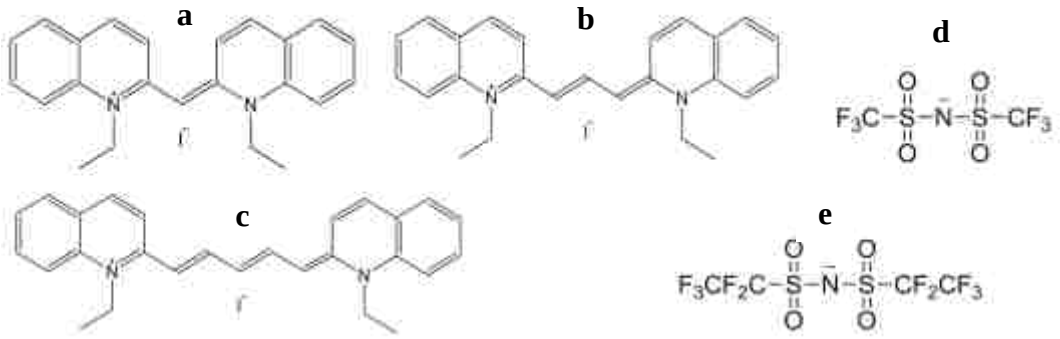

Figure 3.1 Chemical structures of parent compounds (a) PICI, (b) PCI, (c) DDI, and anions (d) NTf_2^- and (e) $BETI^-$.

3.2.3 Microscopy Characterization of NanoGUMBOS

Electron micrographs were obtained for characterization of size and morphology using a JEOL100CX transmission electron microscope (JEOL USA, Inc., Peabody, MA). An aliquot (5 µL) of nanoGUMBOS was dropcasted onto a carbon-coated copper grid and air dried at room temperature.

3.2.4 Absorption and Fluorescence Studies of GUMBOS and NanoGUMBOS

Absorbance measurements were obtained using a Shimadzu UV-3101PC UV-Vis-NIR scanning spectrometer (Shimadzu, Columbia, MD) at room temperature with a slitwidth of 2 nm. Fluorescence emission was performed on a Spex Fluorolog-3 spectrofluorometer (model FL3-22TAU3; Jobin Yvon, Edison, NJ) at room temperature with slitwidths of 5 nm. A 0.4 cm quartz cuvet (Starna Cells) was used to collect the absorbance and fluorescence measurements. A second 0.4 cm quartz cuvet was filled with water for use as a control blank. Fluorescence studies were all performed through

adoption of a synchronous scan protocol with right angle geometry. Fluorescence spectra were corrected for inner filter effects using a standard formula.[6]

3.2.5 Stability Studies of GUMBOS and NanoGUMBOS

Photostability of individual and binary nanoGUMBOS was examined in aqueous suspension by use of fluorescence spectroscopy. Each sample was excited at an excitation wavelength of 524 nm for 3000 s with wide slitwidths of 14 nm. Photostability of [PIC][BETI] and [PIC][NTf_2] nanoGUMBOS was based on specific emission wavelength maximum of 575 nm and 590 nm, respectively. Photostability of binary nanoGUMBOS was examined at an emission wavelength of 670 nm.

Thermal stability of the cyanine-based GUMBOS was investigated by use of thermograviometric analysis. Samples were measured under nitrogen at a rate of 10 °Cmin^{-1} with a temperature range from 23°C up to 600°C. Thermal decomposition of the cyanine-based GUMBOS started between 255°C and 325°C (Table 3.1).

Table 3.1 Thermal decomposition of cyanine-based GUMBOS

GUMBOS	T_{start} (°C)	T_{onset} (°C)
[PIC][NTf_2]	–	355
[PIC][BETI]	–	353
[PC][NTf_2]	325	370
[PC][BETI]	323	362
[DD][NTf_2]	248	363
[DD][BETI]	275	369

The onset temperatures (T_{onset}), at which samples lose weight at a faster speed, ranged from 353°C to 370°C. Overall, these results suggest that cyanine-based GUMBOS have good thermal stability.

3.2.6 Electrochemical Studies of GUMBOS

Electrochemical measurements were performed under anaerobic conditions using an Autolab PGSTAT 302 potentiostat from Eco. Chemie. A three-electrode

system consisting of an Ag/Ag^+ reference electrode, Pt working electrode, and Pt counter electrode was employed. Measurements were conducted in acetonitrile with 0.1 M tetrabutylammonium hexafluorophosphate ($TBAPF_6$) as a supporting electrolyte and ferrocene (Fc^+/Fc) as an internal reference having a formal potential of 0.63 V vs NHE.

3.3 Results and Discussion

3.3.1 Morphological Studies of Individual Cyanine-based NanoGUMBOS

Examination of TEM micrographs of cyanine-based nanoGUMBOS resulted in varying morphologies (Figure 3.2). The distinct diamond-like structure was found to exhibit an average respective length and width of 449 ± 96 nm and 241 ± 63 nm. The nanorods of [PIC][BETI] presented an average length and width of 1.6 ± 0.98 µm and 153 ± 55 nm, respectively. The dimensions of these nanoGUMBOS were similar to values previously reported, except for the width of [PIC][BETI]. This change in morphology was attributed to ordered molecular orientation as a function of the associated counteranion.[20] Nanomaterials of increased methine chain lengths afforded similar morphologies of nanowires and nanorods based on the selected anion. The [PC][NTf_2] and [DD][NTf_2] nanoGUMBOS formed nanowires with respective average lengths and widths of 402 ± 117 nm and 27 ± 7.3 nm for [PC][NTf_2] and 275 ± 67 nm and 24 ± 9.8 nm for [DD][NTf_2]. In contrast, [PC][BETI] nanoGUMBOS were found to have a continuous nanowire network with a width of 46 ± 8.1 nm. Moreover, [DD][BETI] nanoGUMBOS resulted in elongated nanorods with respective average lengths and widths of 11 ± 2.1 µm and 287 ± 120 nm.

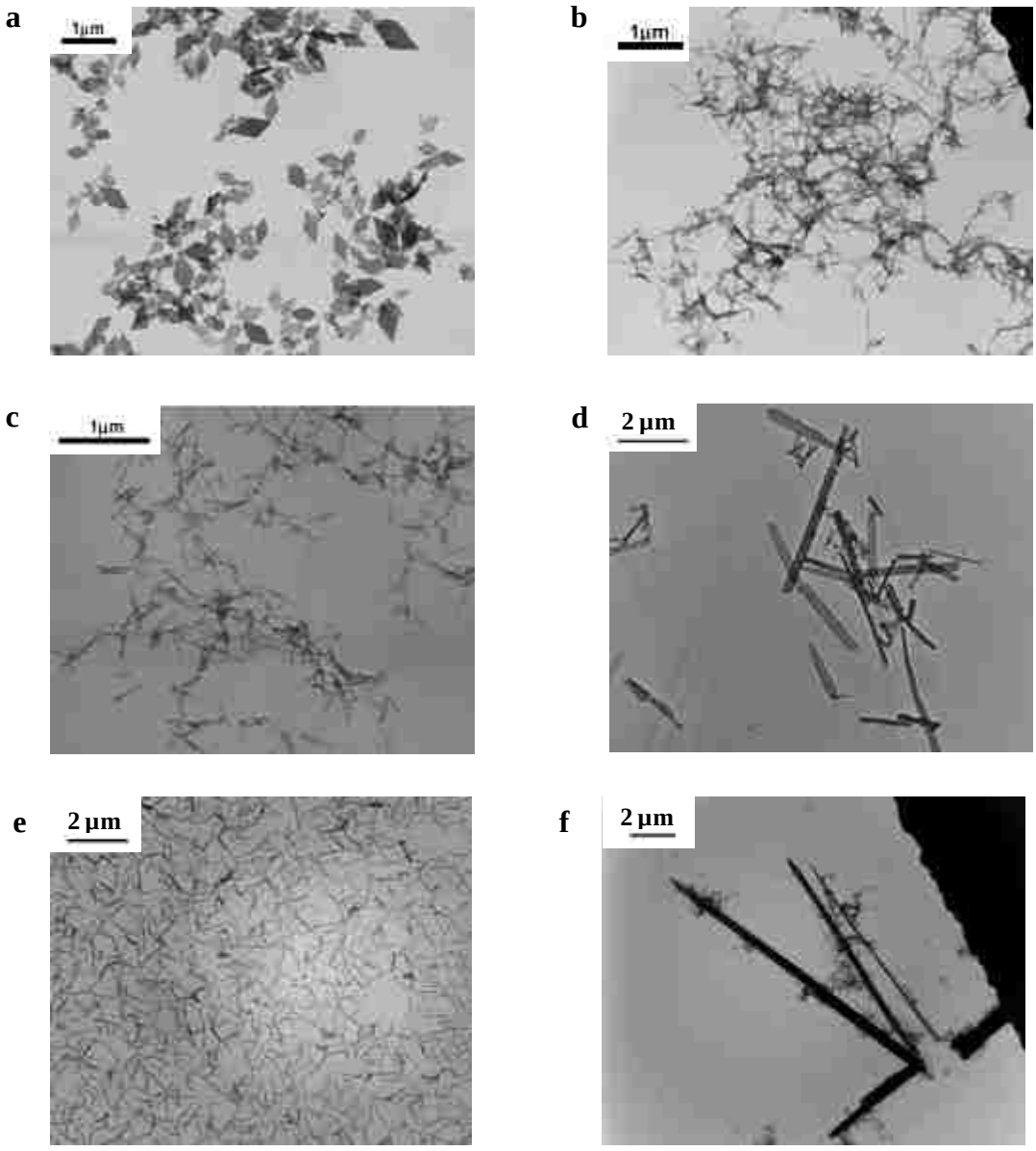

Figure 3.2 TEM micrographs of (a) [PIC][NTf_2], (b) [PC][NTf_2], (c) [DD][NTf_2], (d) [PIC][BETI], (e) [PC][BETI], and (f) [DD][BETI] nanoGUMBOS.

3.3.2 Spectral Properties of Individual Cyanine-based NanoGUMBOS

Examination of absorption spectra of cyanine-based nanoGUMBOS resulted in a distinct change in aqueous dispersion as compared to cyanine-based GUMBOS in ethanolic solution. Absorption spectra of cyanine-based GUMBOS in ethanolic solution were found to exhibit red shifted absorption peaks as the methine chain length increased (Figure 3.3). Specifically, absorption peaks of 490 nm and 524 nm for PIC

GUMBOS, 564 nm and 605 nm for PC GUMBOS, as well as 652 nm and 710 nm for DD GUMBOS were obtained. It is important to note that this shift to longer wavelengths was independent of the associated anion.

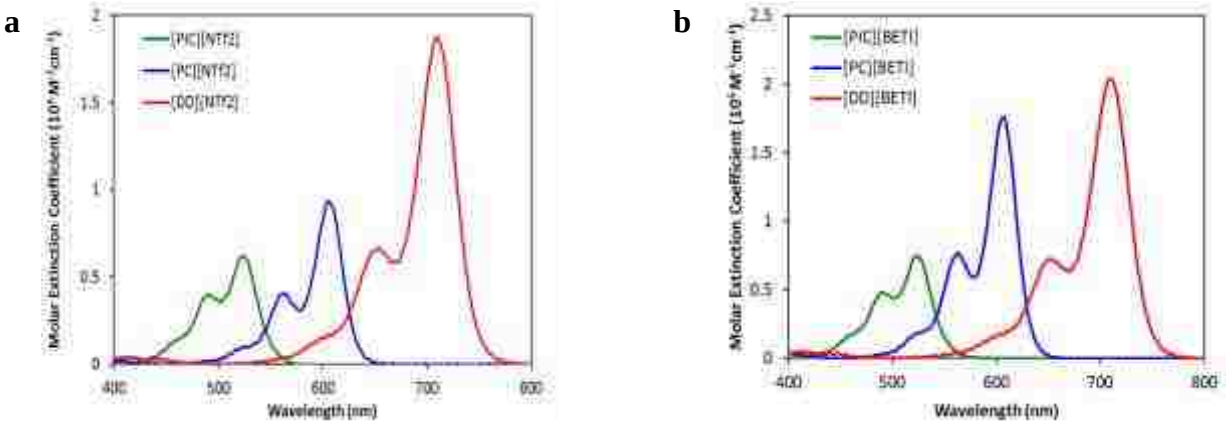

Figure 3.3 Absorption spectra of (a) NTf_2^- anion and (b) $BETI^-$ anion cyanine-based GUMBOS in ethanolic solution.

In contrast, absorption spectra of cyanine-based nanoGUMBOS resulted in broad absorption bands in aqueous dispersion that were dependent on both the methine chain length and associated anion (Figure 3.4). The [PIC][NTf_2] nanoGUMBOS were found to exhibit an absorption peak at 524 nm and a red shifted band at 590 nm, which is evidence of the formation of J-aggregates within the diamond-like nanostructures.[20] The absorption spectrum of [PC][NTf_2] nanoGUMBOS resulted in a blue shifted shoulder and peak at 490 and 550 nm, respectively. Conversely, longer wavelength and less intense absorption were observed for [DD][NTf_2] nanoGUMBOS with multiple peaks at 550, 650, and 695 nm. Interestingly, [PIC][BETI] and [PC][BETI] nanoGUMBOS were found to exhibit similar absorption spectra. The [PIC][BETI] nanoGUMBOS had absorption peaks at 490 and 524 nm, as well as a blue shifted peak at 450 nm with tail broadening in the longer wavelength region that were attributed to the formation of H-aggregates of the dye molecules within the nanorods.[20] The

absorption spectrum of [PC][BETI] nanoGUMBOS resulted in peaks at 595 and 640 nm. In contrast, [DD][BETI] nanoGUMBOS displayed broad absorption with peaks at 515 and 605 nm. Overall, a blue shift in the absorption spectra was observed for the individual cyanine-based nanoGUMBOS as compared to cyanine-based GUMBOS in ethanolic solution. This result was attributed to the formation of H-aggregates within the nanomaterials and is in agreement with studies of PCCl and DDI in aqueous solution.[23,24,25]

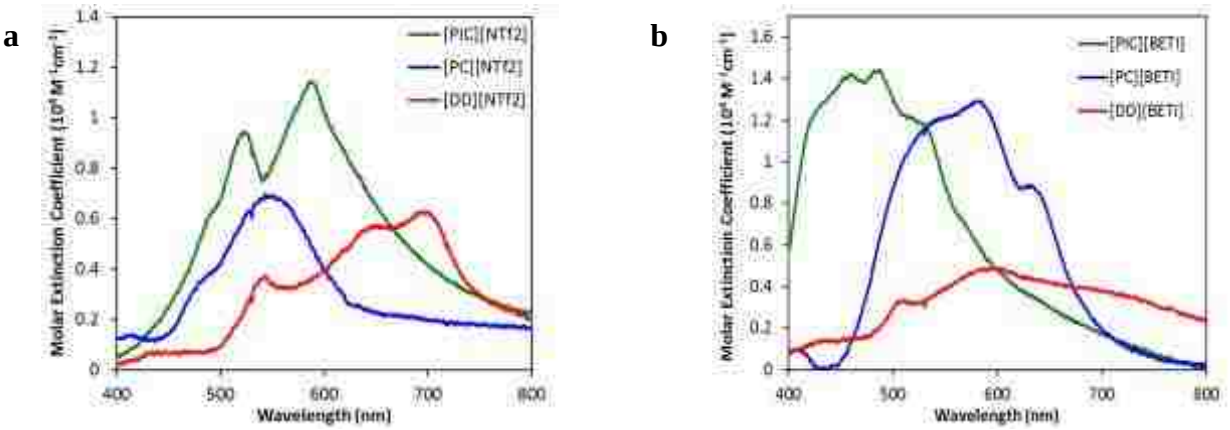

Figure 3.4 Absorption spectra of (a) NTf_2^- anion and (b) $BETI^-$ anion cyanine-based nanoGUMBOS in aqueous suspension.

Examination of fluorescence spectra was found to produce a distinct difference in the cyanine-based nanoGUMBOS with increasing methine chain length when excited at 524 nm (Figure 3.5). The [PIC][NTf_2] nanoGUMBOS resulted in a strong fluorescence peak at 590 nm, while nanoGUMBOS of [PIC][BETI] were found to exhibit a weaker fluorescence peak at ~577 nm. These PIC-based nanoGUMBOS of both anions also revealed a shoulder at 620 nm. This enhanced fluorescence of [PIC][NTf_2] nanoGUMBOS and weak fluorescence of [PIC][BETI] nanoGUMBOS, as compared to the parent compound of PICI in aqueous solution, were attributed to the formation of J- and H-aggregates, respectively.[20] In contrast, fluorescence spectra of increased

methine chain length cyanine-based nanoGUMBOS resulted in minimal fluorescence for both anions. The nanoGUMBOS of [PC][NTf_2], [DD][NTf_2], and [DD][BETI] were found to exhibit a nominal fluorescence peak at 630 nm. Furthermore, [PC][BETI] nanoGUMBOS were found to have a weak fluorescence at 702 nm. This little to no fluorescence confirms the formation of H-aggregates as observed in the absorption spectra.

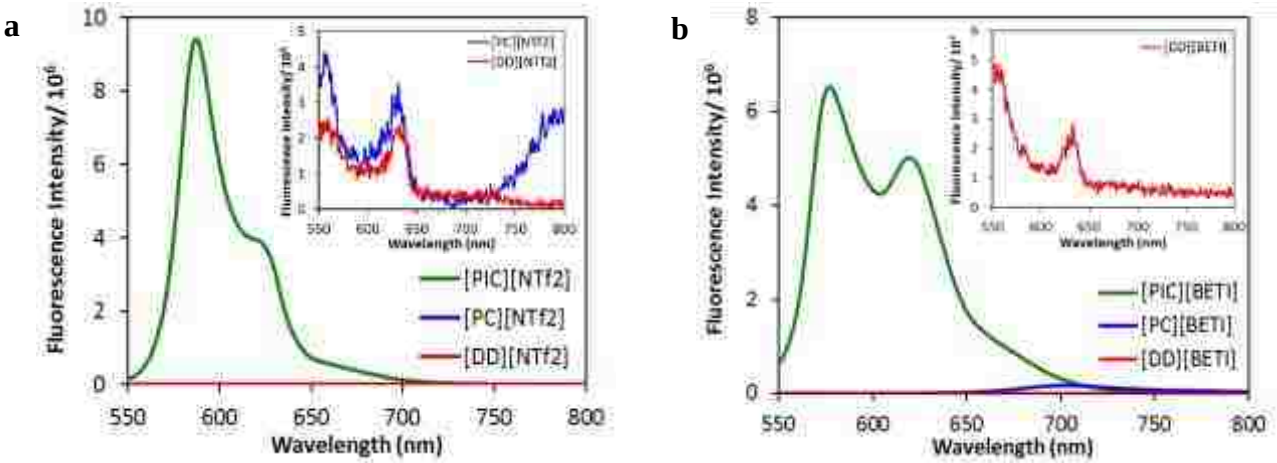

Figure 3.5 Fluorescence spectra of (a) NTf_2^- and (b) $BETI^-$ anion cyanine-based nanoGUMBOS in aqueous suspension when excited at 524 nm. Inset: Magnified fluorescence spectra of [PC][NTf_2] and [DD][NTf_2] shown in panel (a) and [DD][BETI] in panel (b).

3.3.3 Characterization Studies of Binary NanoGUMBOS

Binary nanoGUMBOS were prepared from GUMBOS with similar anions by use of PIC GUMBOS as donor molecules and increased methine chain PC and DD GUMBOS as acceptor molecules. At an equal molar ratio, morphology of the binary nanomaterials resulted in different nanostructures based on the associated anions (Figure 3.6). Binary nanoGUMBOS containing NTf_2^- as an anion, namely [PIC][NTf_2]:[PC][NTf_2] and [PIC][NTf_2]:[DD][NTf_2], were found to have similar formation of hexagonal-shaped nanostructures with an average diameters of 161 ± 119 nm and 260 ± 44 nm, respectively. This was a distinct change in morphology as compared to

the respective diamond-like nanostructures and nanowires of the individual cyanine-based nanoGUMBOS. In contrast, binary nanomaterials paired with $BETI^-$ anion afforded nanorod and nanowire structures. The [PIC][BETI]:[PC][BETI] nanoGUMBOS resulted in a network of nanorods with a respective average length and width of 2.2 ± 0.75 µm and 115 ± 33 nm. The [PIC][BETI]:[DD][BETI] nanoGUMBOS were found to exhibit nanowires with a respective average length and width of 1.5 ± 0.85 µm and 101 ± 37 nm. These nanostructures also varied from the morphology of the nanorods and nanowires of the individual cyanine-based nanoGUMBOS.

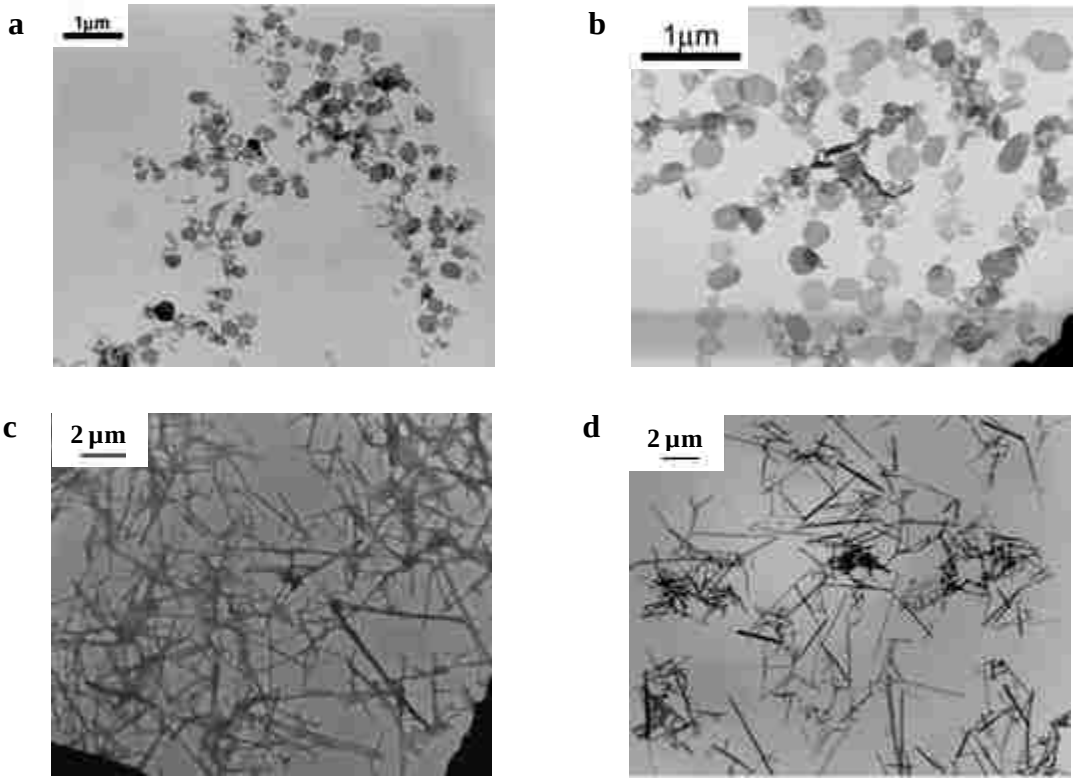

Figure 3.6 TEM micrographs of (a) [PIC][NTf_2]:[PC][NTf_2], (b) [PIC][NTf_2]:[DD][NTf_2], (c) [PIC][BETI]:[PC][BETI], and (d) [PIC][BETI]:[DD][BETI] binary nanomaterials at a 1:1 ratio.

3.3.4 Absorption Studies

Absorption spectra of the binary nanomaterials at varying molar ratios were found to have similar spectral behavior as the donor absorption spectra of PIC

nanoGUMBOS (Figure 3.7). Furthermore, additional absorption peaks were obtained for some of the binary nanoGUMBOS. In that regard, [PIC][NTf_2]:[PC][NTf_2] nanoGUMBOS resulted in a new absorption shoulder around 650 nm. Moreover, [PIC][BETI]:[PC][BETI] nanoGUMBOS were found to reveal absorption peaks for molar ratios of 1:1 and 10:1 at 595 and 640 nm resulting in further broadening of the absorption spectra. This broadening was attributed to the acceptor absorption spectra of individual [PC][BETI] nanoGUMBOS.

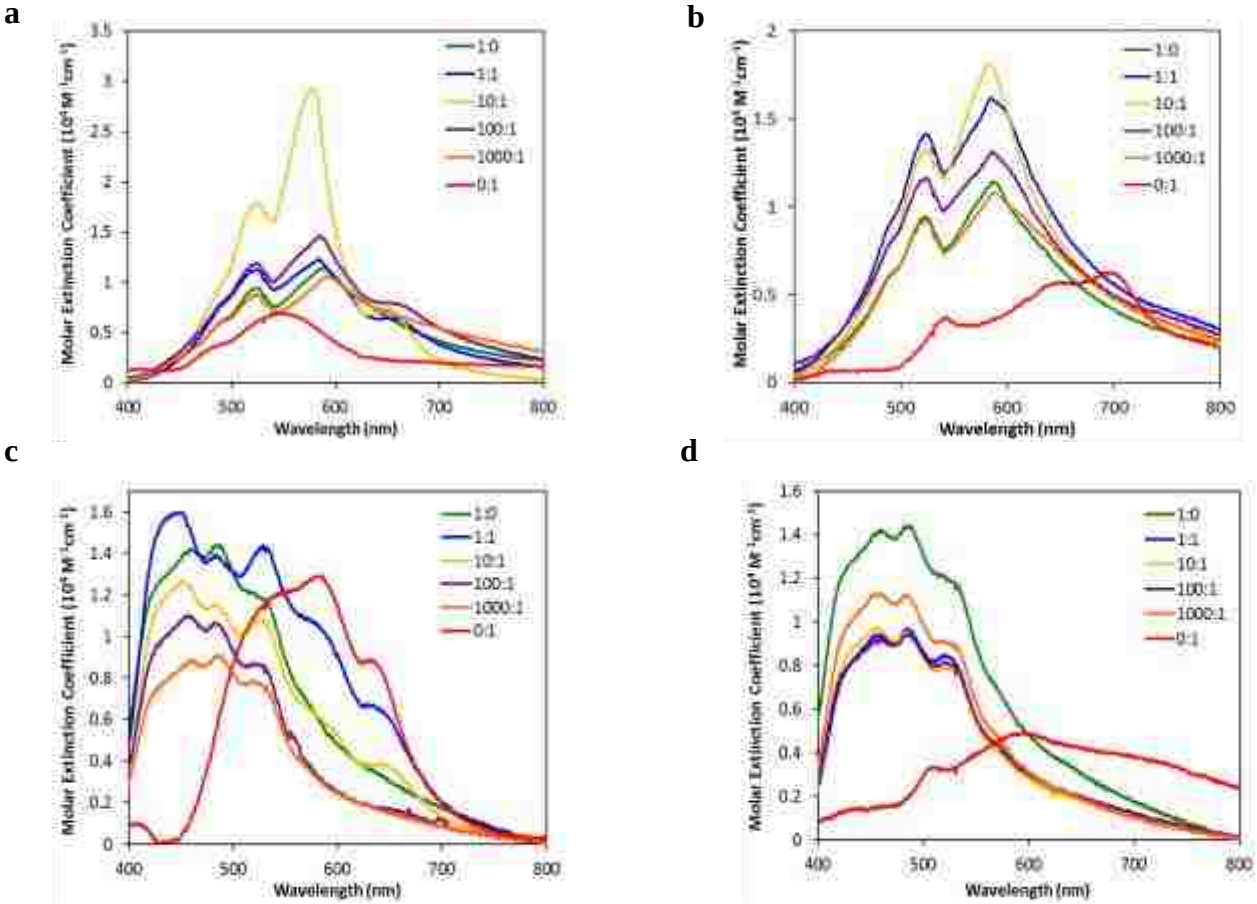

Figure 3.7 Absorption spectra of (a) [PIC][NTf_2]:[PC][NTf_2], (b) [PIC][NTf_2]:[DD][NTf_2], (c) [PIC][BETI]:[PC][BETI], and (d) [PIC][BETI]:[DD][BETI] binary nanoGUMBOS.

3.3.5 Fluorescence Studies

The donor emission and acceptor absorption spectra of cyanine-based nanoGUMBOS suggested the possibility of FRET due to overlap of the absorption and

fluorescence emission spectra (Figure 3.8). The spectral overlap integral (J(λ)) was determined using the following formula

$$J(\lambda) = \frac{\int_0^\infty \varepsilon(\lambda) f(\lambda) \lambda^4 d\lambda}{\int_0^\infty f(\lambda) d\lambda} \quad (1)$$

where ε is the molar extinction coefficient of the acceptor, f(λ) is the normalized emission spectrum of the donor, and λ is the wavelength. The energy transfer efficiency (E) was obtained using the following formula

$$E = 1 - \frac{F_{da}}{F_d} \quad (2)$$

where F_{da} and F_d are the fluorescence intensities of the donor in the presence and absence of the acceptor, respectively. The J(λ) and E values of the binary nanoGUMBOS at a 1:1 molar ratio are compiled in Table 3.2.

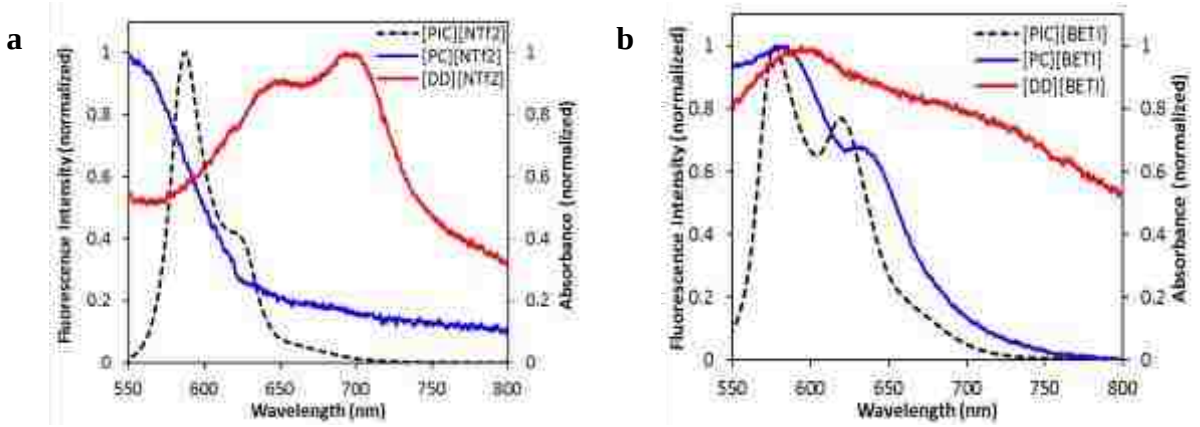

Figure 3.8 Normalized fluorescence (dashed) and absorption (solid) spectra of (a) NTf_2^- and (b) $BETI^-$ cyanine-based nanoGUMBOS in aqueous suspension.

Table 3.2 Spectral overlap integral (J(λ)) and energy transfer efficiency (E) of binary nanoGUMBOS at a 1:1 molar ratio

NanoGUMBOS	J(λ)/ $M^{-1}cm^{-1}nm^4$	E/ %
[PIC][NTf_2]: [PC][NTf_2]	3.86×10^{14}	99
[PIC][NTf_2]:[DD][NTf_2]	5.70×10^{14}	92
[PIC][BETI]: [PC][BETI]	1.30×10^{13}	99
[PIC][BETI]: [DD][BETI]	6.97×10^{14}	89

The highest spectral overlap integral value was obtained for [PIC][BETI]:[PC][BETI] nanoGUMBOS. Energy transfer efficiencies for binary nanoGUMBOS of both anions were found to exhibit high values of 99% in the case of PIC:PC nanoGUMBOS. These high energy transfer efficiencies were attributed to the compact environment of the nanomaterials, presence of J-aggregates from [PIC][NTf_2], and blue shifted absorption of the acceptor molecules due to the formation of H-aggregates. Binary nanomaterials containing the shortest and longest methine chains, [PIC][NTf_2]:[DD][NTf_2] and [PIC][BETI]:[DD][BETI], resulted in lower energy transfer efficiencies of 92% and 89%, respectively. These lower values of PIC:DD binary nanomaterials were due to reduced spectral overlap as compared to PIC:PC binary nanoGUMBOS caused by broadening in the longer wavelength region.

Variations in the fluorescence spectra were observed for binary nanomaterials of both NTf_2^- and $BETI^-$ anions, which were formed with PIC as donor molecules in the presence of PC or DD as acceptor molecules. At an equal molar ratio, binary nanoGUMBOS were found to exhibit a new fluorescence peak at 670 nm, while resulting in a decrease of the donor fluorescence peak (Figure 3.9).

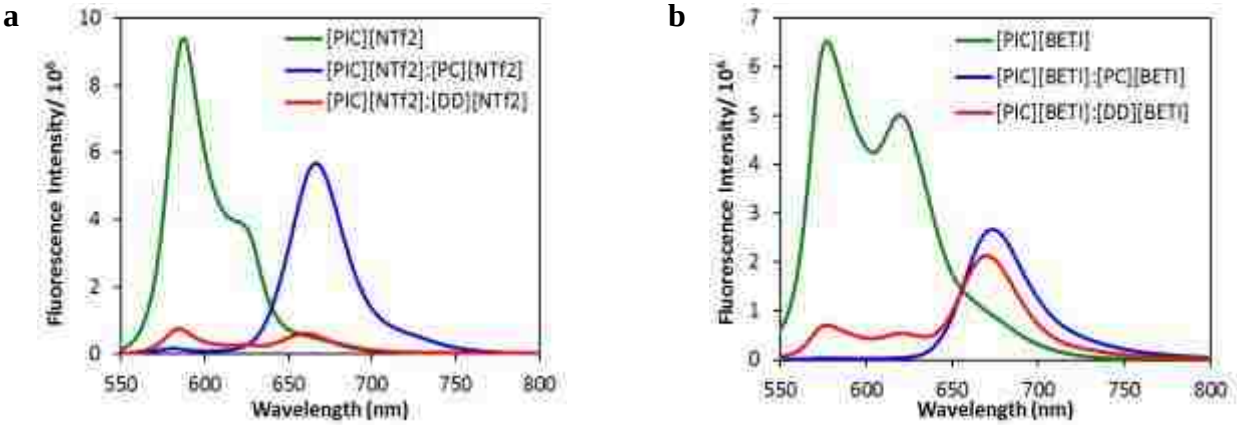

Figure 3.9 Fluorescence spectra of (a) NTf_2^- and (b) $BETI^-$ binary nanoGUMBOS in aqueous suspension at 1:1 molar ratio

The new emission peak was attributed to the occurrence of FRET from the PIC donor molecules to the acceptor molecules. This was a dramatic change from the little to no fluorescence of the individual nanoGUMBOS with longer methine chain lengths.

Binary nanoGUMBOS also resulted in tunable emission at different molar ratios with the same excitation wavelength of 524 nm (Figure 3.10). It was found that as the molar ratios of [PIC][NTf_2]:[PC][NTf_2] and [PIC][BETI]:[PC][BETI] binary nanoGUMBOS increased, the donor fluorescence peaks decreased while the acceptor fluorescence peaks increased due to FRET.

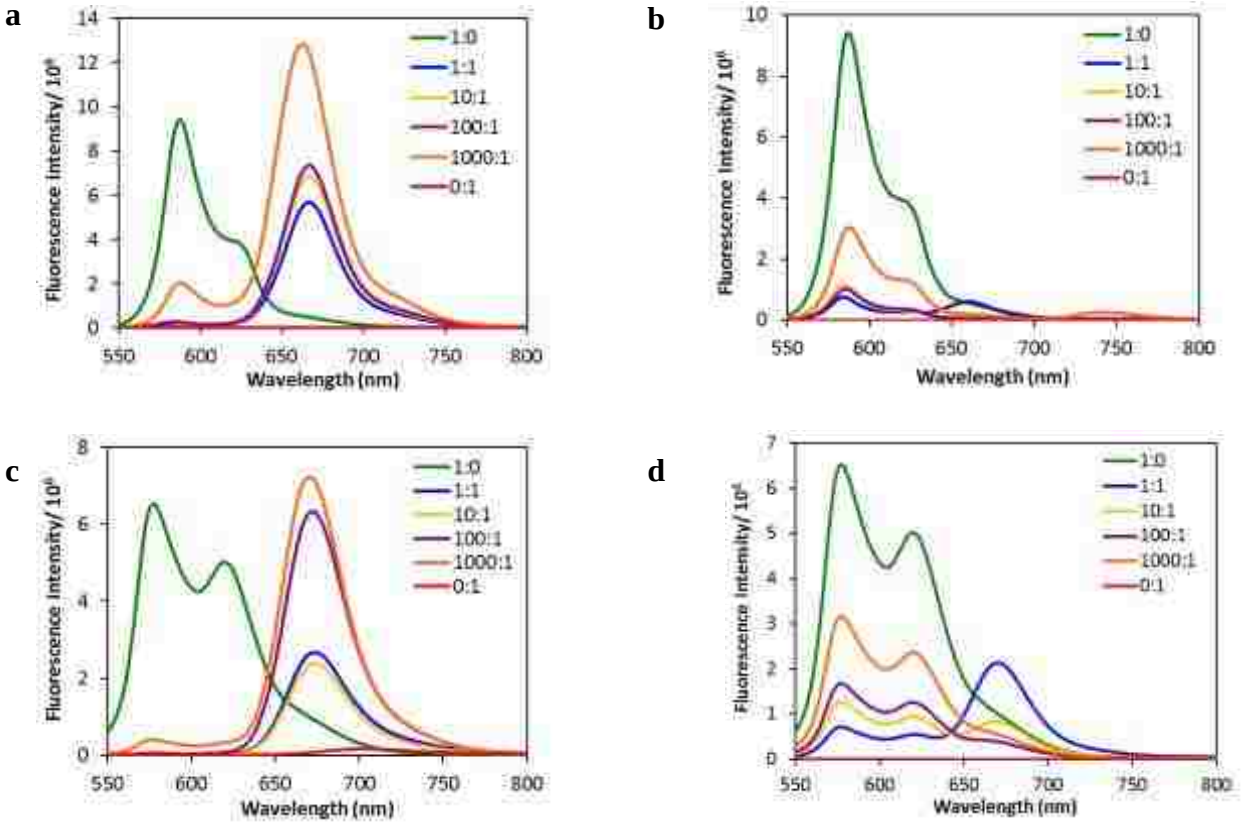

Figure 3.10 Fluorescence spectra of (a) [PIC][NTf_2]:[PC][NTf_2], (b) [PIC][NTf_2]:[DD][NTf_2], (c) [PIC][BETI]:[PC][BETI], and (d) [PIC][BETI]:[DD][BETI] binary nanoGUMBOS.

In contrast, binary nanoGUMBOS containing DD as an acceptor initially resulted in a decrease in the donor fluorescence peaks and increase in acceptor fluorescence peak

at a 1:1 molar ratio, followed by an increase in the donor peak and decrease in the acceptor peak at higher molar ratios. This was due to a decrease in FRET since there was an abundance of donor molecules with respect to acceptor molecules. Interestingly, both donor and acceptor fluorescence peaks were observed for [PIC][NTf_2]:[PC][NTf_2] and [PIC][BETI]:[PC][BETI] binary nanoGUMBOS at a high molar ratio of 1000:1, which was also attributed to the abundance of donor molecules with respect to acceptor molecules. Furthermore, [PIC][NTf_2]:[DD][NTf_2] binary nanoGUMBOS at 1000:1 molar ratio were found to exhibit multiple fluorescence emission at different wavelengths, where a loss of fluorescence intensity at 670 nm resulted in a new fluorescence peak at 745 nm (Figure 3.10b). This spectral behavior revealed the ability to tune the emission wavelength of [PIC][NTf_2]:[DD][NTf_2] binary nanoGUMBOS to the near-infrared region. Thus, the extent of FRET in the various binary nanoGUMBOS demonstrated the wide range of tunability in emission wavelengths and intensities, which is suitable for numerous applications.

3.3.6 Photostability Analysis

Stability of dyes against degradation caused by light, heat, oxygen, and ozone is an important consideration for applications such as biomedical imaging, sensing, and light harvesting.[26] In that regard, photostability of PIC and binary nanoGUMBOS was studied and residual emission intensities were obtained (Figure 3.11). It is important to note that photostability of the individual increased methine chain cyanine-based nanoGUMBOS was not measured due to lack of fluorescence (Figure 3.5).

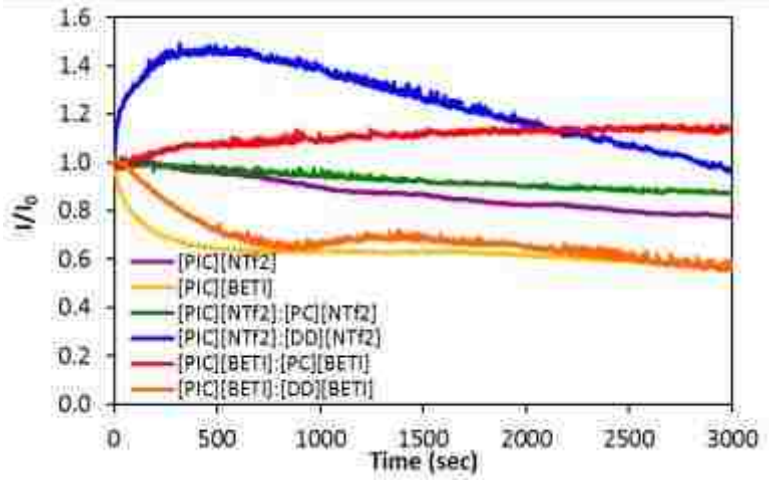

Figure 3.11 Photostability of cyanine-based nanoGUMBOS.

The cyanine-based nanoGUMBOS were found to have residual emission intensities ranging from 53% to 113%. Specifically, gradual decrease was observed for [PIC][NTf_2] and [PIC][NTf_2]:[PC][NTf_2] nanoGUMBOS upon excitation for 3000 s with a residual emission intensity of 75% and 87%, respectively. Photostability of [PIC][NTf_2]:[DD][NTf_2] nanoGUMBOS increased in the first 120 s to 150% followed by a steady decrease with a residual emission intensity of 96%. In contrast, [PIC][BETI] nanoGUMBOS resulted in a decrease in 240 s before reaching a plateau that resulted in a residual emission intensity of 53%. A residual emission intensity of 57% for [PIC][BETI]:[DD][BETI] nanoGUMBOS was obtained with a decrease in photostability in 720 s, followed by a slight increase before continuing to decrease. Conversely, photostability of [PIC][BETI]:[PC][BETI] nanoGUMBOS was found to exhibit the highest residual emission intensity of 113% due to gradual increase of the emission maximum over time. Generally, photostabilities of the cyanine-based nanoGUMBOS composed of NTf_2^- anions were higher than nanoGUMBOS of $BETI^-$ anions, with the exception for [PIC][BETI]:[PC][BETI] nanoGUMBOS. These higher photostabilities were attributed to the presence of J-aggregates from [PIC][NTf_2], which is in agreement with studies of

PEGylated cyanine-based nanoGUMBOS.[13] The high phototstability of [PIC][BETI]:[PC][BETI] nanoGUMBOS was due to greater spectral overlap that enabled improved stability. Overall, the PIC and binary nanoGUMBOS resulted in high photostability that suggest potential in light harvesting and optoelectronic applications.

3.3.8 Electrochemical Energy Levels and Band Gap Calculations

Cyclic voltammetry was performed for the cyanine-based GUMBOS in acetonitrile (Figure 3.12).

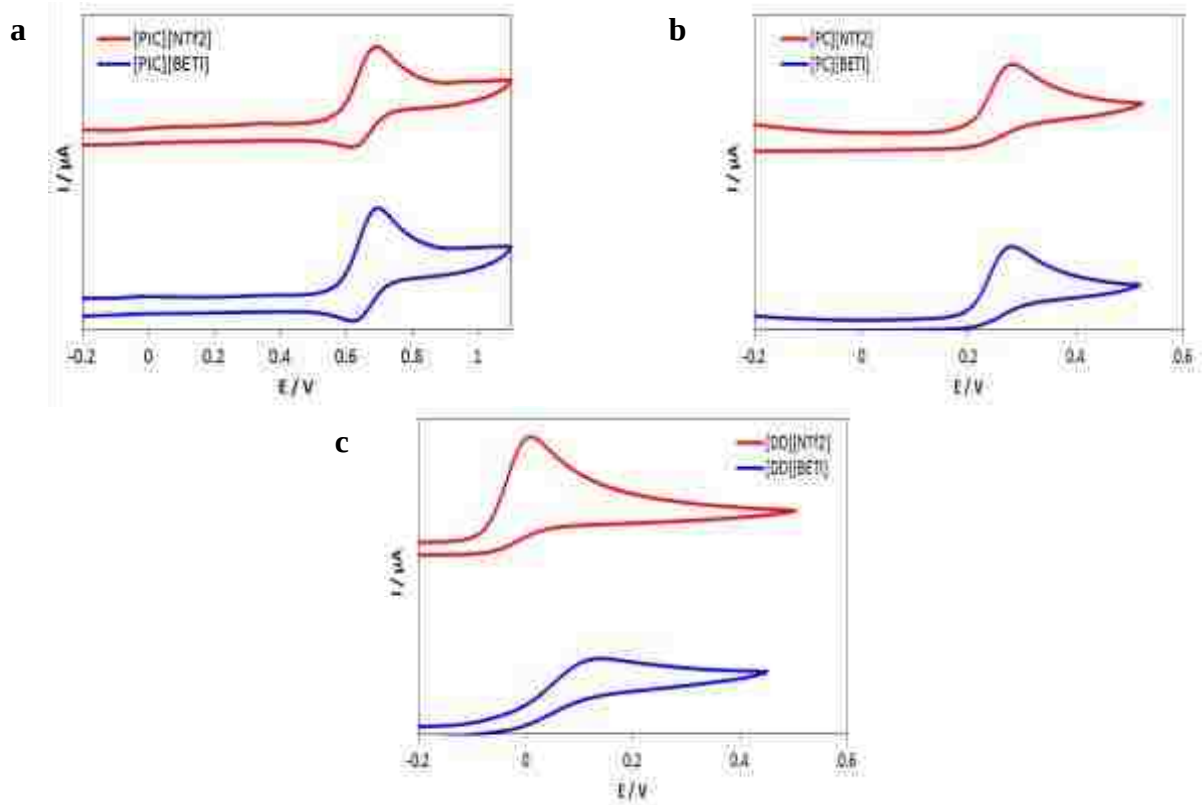

Figure 3.12 Cyclic voltammograms of (a) PIC, (b) PC, (c) DD GUMBOS (1 mM) in acetonitrile with 0.1 M $TBAPF_6$ vs Fc^+/Fc as a reference at 0.1 V/s.

Cyclic voltammograms of PIC GUMBOS revealed a reversible oxidation profile with a potential range from 1.1 V to 0.5 V. In contrast, a quasi-reversible oxidation profile was obtained for PC GUMBOS at potential ranges from 0.5 V to 0.1 V. A quasi-reversible

oxidation profile was also displayed for DD GUMBOS with a potential range from 0.5 V to -0.2 V.

Using the cyclic voltammograms, potentials and energy levels of the cyanine-based GUMBOS were obtained (Table 3.3). Due to the quasi-reversible profile, the oxidation potential (E_{ox}) was calculated from 85% of the maximum peak current. The excited state reduction potential (E^*_{red}) was determined using the oxidation potential by the following equations

$$E^*_{red} = E_{ox} - E_{0-0} \tag{3}$$

$$E_{0-0} = \frac{1240}{\lambda_{int}} \tag{4}$$

where $E_{0\text{-}0}$ represents the 0-0 transition energy state and λ_{int} is the intersect wavelength of the normalized absorption and emission spectra. Similar spectra were observed for both anions that revealed a red shift as the methine chain length increased. The λ_{int} of PIC, PC, and DD GUMBOS was 539, 619, and 727 nm, respectively. The band gap of the cyanine-based GUMBOS was obtained by the onset wavelength (λ_{onset}) at which a negative tangent line of the lowest energy absorption peak intersects with a linear tangent line of the absorption tail. The λ_{onset} of PIC, PC, and DD GUMBOS was 556, 635, and 745 nm, respectively. Energy levels of the cyanine-based GUMBOS were calculated by the following equations

$$E_{HOMO}(eV) = -1e^-[E_{pa}(V\ vs\ Fc^+/Fc) + 4.8(V\ Fc^+/Fc\ vs\ Zero)] \tag{5}$$

$$E_{LUMO}(eV) = E_{HOMO} + E_g \tag{6}$$

where E_{HOMO} is the highest occupied molecular orbital (HOMO) energy level calculated vs vacuum with Fc^+/Fc as a reference and E_{pa} is the anodic potential. The lowest

unoccupied molecular orbital energy level (E_{LUMO}) is obtained from the sum of the HOMO value and band gap.

Table 3.3 Redox potentials and band gap of PIC GUMBOS obtained from UV-Vis absorption

Dyes	E_{ox}[a] (V)	$E_{0\text{-}0}$[a] (V)	E^*_{red}[b] (V)	HOMO[c] (eV)	LUMO[c] (eV)	E_g (eV)
[PIC][NTf_2]	1.29	2.30	-1.01	-5.50	-3.27	2.23
[PIC][BETI]	1.31	2.30	-0.99	-5.56	-3.33	2.23
[PC][NTf_2]	0.962	2.00	-1.04	-5.13	-3.18	1.95
[PC][BETI]	0.972	2.00	-1.03	-5.14	-3.19	1.95
[DD][NTf_2]	0.632	1.71	-1.08	-4.80	-3.14	1.66
[DD][BETI]	0.701	1.71	-1.01	-4.87	-3.21	1.66

[a]The potentials were reported as V vs NHE. [b]The excited state reduction potential was obtained by equation $E^*_{red} = E_{ox} - E_{0-0}$. [c]The LUMO value was calculated by equation $E_{LUMO}(eV) = E_{HOMO} + E_g$.

The electrochemical properties of the cyanine-based GUMBOS revealed a decrease in oxidation potential with increased methine chain length. This resulted in a decrease in the HOMO energy level and reduced the band gap of the GUMBOS, which was expected due to the increase in wavelength as the methine chain length increased. The cyanine-based GUMBOS were found to have suitable potentials for possible application as sensitizers in dye-sensitized solar cells. The oxidation and excited state reduction potential of the dye are favorable for electron transfer to the conduction band of a titanium dioxide semiconductor (-0.5 V vs NHE), as well as an iodide/triiodie redox couple electrolyte (0.4 V vs NHE).

3.4 Conclusions

In summary, variable methine chain length cyanine-based GUMBOS were synthesized to form binary nanomaterials with controlled morphology. These binary nanoGUMBOS were found to exhibit broad absorption and tunable emission for non-fluorescent acceptor molecules by changing the molar ratio due to the occurrence of FRET. Multiple fluorescence peaks were observed for [PIC][NTf_2]:[DD][NTf_2]

nanoGUMBOS that extended to the near-infrared region. High energy transfer efficiencies were attributed to the compact environment of the nanomaterials, formation of J- and H-aggregates, and significant overlap of the absorption and emission spectra. Furthermore, high photostability and thermal stability were obtained for the binary materials. The tunable emission of these binary nanomaterials suggest interesting properties for potential applications in sensing and light harvesting in the visible to near-infrared region. In addition, electrochemical properties of the cyanine-based GUMBOS were observed to have suitable potentials for use as sensitizers in dye-sensitized solar cells. Moreover, the ability to tune these GUMBOS enables potential use in optoelectronics.

3.5 References

1. West, J. L.; Halas, N. J., Engineered nanomaterials for biophotonics applications: Improving sensing, imaging, and therapeutics. *Annu. Rev. Biomed. Eng.* **2003,** *5*, 285-292.

2. Goldberg, M.; Langer, R.; Jia, X. Q., Nanostructured materials for applications in drug delivery and tissue engineering. *J. Biomater. Sci.-Polym. Ed.* **2007,** *18* (3), 241-268.

3. Xia, Y. N.; Yang, P. D.; Sun, Y. G.; Wu, Y. Y.; Mayers, B.; Gates, B.; Yin, Y. D.; Kim, F.; Yan, Y. Q., One-dimensional nanostructures: Synthesis, characterization, and applications. *Adv. Mater.* **2003,** *15* (5), 353-389.

4. Arico, A. S.; Bruce, P.; Scrosati, B.; Tarascon, J. M.; Van Schalkwijk, W., Nanostructured materials for advanced energy conversion and storage devices. *Nat. Mater.* **2005,** *4* (5), 366-377.

5. Kamat, P. V., Meeting the clean energy demand: Nanostructure architectures for solar energy conversion. *J. Phys. Chem. C* **2007,** *111* (7), 2834-2860.

6. Lakowicz, J. R., *Principles of Fluorescence Spectroscopy*. 3 ed.; Springer: New York, 2006.

7. Peng, A. D.; Xiao, D. B.; Ma, Y.; Yang, W. S.; Yao, J. N., Tunable emission from doped 1,3,5-triphenyl-2-pyrazoline organic nanoparticles. *Adv. Mater.* **2005,** *17* (17), 2070-2073.

8. Zhao, Y. S.; Fu, H. B.; Hu, F. Q.; Peng, A. D.; Yang, W. S.; Yao, J. N., Tunable emission from binary organic one-dimensional nanomaterials: An alternative approach to white-light emission. *Adv. Mater.* **2008,** *20* (1), 79-83.

9. Zheng, J. Y.; Zhang, C. A.; Zhao, Y. S.; Yao, J. N., Detection of chemical vapors with tunable emission of binary organic nanobelts. *Phys. Chem. Chem. Phys.* **2010,** *12* (40), 12935-12938.

10. Tesfai, A.; El-Zahab, B.; Kelley, A. T.; Li, M.; Garno, J. C.; Baker, G. A.; Warner, I. M., Magnetic and Nonmagnetic Nanoparticles from a Group of Uniform Materials Based on Organic Salts. *ACS Nano* **2009,** *3* (10), 3244-3250.

11. Bwambok, D. K.; El-Zahab, B.; Challa, S. K.; Li, M.; Chandler, L.; Baker, G. A.; Warner, I. M., Near-Infrared Fluorescent NanoGUMBOS for Biomedical Imaging. *ACS Nano* **2009,** *3* (12), 3854-3860.

12. Das, S.; de Rooy, S. L.; Jordan, A. N.; Chandler, L.; Negulescu, I. I.; El-Zahab, B.; Warner, I. M., Tunable Size and Spectral Properties of Fluorescent NanoGUMBOS in Modified Sodium Deoxycholate Hydrogels. *Langmuir* **2012,** *28* (1), 757-765.

13. Lu, C.; Das, S.; Magut, P. K. S.; Li, M.; El-Zahab, B.; Warner, I. M., Irradiation Induced Fluorescence Enhancement in PEGylated Cyanine-Based NIR Nano- and Mesoscale GUMBOS. *Langmuir* **2012,** *28* (40), 14415-14423.

14. Cole, M. R.; Li, M.; El-Zahab, B.; Janes, M. E.; Hayes, D.; Warner, I. M., Design, Synthesis, and Biological Evaluation of beta-Lactam Antibiotic-Based Imidazolium- and Pyridinium-Type Ionic Liquids. *Chem. Bio. Drug Des.* **2011,** *78* (1), 33-41.

15. Regmi, B. P.; Monk, J.; El-Zahab, B.; Das, S.; Hung, F. R.; Hayes, D. J.; Warner, I. M., A novel composite film for detection and molecular weight determination of organic vapors. *J. Mater. Chem.* **2012,** *22* (27), 13732-13741.

16. Dumke, J. C.; El-Zahab, B.; Challa, S.; Das, S.; Chandler, L.; Tolocka, M.; Hayes, D. J.; Warner, I. M., Lanthanide-Based Luminescent NanoGUMBOS. *Langmuir* **2010,** *26* (19), 15599-15603.

17. de Rooy, S. L.; El-Zahab, B.; Li, M.; Das, S.; Broering, E.; Chandler, L.; Warner, I. M., Fluorescent one-dimensional nanostructures from a group of uniform materials based on organic salts. *Chem. Commun.* **2011,** *47* (31), 8916-8918.

18. Das, S.; Bwambok, D.; Ei-Zahab, B.; Monk, J.; de Rooy, S. L.; Challa, S.; Li, M.; Hung, F. R.; Baker, G. A.; Warner, I. M., Nontemplated Approach to Tuning the Spectral Properties of Cyanine-Based Fluorescent NanoGUMBOS. *Langmuir* **2010,** *26* (15), 12867-12876.

19. de Rooy, S. L.; Das, S.; Li, M.; El-Zahab, B.; Jordan, A.; Lodes, R.; Weber, A.; Chandler, L.; Baker, G. A.; Warner, I. M., Ionically Self-Assembled, Multi-Luminophore One-Dimensional Micro- and Nanoscale Aggregates of Thiacarbocyanine GUMBOS. *J. Phys. Chem. C* **2012,** *116* (14), 8251-8260.

20. Jordan, A. N.; Das, S.; Siraj, N.; de Rooy, S. L.; Li, M.; El-Zahab, B.; Chandler, L.; Baker, G. A.; Warner, I. M., Anion-controlled morphologies and spectral features of cyanine-based nanoGUMBOS - an improved photosensitizer. *Nanoscale* **2012,** *4* (16), 5031-5038.

21. Davydov, A. S., *Theory of Molecular Excitons*. McGraw-Hill: New York, 1962.

22. Kasha, M.; Rawls, H. R.; Ashraf El-Bayoumi, M., The Exciton Model in Molecular Spectroscopy. *Pure Appl Chem* **1965,** *11*, 371-392.

23. Chen, S. Y.; Horng, M. L.; Quitevis, E. L., Picosecond Spectroscopic Studies of Electronic-Energy Relaxation in H-aggregates of 1,1'-diethyl-2,2'-dicarbocyanine on Colloidal Silica. *J. Phys. Chem.* **1989,** *93* (9), 3683-3688.

24. Gadde, S.; Batchelor, E. K.; Kaifer, A. E., Controlling the Formation of Cyanine Dye H- and J-Aggregates with Cucurbituril Hosts in the Presence of Anionic Polyelectrolytes. *Chem. Eur. J.* **2009,** *15* (24), 6025-6031.

25. Barazzouk, S.; Lee, H.; Hotchandani, S.; Kamat, P. V., Photosensitization aspects of pinacyanol H-aggregates. Charge injection from singlet and triplet excited states into SnO2 nanocrystallites. *J. Phys. Chem. B* **2000,** *104* (15), 3616-3623.

26. Mishra, A.; Behera, R. K.; Behera, P. K.; Mishra, B. K.; Behera, G. B., Cyanines during the 1990s: A review. *Chem. Rev.* **2000,** *100* (6), 1973-2011.

CHAPTER 4
DYE-SENSITIZED SOLAR CELL USING CYANINE-BASED GUMBOS

4.1 Introduction

Renewable energy is a major concern due to increased world energy consumption. In particular, solar energy is a continuous and abundant renewable source that uses devices known as solar cells to convert sunlight to electricity. Specifically, devices such as conventional silicon solar cells have been reported to have a high conversion efficiency of 24.7%.[1] Unfortunately, these solar cells require expensive manufacturing for production of high purity single crystals. Devices known as dye-sensitized solar cells (DSSCs) are a promising low cost alternative to silicon solar cells that employ nanocrystalline titanium dioxide (TiO_2) particles (Figure 4.1).

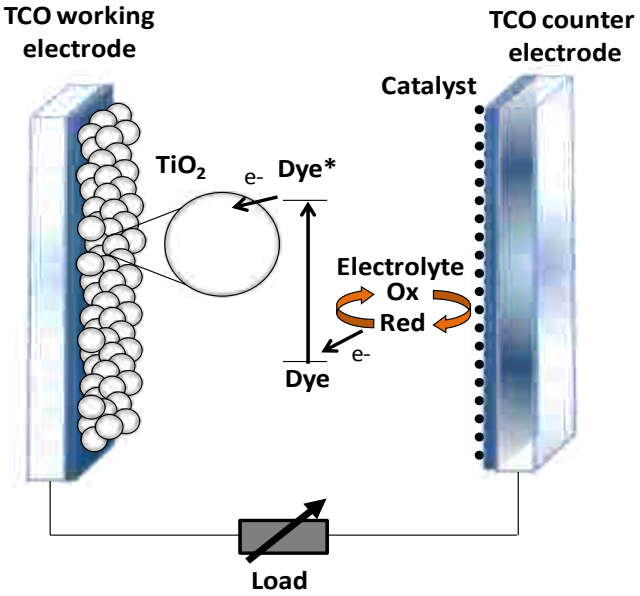

Figure 4.1 Diagram of a DSSC consisting of a dye sensitizer, TiO_2 working electrode, catalyst counter electrode, and electrolyte.

Initially developed by Gratzel and O'Regan in 1991, this DSSC consisted of a dye derived from a ruthenium complex adsorbed on the surface of TiO_2 nanoparticles that resulted in the generation of a conversion efficiency of 7.9%.[2] Since development,

research related to DSSCs continues to increase over the years. As a result, a conversion efficiency of 11% has been achieved for DSSCs using ruthenium complexes.[3,4]

An important function for DSSCs is the capability to transport electrons to an external load. Electron transport is achieved by a working electrode that consists of a wide band gap oxide semiconductor deposited on a TCO glass substrate. A variety of nanostructures has been studied to optimize conversion efficiency including nanoparticles,[3,4] nanotubes,[5,6,7] and nanorods.[8,9] In particular, TiO_2 electrospun nanofibers have also been reported in DSSCs.[10,11,12] Recently, Liu *et al.* have demonstrated the use of electrospinning to prepare polymer nanofibers doped with TiO_2 nanoparticles and a ruthenium complex.[13] This technique combines the advantages of using nanostructures for increased surface area, as well as maintaining the strong interaction between the dye and the surface of TiO_2. However, to the best of our knowledge, this preparation technique has not been applied in DSSCs. The electrospinning method is a direct, facile, and controllable approach to fabricate fibers at a range of nanometers to micrometers (Figure 4.2).[14] This system employs an applied voltage at the tip of a needle to overcome the surface tension of a TiO_2 polymeric solution. Once this occurs, fibers are produced and collected at a given distance from the needle tip. The diameter of the fibers is controlled by parameters such as the applied voltage, flow rate, solution viscosity, and surface tension.

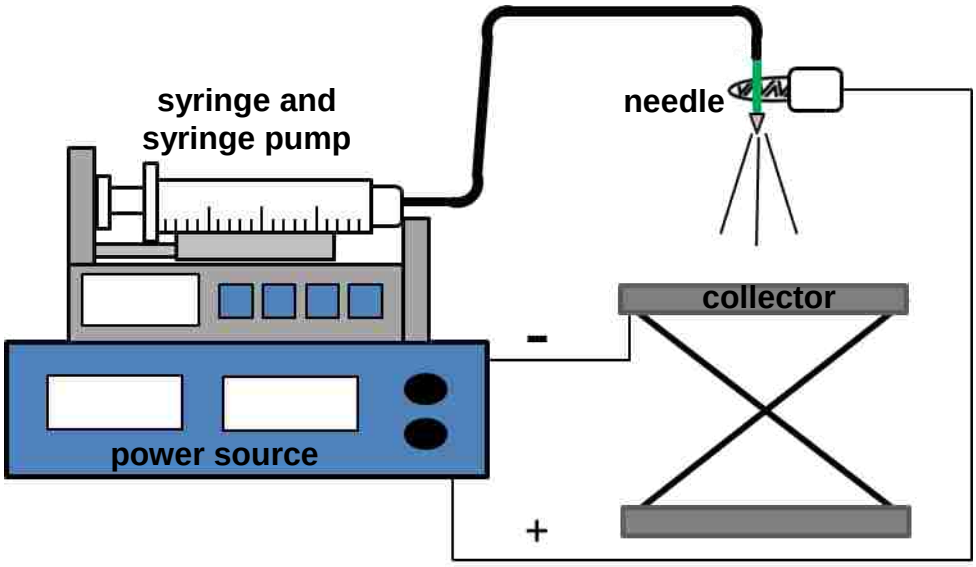

Figure 4.2 Schematic of electrospinning apparatus consisting of a power source, syringe pump, syringe, needle, and collector.

Another important component of DSSCs is the photosensitizing dye which is used to absorb photons from sunlight and transfer electrons to generate current. Ideal dye sensitizers absorb photons in the visible and near-infrared regions below 920 nm of the solar irradiance spectrum. Dye sensitizers also possess suitable redox properties for efficient electron transfer to overcome possible recombination and reduce loss of efficiency throughout the solar cell. For this reason, the oxidation potential and excited state oxidation potential of the sensitizer are closely matched with the potentials of the iodide/triiodide electrolyte (0.4 V vs NHE) and conduction band of TiO_2 (-0.5 V vs NHE), respectively. The ideal spectral and redox properties of dye sensitizers can be optimized by the structure of the dye.

Dyes derived from ruthenium complexes have been typically used in DSSCs. Unfortunately, several disadvantages are associated with current ruthenium complex photosensitizers, which can be attributed to limited supply and expense of metals, as

well as reduced absorption in the near-infrared region of the electromagnetic spectrum. Alternatively, organic dyes as photosensitizers has been reported as alternative to for solar cell application allow for the design of structures to be tailored for optimal spectral and electrochemical properties. A variety of organic dyes such as coumarins,[15,16,17] indolines,[18,19] and triphenylamines[20,21] have been synthesized at low cost that exhibit desirable properties such as high molar extinction coefficients and broad absorption spectra. In particular, cyanine dyes have also been investigated as sensitizers with conversion efficiencies ranging from 3.1% to 5.4%.[22,23,24]

Although organic dyes have been found to provide adequate conversion efficiencies by tailoring the structures, a challenge of these dyes is the presence of aggregation that can reduce conversion efficiency. The incorporation of coadsorbates such as chenodeoxycholic acid (CDCA) and 4-tert-butylpyridine (TBP) in DSSCs have been found to limit aggregation and improve conversion efficiency in organic dyes such as indoline and coumarin.[19,16] In contrast, beneficial characteristics have been reported in recent studies by controlling dye aggregates. In particular, the presence of aggregation in cyanine dyes has also been investigated for potential aid in optimizing conversion efficiency of DSSCs.[25] In this regard, the use of controlled J-aggregates of a merocyanine dye has been reported to achieve a conversion efficiency of 4.5% by Sayama *et al.*[26]

As previously mentioned, a new class of materials referred to as a **g**roup of **u**niform **m**aterials **b**ased on **o**rganic **s**alts (GUMBOS) and nanomaterials derived from GUMBOS (nanoGUMBOS) have been found to exhibit interesting physiochemical properties that can be tuned for multiple functions based on the selected cations and

anions. In previous studies, cyanine-based nanoGUMBOS were prepared by use of a simple reprecipitation method and found to exhibit controlled morphology and aggregation by variation of the associated anion.[27] Broad absorption of the cyanine-based nanomaterials was also observed due to differences in molecular self-assembly ordering, i.e. H- and J-aggregation. In addition, electrochemical properties of the cyanine-based GUMBOS were reported to have suitable potential values that favor electron injection and regeneration processes required in DSSCs. The present work entails the investigation of cyanine-based GUMBOS in DSSCs using an electrospinning method for formation of nanofibers. The TiO_2 electrode was composed of nanofibers doped with TiO_2 nanoparticles and cyanine-based GUMBOS. Photovoltaic performances of the solar cells were found to exhibit improved energy efficiency by use of electrospun nanofibers as compared to nanoparticles.

4.2 Materials and Methods

4.2.1 Syntheses of Cyanine-based GUMBOS

Cyanine-based GUMBOS were synthesized by an anion exchange reaction of pseudoisocyanine (PIC) iodide with lithium bis(trifluoromethanesulfonyl)imide ($LiNTf_2$) and lithium bis(perfluoroethylsulfonyl)imide (LiBETI) using a method previously reported.[27] Briefly, a mixture of PICI and $LiNTf_2$ (1.1 eq) was dissolved in a biphasic solution of methylene chloride and water (2:1, v/v) and stirred for one day at room temperature. The methylene chloride layer was collected and washed several times with fresh deionized water to completely remove residual LiI byproduct. Subsequently, the methylene chloride was removed under vacuum at 40 °C by use of a rotary

evaporator followed by freeze-drying overnight to afford solid [PIC][NTf_2]. A similar procedure was implemented to synthesize [PIC][BETI].

4.2.2 Preparation of TiO_2 Electrodes

The nanofibers were electrospun directly on fluorine-doped tin oxide glass substrate (FTO, 10 cm x 10 cm) from a solution of 0.3 g poly(vinylpyrrolidone) (PVP) doped with 0.03 g TiO_2 powder and 4 mM cyanine-based GUMBOS in ethanol (Figure 4.3). Formation of the nanofibers was obtained using a syringe, 23 gauge needle, and an applied voltage of 15 kV at a distance of 10 cm.

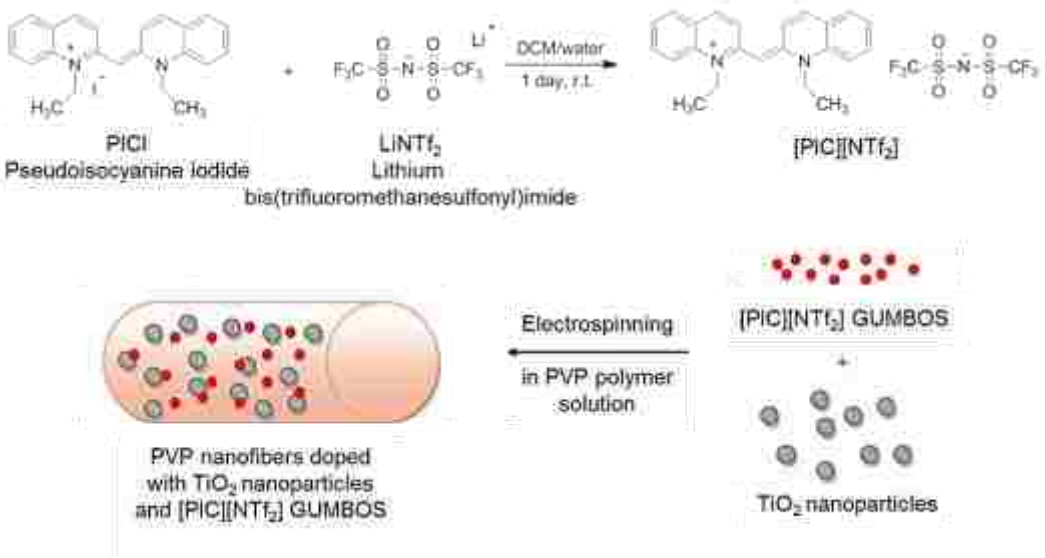

Figure 4.3 Synthesis of electrospun PVP nanofibers doped with TiO_2 nanoparticles and [PIC][NTf_2] GUMBOS.

Two procedures were used to form TiO_2 nanoparticles for comparison with the electrospun nanofibers. A paste of TiO_2 nanoparticles was prepared as reported by Lee *et al.* in which 0.5 g of anatase TiO_2 powder (< 25 nm) and 0.2 g of polyethylene glycol (PEG, M_w = 14,000 g/mol) were added to 100 µl of Triton X-100 in 3 ml of acetic acid (0.1 M).[28] In addition, a solution of TiO_2 nanoparticles was synthesized as follows: 25 ml of titianium (IV) isopropoxide and 4 ml of 2-propanol were added to 150 ml of deionized

water over 20 min. Nitric acid (70%, 2.5 ml) was added within 10 min, and the solution was stirred for 12 h at 70 °C. Polyethylene glycol (10% w/w) was added to the solution that was then placed under vacuum at 60 °C by use of a rotary evaporator. Electrodes were prepared using TiO_2 nanoparticle paste and solution by the doctor-blading method, followed by heating for 30 min at 450 °C. Electron micrographs were obtained to investigate the morphology of the TiO_2 nanomaterials by use of a JSM-6610, JAM-6610LV high and low vacuum scanning electron microscope (JOEL USA, Inc. Peabody, MA).

4.2.3 Solar Cell Fabrication and Characterization

The TiO_2 electrodes composed of nanoparticles were soaked overnight in 1 mM PIC-based GUMBOS ethanolic solutions. Subsequently, the TiO_2 electrodes were carefully cleaned with ethanol and dried. Platinum (Pt) counter electrodes were prepared by coating FTO glass substrates with 5 mM solution of H_2PtCl_6 in 2-propanol, followed by heating for 20 min at 400 °C. The solar cell was assembled by sealing the dye/TiO_2 electrode and Pt counter electrode together with a thermal melt polymer film (Figure 4.4). An iodide/triiodide electrolyte solution, consisting of 0.5 M lithium iodide and 50 mM iodine mixed in acetonitrile, was incorporated into the solar cell through two holes drilled in the Pt counter electrode.

Figure 4.4 Photograph image of a fabricated DSSC with use of a quarter as a scale.

Solar cell current-voltage (*I*–*V*) characteristics were measured by use of a Keithley 2400 sourcemeter and xenon arc lamp with AM 1.5 G filter (Figure 4.5). The solar simulator was calibrated to one sun with a light power density of 100 $mWcm^{-2}$.

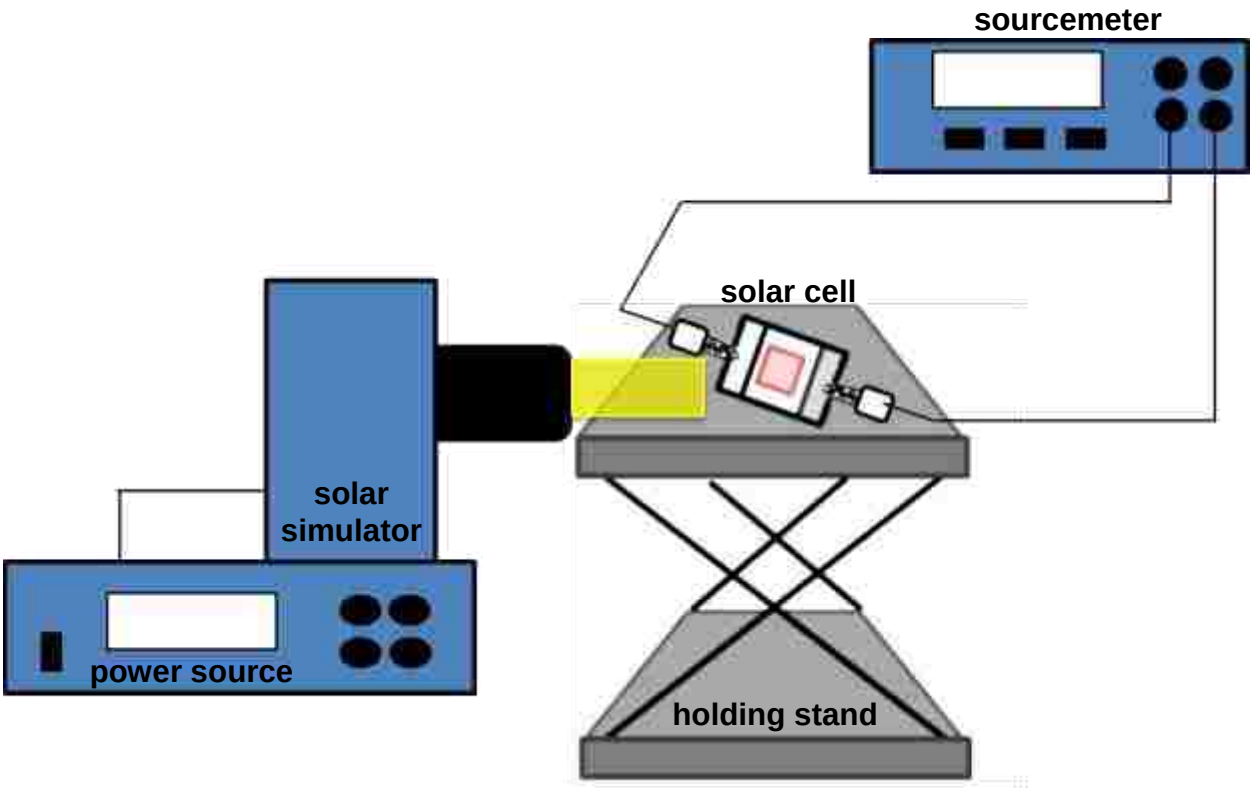

Figure 4.5 Diagram of solar cell instrumentation that includes a power source, solar simulator, solar cell, holding stand, and sourcemeter.

4.3 Results and Discussion

4.3.1 Morphology of TiO_2 Electrodes

Examination of scanning electron micrographs of TiO_2 electrodes were found to exhibit nanostructures for all TiO_2 preparation methods. Formation of TiO_2 electrodes prepared from TiO_2 paste and TiO_2 solution consisted of clusters of nanoparticles that produced a uniform coverage on the glass substrate (Figure 4.6 and 4.7). In contrast, one-dimensional TiO_2 nanofibers were found to be were randomly deposited on the glass substrate with a diameter of 139 ± 34 nm (Figure 4.8).

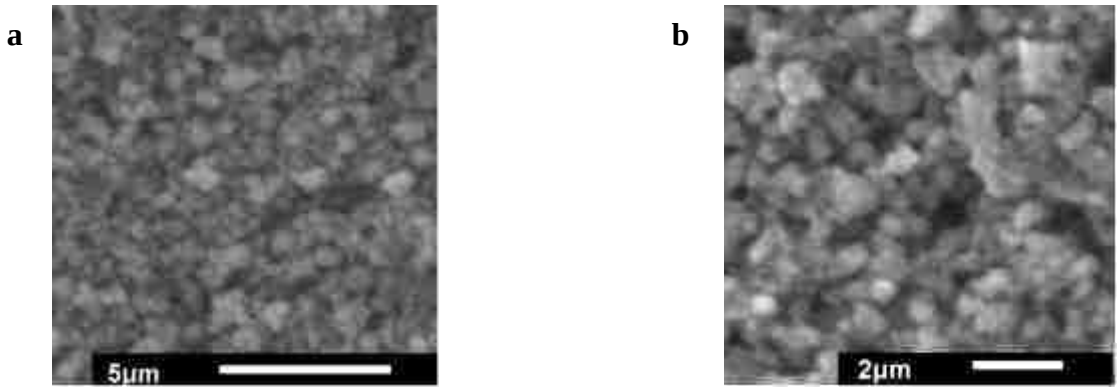

Figure 4.6 (a) Scanning electron micrographs of TiO_2 nanoparticles on an FTO electrode via TiO_2 paste. (b) Magnification of panel (a).

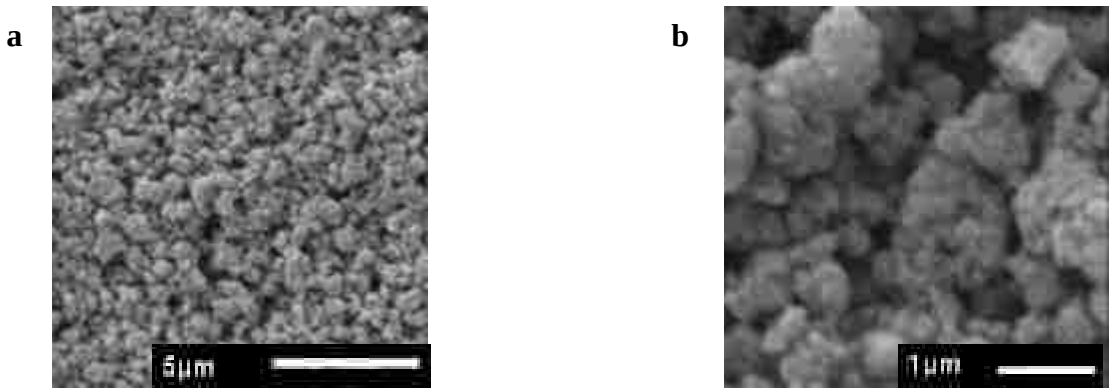

Figure 4.7 (a) Scanning electron micrographs of TiO_2 nanoparticles on an FTO electrode by use of TiO_2 solution. (b) Magnification of panel (a).

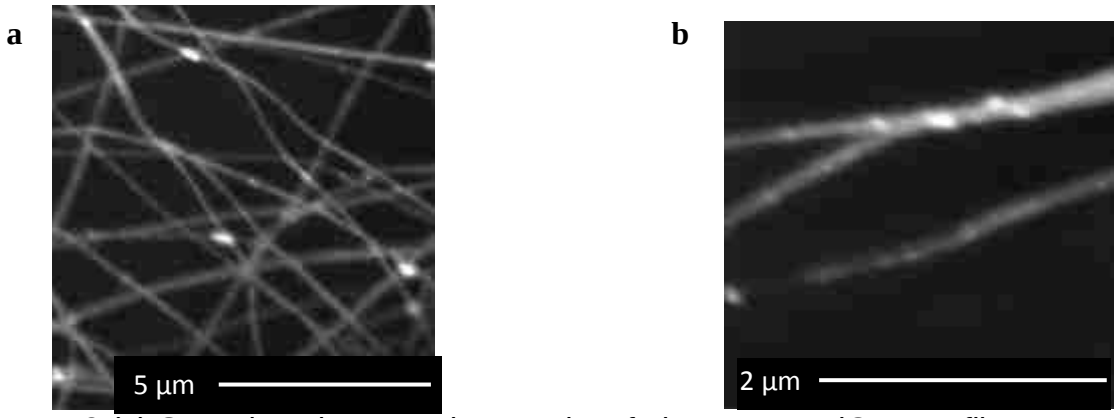

Figure 4.8 (a) Scanning electron micrographs of electrospun TiO_2 nanofibers on an FTO electrode. (b) Magnification of panel (a).

4.3.2 Performance of DSSCs with Cyanine-based GUMBOS

The I-V characteristics of DSSCs using the TiO_2 preparation methods with a ruthenium complex N719, PICI, and [PIC][BETI] GUMBOS were obtained (Figure 4.9

and 4.10). The photovoltaic performances including the short-circuit photocurrent density (J_{sc}), open-circuit photovoltage (V_{oc}), fill factor (FF), and overall power conversion efficiency (η) of the solar cell devices were collected (Table 4.1). For the device containing N719, the following parameters were obtained: J_{sc} (2.3 $mAcm^{-2}$), V_{oc} (0.72 V), FF (0.54), and η (0.89%). For the device containing PICI, J_{sc}, V_{oc}, FF, and η were found to be 0.30 $mAcm^{-2}$, 0.19 V, 0.25, and 0.014%. Similarly, the device composed of [PIC][BETI] GUMBOS resulted in the following characteristics: J_{sc} (0.36 $mAcm^{-2}$), V_{oc} (0.16 V), FF (0.25), and η (0.014%). In contrast, the device comprised of electrospun nanofibers and [PIC][NTf_2] GUMBOS was also measured and found to yield J_{sc}, V_{oc}, FF, and η values of 3.0 $mAcm^{-2}$, 0.47 V, 0.52, and 0.73%.

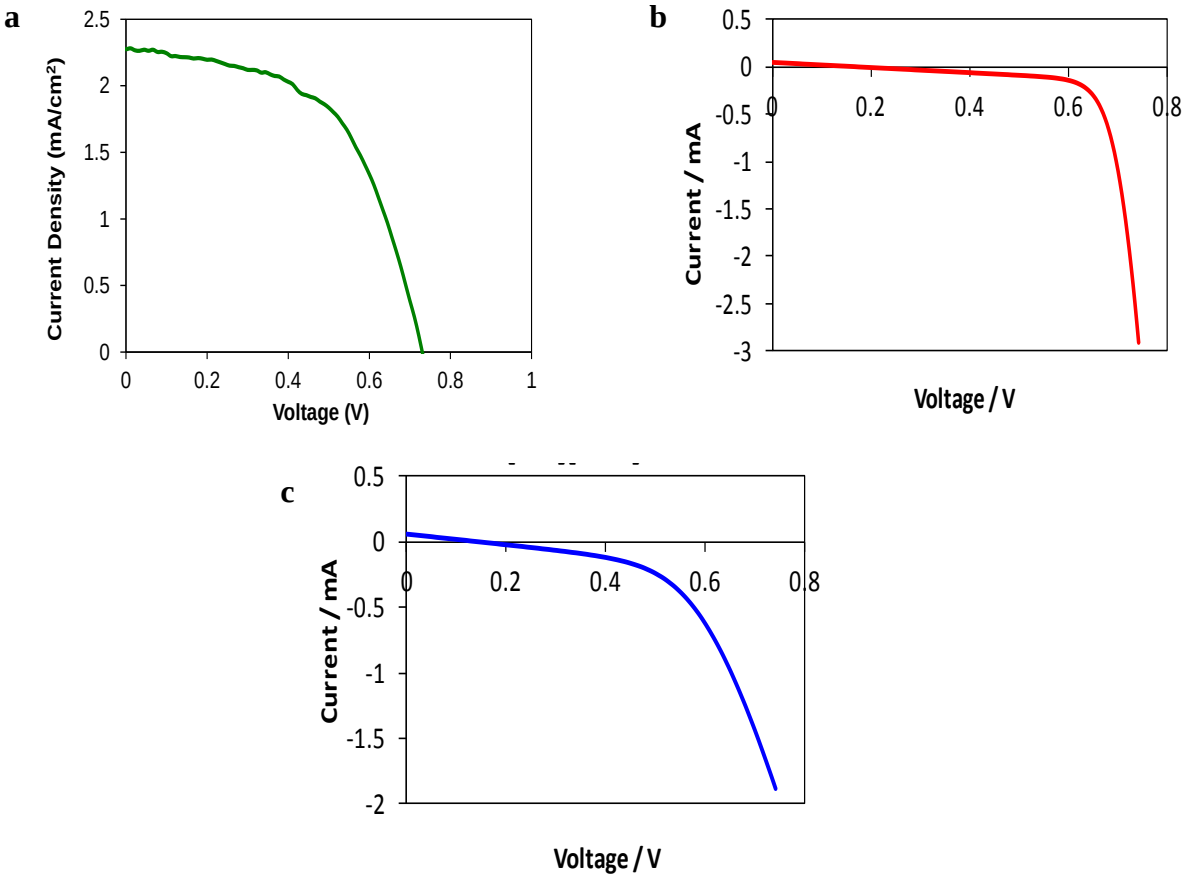

Figure 4.9 I-V plots of DSSCs composed of (a) N719, (b) PICI, and (c) [PIC][BETI] GUMBOS using TiO_2 nanoparticles.

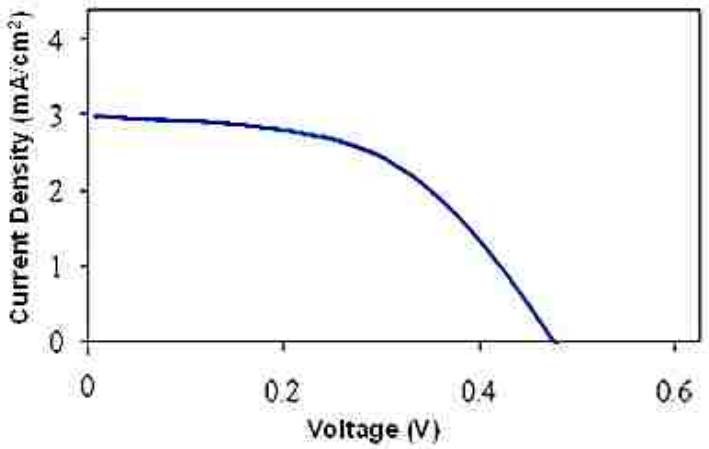

Figure 4.10 I-V plot of a DSSC consisting of [PIC][NTf_2] GUMBOS electrospun using doped nanofibers.

Table 4.1 Photovoltaic performances of dye-sensitized solar cells using [a]TiO_2 solution, [b]paste, and [c]electrospinning methods

GUMBOS	J_{sc}/ mAcm^{-2}	V_{oc}/ V	FF	η/ %
N719[a]	2.3	0.72	0.54	0.89
PICI [b]	0.30	0.19	0.25	0.014
[PIC][BETI][b]	0.36	0.157	0.25	0.014
[PIC][NTf_2][c]	2.99	0.47	0.52	0.73

The performance of the solar cell containing a common dye derived from a ruthenium complex, N719, and using a TiO_2 solution method was found to exhibit a low conversion efficiency of 0.89%. This low efficiency was attributed to the TiO_2 coating, which required further optimization. The performance of the TiO_2 paste devices was similar for both the cyanine parent compound and GUMBOS with a negligible conversion efficiency of 0.014%. This low efficiency may be attributed to desorption of the dye on the TiO_2 surface. This desorption might be a result of the lack of an anchoring group in the dye structure to bind to the TiO_2 surface. In contrast, higher conversion efficiency was observed using the electrospinning technique with [PIC][NTf_2] GUMBOS. This increase in efficiency was attributed to improved interaction between the dye and TiO_2 surface. As mentioned earlier, the dye was incorporated with the TiO_2/PVP solution during electrospinning. This allowed for better contact of the dye

molecule on the TiO_2 surface within the confinement of the nanofiber. It is important to note that since the cyanine GUMBOS were prepared in ethanolic solution their absorption properties are the same.[27] Therefore, this increase in efficiency was not due to the use of a different dye. Similar to TiO_2 paste devices, the conversion efficiency of the electrospinning technique may also be enhanced by use of anchoring groups in the dye structure.

4.4 Conclusions

For the first time, cyanine-based GUMBOS were applied in DSSCs. Preparation of TiO_2 electrodes from TiO_2 paste and nanoparticle solution were found to yield uniform surface coverage. The formation of nanofibers via an electrospinning technique was also used to prepare electrodes. Performances of DSSCs composed of these TiO_2 electrodes with cyanine-based GUMBOS were measured. Photovoltaic characteristics of the solar cells were found to exhibit an improved conversion efficiency of 0.73% by use of electrospun nanofibers as compared to nanoparticles that resulted in negligible conversion efficiency. This lack of efficiency was attributed to limited interaction between the dyes and the TiO_2 surface. The interaction may be optimized by modification of the dye structures with an anchoring group, which is currently under investigation.

4.5 References

1. Zhao, J. H.; Wang, A. H.; Green, M. A.; Ferrazza, F., 19.8% efficient "honeycomb" textured multicrystalline and 24.4% monocrystalline silicon solar cells. *Appl. Phys. Lett.* **1998,** *73* (14), 1991-1993.

2. Oregan, B.; Gratzel, M., A Low-Cost, High-Efficiency Solar Cell Based on Dye-Sensitized Colloidal TiO2 Films. *Nature* **1991,** *353* (6346), 737-740.

3. Nazeeruddin, M. K.; De Angelis, F.; Fantacci, S.; Selloni, A.; Viscardi, G.; Liska, P.; Ito, S.; Bessho, T.; Gratzel, M., Combined experimental and DFT-TDDFT computational study of photoelectrochemical cell ruthenium sensitizers. *J. Am. Chem. Soc.* **2005,** *127* (48), 16835-16847.

4. Chiba, Y.; Islam, A.; Watanabe, Y.; Komiya, R.; Koide, N.; Han, L., Dye-Sensitized Solar Cells with Conversion Efficiency of 11.1%. *Jpn. J. Appl. Phys.* **2006,** *45* (25), L638-L640.

5. Mor, G. K.; Shankar, K.; Paulose, M.; Varghese, O. K.; Grimes, C. A., Use of Highly-Ordered TiO2 Nanotube Arrays in Dye-Sensitized Solar Cells. *Nano Lett.* **2006,** *6* (2), 215-218.

6. Zhu, K.; Neale, N. R.; Miedaner, A.; Frank, A. J., Enhanced Charge-Collection Efficiencies and Light Scattering in Dye-Sensitized Solar Cells Using Oriented TiO2 Nanotubes Arrays. *Nano Lett.* **2007,** *7* (1), 69-74.

7. Jennings, J. R.; Ghicov, A.; Peter, L. M.; Schmuki, P.; Walker, A. B., Dye-Sensitized Solar Cells Based on Oriented TiO2 Nanotube Arrays: Transport, Trapping, and Transfer of Electrons. *J. Am. Chem. Soc.* **2008,** *130* (40), 13364-13372.

8. Adachi, M.; Murata, Y.; Takao, J.; Jiu, J.; Sakamoto, M.; Wang, F., Highly Efficient Dye-Sensitized Solar Cells with a Titania Thin-Film Electrode Composed of a Network Structure of Single-Crystal-like TiO2 Nanowires Made by the "Oriented Attachment" Mechanism. *J. Am. Chem. Soc.* **2004,** *126* (45), 14943-14949.

9. Liu, B.; Aydil, E. S., Growth of Oriented Single-Crystalline Rutile TiO2 Nanorods on Transparent Conducting Substrates for Dye-Sensitized Solar Cells. *J. Am. Chem. Soc.* **2009,** *131* (11), 3985-3990.

10. Song, M. Y.; Kim, D. K.; Ihn, K. J.; Jo, S. M.; Kim, D. Y., Electrospun TiO2 electrodes for dye-sensitized solar cells. *Nanotechnology* **2004,** *15* (12), 1861-1865.

11. Fujihara, K.; Kumar, A.; Jose, R.; Ramakrishna, S.; Uchida, S., Spray deposition of electrospun TiO2 nanorods for dye-sensitized solar cell. *Nanotechnology* **2007,** *18* (36), 1-5.

12. Chuangchote, S.; Sagawa, T.; Yoshikawa, S., Efficient dye-sensitized solar cells using electrospun TiO2 nanofibers as a light harvesting layer. *Appl. Phys. Lett.* **2008,** *93* (3), 1-3.

13. Liu, L.; Li, B.; Zhang, J.; Qin, R.; Zhao, H.; Ren, X., Electrospinning preparation and characterization of a new kind of composite nanomaterials: One-dimensional

composite nanofibers doped with TiO2 nanoparticles and Ru(II) complex. *Mater. Res. Bull.* **2009,** *44* (11), 2081-2086.

14. Thavasi, V.; Singh, G.; Ramakrishna, S., Electrospun nanofibers in energy and environmental applications. *Energy Environ. Sci.* **2008,** *1* (2), 205-221.

15. Hara, K.; Sayama, K.; Arakawa, H.; Ohga, Y.; Shinpo, A.; Suga, S., A coumarin-derivative dye sensitized nanocrystalline TiO2 solar cell having a high solar-energy conversion efficiency up to 5.6%. *Chem. Commun.* **2001,** (6), 569-570.

16. Hara, K.; Dan-oh, Y.; Kasada, C.; Ohga, Y.; Shinpo, A.; Suga, S.; Sayama, K.; Arakawa, H., Effect of Additives on the Photovoltaic Performance of Coumarin-Dye-Sensitized Nanocrystalline TiO2 Solar Cells. *Langmuir* **2004,** *20* (10), 4205-4210.

17. Wang, Z. S.; Cui, Y.; Dan-Oh, Y.; Kasada, C.; Shinpo, A.; Hara, K., Molecular Design of Coumarin Dyes for Stable and Efficient Organic Dye-Sensitized Solar Cells. *J. Phys. Chem. C* **2008,** *112* (43), 17011-17017.

18. Horiuchi, T.; Miura, H.; Uchida, S., Highly efficient metal-free organic dyes for dye-sensitized solar cells. *J. Photochem. Photobiol. A-Chem.* **2004,** *164* (1-3), 29-32.

19. Ito, S.; Miura, H.; Uchida, S.; Takata, M.; Sumioka, K.; Liska, P.; Comte, P.; Pechy, P.; Graetzel, M., High-conversion-efficiency organic dye-sensitized solar cells with a novel indoline dye. *Chem. Commun.* **2008,** (41), 5194-5196.

20. Liang, M.; Xu, W.; Cai, F. S.; Chen, P. Q.; Peng, B.; Chen, J.; Li, Z. M., New triphenylamine-based organic dyes for efficient dye-sensitized solar cells. *J. Phys. Chem. C* **2007,** *111* (11), 4465-4472.

21. Liang, Y.; Cheng, F.; Liang, J.; Chen, J., Triphenylamine-Based Ionic Dyes with Simple Structures: Broad Photoresponse and Limitations on Open-Circuit Voltage in Dye-Sensitized Solar Cells. *J. Phys. Chem. C* **2010,** *114* (37), 15842-15848.

22. Sayama, K.; Tsukagoshi, S.; Mori, T.; Hara, K.; Ohga, Y.; Shinpou, A.; Abe, Y.; Suga, S.; Arakawa, H., Efficient sensitization of nanocrystalline TiO2 films with cyanine and merocyanine organic dyes. *Sol. Energy Mater. Sol. Cells* **2003,** *80* (1), 47-71.

23. Chen, Y. S.; Li, C.; Zeng, Z. H.; Wang, W. B.; Wang, X. S.; Zhang, B. W., Efficient electron injection due to a special adsorbing group's combination of carboxyl and hydroxyl: dye-sensitized solar cells based on new hemicyanine dyes. *J. Mater. Chem.* **2005,** *15* (16), 1654-1661.

24. Geiger, T.; Kuster, S.; Yum, J. H.; Moon, S. J.; Nazeeruddin, M. K.; Gratzel, M.; Nuesch, F., Molecular Design of Unsymmetrical Squaraine Dyes for High Efficiency Conversion of Low Energy Photons into Electrons Using TiO2 Nanocrystalline Films. *Adv. Funct. Mater.* **2009,** *19* (17), 2720-2727.

25. Ehret, A.; Stuhl, L.; Spitler, M. T., Spectral sensitization of TiO2 nanocrystalline electrodes with aggregated cyanine dyes. *J. Phys. Chem. B* **2001,** *105* (41), 9960-9965.

26. Sayama, K.; Tsukagoshi, S.; Hara, K.; Ohga, Y.; Shinpou, A.; Abe, Y.; Suga, S.; Arakawa, H., Photoelectrochemical properties of J aggregates of benzothiazole merocyanine dyes on a nanostructured TiO2 film. *J. Phys. Chem. B* **2002,** *106* (6), 1363-1371.

27. Jordan, A. N.; Das, S.; Siraj, N.; de Rooy, S. L.; Li, M.; El-Zahab, B.; Chandler, L.; Baker, G. A.; Warner, I. M., Anion-controlled morphologies and spectral features of cyanine-based nanoGUMBOS - an improved photosensitizer. *Nanoscale* **2012,** *4* (16), 5031-5038.

28. Lee, B.; Hwang, D.-K.; Guo, P.; Ho, S.-T.; Buchholtz, D. B.; Wang, C.-Y.; Chang, R. P. H., Materials, Interfaces, and Photon Confinement in Dye-Sensitized Solar Cells. *J. Phys. Chem. B* **2010,** *114* (45), 14582-14591.

CHAPTER 5
CONCLUSIONS AND FUTURE WORK

5.1 Concluding Remarks

This dissertation work involved the use of novel dye GUMBOS and nanomaterials derived from GUMBOS for potential application as sensitizers in DSSCs. In the first chapter, an overview of solar cells with a focus on DSSCs was presented. Studies related to key components of DSSCs were reported, and analytical techniques used in this work were discussed.

The synthesis and characterization of nanoGUMBOS using cyanine dyes was examined in the second chapter. These cyanine nanomaterials were prepared by use of a simple reprecipitation method and found to exhibit controlled morphology and aggregation by variation of the associated anion. In addition, broad absorption of the cyanine-based nanoGUMBOS was reported due to differences in molecular self-assembly ordering (e.g., H- *vs.* J-aggregation). Furthermore, electrochemical properties of the cyanine-based GUMBOS resulted in suitable potential values that favor electron injection and regeneration processes required in DSSCs.

Studies to further broaden absorption, particularly in the near-infrared region of the electromagnetic spectrum, were investigated in the third chapter. Previously studied GUMBOS were combined with novel increased methine chain length cyanine-based GUMBOS to form binary nanomaterials. Spectral properties of these binary nanoGUMBOS were found to yield broad absorption and tunable emission that extended to the near-infrared region by adjusting the molar ratio, which was attributed to FRET. Additionally, electrochemical properties of these cyanine GUMBOS were also

found to exhibit adequate potential values that suggest possible use as photosensitizers in DSSCs.

In the fourth chapter, the incorporation of cyanine-based GUMBOS in DSSCs was reported. Photovoltaic performances of the solar cells were found to exhibit a conversion efficiency of 0.73% by use of electrospun nanofibers as compared to nanoparticles that resulted in negligible conversion efficiency. This lack of efficiency was attributed to limited interaction between the sensitizers and TiO_2 surface. Therefore, this interaction may be optimized by modification of the dye structures with an anchoring group.

5.2 Future Work

Examination of the electrochemical properties of cyanine-based nanomaterials will also be examined. The electrochemical studies involved in this dissertation were conducted in solution. However, nanomaterials can exhibit different characteristics as compared to bulk materials. Therefore, it is important to measure the potential of the cyanine-based nanoGUMBOS to confirm use in DSSCs. These studies will require increased concentration of nanomaterials for sufficient analysis by use of cyclic voltammetry. The fabrication of a working electrode comprised of cyanine-based nanoGUMBOS deposited on FTO glass substrates can be used to obtain a concentrated sample of nanoGUMBOS. The selection of a suitable aqueous electrolyte will also be necessary to allow for optimized analysis.

This thin film approach can also be applied for investigation of the electron transfer process between the sensitizer and TiO_2 surface by depositing TiO_2 followed by concentrated nanoGUMBOS. The preparation of TiO_2 electrodes with cyanine-based

nanoGUMBOS can be examined using both electrochemical and spectral techniques, i.e. cyclic voltammetry, UV-Vis absorption and fluorescence spectroscopy. After further testing and optimizing DSSCs using the cyanine based-GUMBOS and nanoGUMBOS, modification to other significant components in DSSCs will be explored in the presence of these materials such as investigating various oxide semiconductor nanostructures and ionic liquid electrolytes.

APPENDIX: LETTERS OF PERMISSION

Atiya Jordan <ajorda6@lsu.edu> Fri, Nov 16, 2012 at 4:12 PM

To: contracts-copyright@rsc.org

To Whom It May Concern:

I am the first author of "Anion-controlled morphologies and spectral features of cyanine-based nanoGUMBOS – an improved photosensitizer" published this year in Nanoscale. I would like to request permission to use this article in my dissertation. Please let me know what forms and information is necessary to may this possible.

Regards,

Atiya Jordan
PhD Candidate
Warner Research Group
Department of Chemistry
Louisiana State University

CONTRACTS-COPYRIGHT (shared) <Contracts-Copyright@rsc.org> Wed, Nov 21, 2012 at 4:55 AM

To: Atiya Jordan <ajorda6@lsu.edu>

Dear Atiya

The Royal Society of Chemistry (RSC) hereby grants permission for the use of your paper(s) specified below in the printed and microfilm version of your thesis. You may also make available the PDF version of your paper(s) that the RSC sent to the corresponding author(s) of your paper(s) upon publication of the paper(s) in the following ways: in your thesis via any website that your university may have for the deposition of theses, via your university's Intranet or via your own personal website. We are however unable to grant you permission to include the PDF version of the paper(s) on its own in your institutional repository. The Royal Society of Chemistry is a signatory to the STM Guidelines on Permissions (available on request).

Please note that if the material specified below or any part of it appears with credit or acknowledgement to a third party then you must also secure permission from that third party before reproducing that material.

Please ensure that the thesis states the following:

Reproduced by permission of The Royal Society of Chemistry

and include a link to the paper on the Royal Society of Chemistry's website.

Please ensure that your co-authors are aware that you are including the paper in your thesis.

Regards

Gill Cockhead

Publishing Contracts & Copyright Executive

Gill Cockhead (Mrs), Publishing Contracts & Copyright Executive
Royal Society of Chemistry, Thomas Graham House
Science Park, Milton Road, Cambridge CB4 0WF, UK
Tel +44 (0) 1223 432134, Fax +44 (0) 1223 423623
http://www.rsc.org

VITA

Atiya Nicole Jordan was born in Philadelphia, Pennsylvania, to Jimmy and Vendella Jordan. She grew up in Virginia, by way of North Carolina. Atiya attended Hunt Valley and Orange Hunt Elementary Schools prior to enrollment at Washington Irving Middle School in Springfield, VA. Atiya graduated from West Springfield High School in 2004. She received her Bachelor of Science (*Cum Laude*) with a dual major in Forensic Science and Chemistry from Virginia Commonwealth University in May 2008. As an undergraduate, Atiya was a class facilitator for an intense focused learning course for General Chemistry. She also participated in a summer internship at Pharmaceutical Product Development Inc. in Richmond, VA. Upon graduation, Atiya matriculated to graduate school at Louisiana State University (LSU) in August 2008. She began her doctoral studies in analytical chemistry under the mentorship of Dr. Isiah M. Warner. During her time in graduate school, Atiya had the opportunity to travel to China twice for international conferences through a National Science Foundation program known as the International Materials Institute for Solar Energy and Environment. Atiya has received several honors during her graduate school career at LSU including the *Board of Regents Fellowship, American Association of University Women Eleanor Earle Memorial Scholarship,* and *Ford Foundation Dissertation Fellowship Honorable Mention*. Atiya graduated with the degree of Doctor of Philosophy in chemistry from Louisiana State University in May 2012. Her publications, conference presentations, as well as honors and awards are listed below.

PUBLICATIONS

Jordan, A. N.; Das, S.; Siraj, N.; de Rooy, S. L.; Baker, G. A.; Warner, I. M. Near-Infrared Emitting Binary Nanomaterials. To be submitted for publication, 2013.

Jordan, A. N.; Das, S.; Siraj, N.; de Rooy, S. L.; Li, M.; El-Zahab, B.; Chandler, L.; Baker, G. A.; Warner, I. M. Anion-controlled Morphologies and Spectral Features of Cyanine-based NanoGUMBOS–An Improved Photosensitizer, *Nanoscale*, 2012, 4, 5031-5038.

de Rooy, S. L.; Das, S.; Li, M.; El-Zahab, B.; **Jordan, A. N.**; Lodes, R.; Weber, A.; Chandler, L.; Baker, G. A.; Warner, I. M. Ionically Self-Assembled, Multi-Luminophore One-Dimensional Thiacarbocyanine Micro and Nanoscale GUMBOS. *Journal of Physical Chemistry*, 2012, 116, 8251-8260.

Das, S.; de Rooy, S. L.; **Jordan, A. N.**; Chandler, L.; Negulescu, I. I.; El-Zahab, B.; Warner, I. M. Tunable Size and Spectral Properties of Fluorescent NanoGUMBOS in Modified Sodium Deoxycholate Hydrogels. *Langmuir*, 2011, 28, 757-765.

ORAL PRESENTATIONS

Cyanine NanoGUMBOS as Sensitizers for Applications in Dye-sensitized Solar Cells. Presented at the 245th ACS National Meeting, New Orleans, LA, April 7-11, 2013.
High Energy Transfer Efficiency Binary NanoGUMBOS for Application in Dye-sensitized Solar Cells. Presented at the 68th Annual Southwest Regional Meeting of the American Chemical Society, Baton Rouge, LA, Nov 4-7, 2012.

Dye GUMBOS and NanoGUMBOS as Photosensitizers for Application in Dye-Sensitized Solar Cells. Presented at the 39th Annual NOBCChE Conference, Washington, D.C., Sept 25-28, 2012.

Invited speaker. Cyanine GUMBOS and NanoGUMBOS for Application in Dye-sensitized Solar Cells. Presented at Virginia Commonwealth University, Richmond, VA, April 24, 2012.

Evaluation of Morphology and Spectral Properties of Nanomaterials Derived from Pseudoisocyanine-based GUMBOS. Presented at the 38th Annual NOBCChE Conference, Houston, TX, April 19-22, 2011.

Tunable Morphology and Spectral Properties of Pseudoisocyanine-based NanoGUMBOS. Presented at the 66th Southwest and 62nd Southeastern Regional Meeting of the American Chemical Society, New Orleans, LA, Nov 30-Dec 4, 2010.

POSTER PRESENTATIONS

Jordan, A. N.; Galpothdeniya, I.; de Rooy, S. L.; Das, S.; Siraj, N.; Warner, I. M. Ionic Liquids and GUMBOS for Applications in Sensing and Light Harvesting. Presented at the Nanotechnology for Defense Conference, Summerlin, NV, Aug 6-9, 2012.

Johnson, K.; **Jordan, A.N.**; McNeel, K.; Das, S.; Warner, I. M. Investigation of Trihexyl(tetradecyl)phosphonium Merocyanine for Use in Dye-Sensitized Solar Cells. Presented at the Summer Undergraduate Research Forum, Baton Rouge, LA, July 26, 2012.

Jordan, A. N.; Das, S.; Siraj, N.; de Rooy, S. L.; Li, M.; El-Zahab, B.; Chandler, L.; Baker, G. A.; Warner, I. M. Morphological, Spectral, and Electrochemical Properties of Pseudoisocyanine-based NanoGUMBOS: Application in Dye-Sensitized Solar Cells. Presented at the International Materials Institute for Solar Energy and Environment – Dye-Sensitized Solar Cells Workshop, Xiamen, China, Oct 24-28, 2011.

Knapp, E.; **Jordan, A. N.**; Cole, M. R.; Das, S.; Warner, I. M. Merocyanine Phosphonium GUMBOS: Synthesis and Characterization for Dye-Sensitized Solar Cells. Presented at the Summer Undergraduate Research Forum, Baton Rouge, LA, July 28, 2011.

Jordan, A. N.; Das, S.; de Rooy, S. L.; El-Zahab, B. Warner, I. M. Tunable Morphology and Spectral Properties of Cyanine Dye GUMBOS. Presented at the Nanotechnology for Defense Conference, Atlanta, GA, May 3-6, 2010.

Jordan, A. N.; Das, S.; de Rooy, S. L.; Li, M. El-Zahab, B. Warner, I. M. Pseudoisocyanine-based GUMBOS as Sensitizers for Dye-Sensitized Solar Cells. Presented at the Southwest Regional NOBCChE Conference, Baton Rouge, LA, March 13, 2010.

Jordan, A. N.; Das, S.; de Rooy, S. L.; Li, M. El-Zahab, B. Warner, I. M. Cyanine Dye NanoGUMBOS as Sensitizers for Dye-Sensitized Solar Cells. Presented at the 2nd US-China Workshop on Nanostructured Materials for Global Energy and Environmental Challenges, Jiangsu, China, Oct 15-17, 2009.

HONORS AND AWARDS

2013 James Robinson Outstanding Research in Analytical Sciences Award

2012 Procter & Gamble, Focusing on Industrial Recruitment of Scientific Talent (FIRST) Conference

2012 Dow Chemical Company, Building Engineering and Science Talent (BEST) Symposium

2012 Ford Foundation Dissertation Fellowship Honorable Mention

2012 American Association of University Women Eleanor Earle Memorial Scholarship

2012 62nd Meeting of Nobel Laureates Graduate Student Nominee

2009 Teaching Assistant Scholars Award

2008 Louisiana Board of Regents Graduate Fellowship

PROFESSIONAL AFFILIATIONS

2011-Present	Iota Sigma Pi National Honor Society of Women in Chemistry
2008-Present	American Chemical Society
2008-Present	National Organization for the Professional Advancement of Black Chemists and Chemical Engineers (NOBCChE)